University of Nevada, Reno

Observed and Simulated Urban Heat Island and Urban Cool Island in Las Vegas

A thesis submitted in partial fulfillment of the requirements for the degree of Master of Science in Atmospheric Science

by

Daniel O. Sauceda

Dr. John Mejia/Thesis Advisor

December, 2014

THE GRADUATE SCHOOL

We recommend that the thesis
prepared under our supervision by

DANIEL O. SAUCEDA

Entitled

Observed And Simulated Urban Heat Island And Urban Cool Island In Las Vegas

be accepted in partial fulfillment of the
requirements for the degree of

MASTER OF SCIENCE

John Mejia, Advisor

Sajjad Ahmad, Committee Member

Justin Huntington, Graduate School Representative

David W. Zeh, Ph.D., Dean, Graduate School

December, 2014

Abstract

This research investigates the urban climate of Las Vegas and establishes long-term trends relative to the regional climate in an attempt to identify climate disturbances strictly related to urban growth. An experimental surface station network (DRI-UHI) of low-cost surface temperature (T2m) and relative humidity (RH) sensors were designed to cover under-sampled low-intensity residential urban areas, as well as complement the in-city and surrounding rural areas. In addition to the analysis of the surface station data, high-resolution gridded data products (GDPs) from Daymet (1km) and PRISM (800 m) and results from numerical simulations were used to further characterize the Las Vegas climate trends. The Weather Research and Forecasting (WRF) model was coupled with three different models: the Noah Land Surface Model (LSM) and a single- and multi-layer urban canopy model (UCM) to assess the urban related climate disturbances; as well as the model sensitivity and ability to characterize diurnal variability and rural/urban thermal contrasts. The simulations consisted of 1 km grid size for five, one month-long hindcast simulations during November of 2012: (i) using the Noah LSM without UCM treatment, (ii) same as (i) with a single-layer UCM (UCM1), (iii) same as (i) with a multi-layer UCM (UCM2), (iv) removing the City of Las Vegas (NC) and replacing it with predominant land cover (shrub), and (v) same as (ii) with increasing the albedo of rooftops from 0.20 to 0.65 as a potential adaptation scenario known as "white roofing".

T2m long-term trends showed a regional warming of minimum temperatures (T_{min}) and negligible trends in maximum temperatures (T_{max}). By isolating the regional temperature trends, an observed urban heat island (UHI) of ~1.63°C was identified as

well as a daytime urban cool island (UCI) of ~0.15°C. GDPs agree with temperature trends but tend to underpredict UHI intensity by ~1.05°C. The WRF-UCM showed strong correlations with observed T2m ($0.85 < \rho < 0.95$) and vapor pressure (e_a; $0.83 < \rho < 0.88$), and moderate-to-strong correlations for RH ($0.64 < \rho < 0.81$) at the 95% confidence level. UCM1 shows the best skill and adequately simulates most of the UHI and UCI observed characteristics. Differences of LSM, UCM1, and UCM2 minus NC show simulated effects of warmer in-city T_{min} for LSM and UCM2, and cooler in-city T_{max} for UCM1 and UCM2. Finally, the white roofing scenario for Las Vegas was not found to significantly impact the UHI effect but has the potential to reduce daytime temperature by 1°-2°C.

Acknowledgements

First and foremost I would like to thank my advisor Dr. John Mejia for giving me the opportunity to work with him on this interesting project. He has taught me how to become a better scientist through developing skill sets I didn't think I had. I would also like to acknowledge my committee members Dr. Justin Huntington and Dr. Sajjad Ahmad for taking interest in my work, and assisting at advising me alongside John. I'd personally like to thank Dr. Michael Kaplan for bringing me into the Desert Research Institute (DRI) community. Without him and Benjamin Hatchett I would not have had this opportunity. Our research would not be possible without the funding of the NSF-EPSCoR, and the DRI Graduate Support. In assistance to the DRI-UHI observational network, I'd like to thank Leonardo Hernandez who helped designed and setup the network. Also the Clark County School District (CCSD), Summerlin Golf Course, Wildhorse Golf Course, Mike Roos, and volunteers at DRI South for letting us set up our instruments on their properties. To the graduate students: Andy Joros, KC King, Sandra Theiss, Matt Fearon, Nick Nauslar, and others who have helped me with data analysis and given me advice on surviving graduate school, I appreciate the sentiments. A special thanks to Daniel McEvoy for adding more insight to this thesis by providing me with material to upgrade my analysis. Lastly, I'd like to thank my parents Rick and Letty, and my brother Richie for their encouragement and belief in me to accomplish tasks I set out to finish.

Table of Contents

List of Tables

List of Figures

List of Appendices

1. Introduction

1.1 Urban Climate

The City of Las Vegas has grown extensively in population and size over the last five decades (Figure 1). Changing the natural land use/land cover (LULC) into a city environment can have an impact on air quality, local climate, and weather (Taha, 1997). These impacts further include socioeconomic and health factors (Huang et al., 2011). Urban development generally causes temperatures to increase due to greater heat storage by impervious surfaces leading to a phenomenon known as the urban heat island (UHI) effect. The UHI is a common phenomenon among large cities as surface areas with large amounts of impervious materials absorb heat during the daytime that is later released during nighttime/early morning hours (Oke and Maxwell, 1975). This characterizes a warmer urban environment relative to the suburban and rural surroundings that is most significant during the nighttime and early morning (Fast et al., 2005; Kim and Baik, 2005; Guhathakurta and Gober, 2010).

Extreme temperatures from heat waves can be enhanced by the UHI, making residents vulnerable to heat exhaustion. Along with higher dewpoint temperatures (T_d), increases in air temperature can affect the human thermal comfort. The human body can become restricted from evaporating moisture (i.e. sweat) to cool itself as the environment reaches its threshold to absorb moisture (Kunkel et al., 1996). Wind speeds are also influenced by the urban environment. Surface roughness of urban materials and building structures can slow down wind speeds (Kim and Kim, 2009; Yushkov et al., 2009). Slower wind speeds also favor an increase in anthropogenic emissions by reducing

turbulent mixing processes that are responsible for the dispersion of pollutants (Allwine and Whiteman, 1988). Furthermore, reduced winds can slow down the transport of warmer air allowing the UHI to persist for a longer period of time.

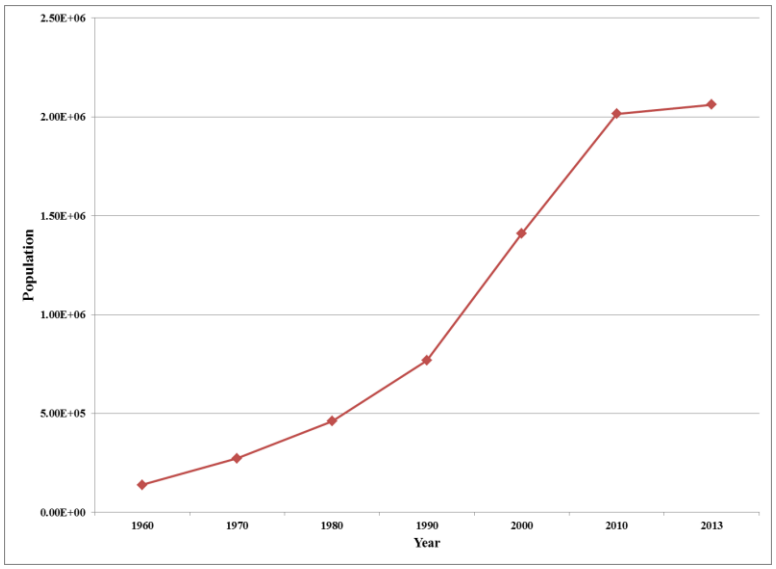

Fig. 1. The metropolitan population of Las Vegas, Nevada provided by the US Census Bureau. *Source: census.gov.*

The urban cool island (UCI) is an inverse effect of the UHI in which rural arid surrounding environments tend to be warmer than the urban area. The UCI is most significant during the daytime. Contributions that influence the UCI include: enhanced evapotranspiration (ET) from foreign vegetation which includes turf grass from lawns and golf courses (Hart and Sailor, 2009; Mendonca, 2009; Li et al., 2011; Lindén, 2011; Middel et al., 2012); evaporative cooling from open water surfaces such as artificial ponds and lakes within or nearby the city (Mendonca, 2009; Lindén, 2011); urban shading from buildings and trees (Hart and Sailor, 2009; Lindén, 2011); and surfaces

characterized by higher albedo (Mendonca, 2009; Akbari et al., 2012). Surfaces shaded by urban features tend to absorb less solar energy due to the density of buildings, trees, and other urban structures (Hart and Sailor, 2009).

Urban environments impact all the components of the surface energy balance (SEB) which include: shortwave and longwave radiation exchanges, latent and sensible heat fluxes, and albedo (Oke, 1987). A difference in albedo between urban surfaces affects the amount of absorbed incoming solar radiation. For example, brighter urban objects (e.g., light concrete surfaces and white roofs) reflect more light than darker objects (e.g., dark pavement and ponds). Urban geometry can be of importance as large buildings increase the UHI when warm air is exerted by these buildings along with paved streets and anthropogenic activities (Wallace and Hobbs, 2006). The limited spacing between houses and buildings has a tendency to trap outgoing radiation, and further add to the cities warming (Aguado and Burt, 2007). Furthermore, tall buildings can create shading during the daylight hours and reduce heat storage resulting in less upwelling longwave radiation during the night (Roberts et al., 2006). However, estimating the net thermal effect of buildings can be challenging and may vary depending on the urban orientation, city geometry, and surface characteristics. Fast et al. (2005) showed from observations during the summer of 2001 that downtown Phoenix, AZ, tends to be warmer outside and to the west of the downtown central core.

1.2 UHI Impacts

Previous studies have shown that precipitation patterns can be modulated as a warmer city creates more buoyant boundary layer parcels fostering rising motions, thus

increasing the likelihood for the development of convection and precipitation downwind of a city (Van Heerwaarden and Vilà-Guerau De Arellano, 2008). Additionally, urban pollution increases aerosol loadings that can serve as condensation nuclei and reduce the intensity and magnitude of downwind precipitation (Changnon, 1981; Van Den Heever and Cotton, 2007).

Due to the climate perturbations and human health threats associated with the UHI and the rapid growth of cities, it is necessary for cities to have a plan for adaptation and mitigation (NCA, 2013). Mitigation and adaptation strategies can help decrease pollution concentrations while cooling strategies such as white roofing (Jacobson and Ten Hoeve, 2012), cool paving (Li et al., 2013), and increasing the green fraction (Smith and Roebber, 2011) can help reduce the UHI impacts. Using a computer model, Jacobson and Ten Hoeve (2012) simulated a white roofing scenario for the globe. Results totaled a population-weighted cooling of 0.02°C, however, global temperatures still continued to rise. Li et al. (2013) investigated the hydraulic and thermal performances of cool pavements showing that interlocking cool pavers infiltrate 0.4 cm s^{-1} more than non-interlocking cool pavers. This helps prevent intense runoff and cools the surface through diffuse evaporation. In addition, the albedo of cool pavements helped reduce pavement temperatures by ~15-35°C depending on the moisture infiltrated. Smith and Roebber (2011) modeled a green roofing summer scenario for Chicago, Illinois, and showed that vegetation on rooftops increased ET and albedo to cool the urban environment by ~3°C. Other green strategies suggest building more parks and planting more trees (Kloss and Calarusse, 2006; EPA, 2008; NCA, 2013). Cooling the urban environment will lead to

less usage of air conditioning thus reducing electrical consumption (Shorr et al., 2009). For example, the Houston Advanced Research Center (HARC) has taken initiative on using several of the mentioned methods to mitigate the UHI in Dallas, Texas. The Dallas Sustainable Skyline Initiative is a project of the US Environmental Protection Agency in which mitigation activities include: planting trees in hotspots of the city; installing cool roofs (white roofs and green roofs); and using cool pavements to increase albedo and minimize stormwater runoff (HARC, 2009). HARC describes how the benefits of these strategies outweigh the costs based on the potential amount of energy it can save.

The UHI can affect water demand as warmer temperatures result in higher evaporation and ET rates, and therefore providing the need to increase irrigation water requirements (Gober et al., 2010). Thus, further stressing the effects of episodic droughts and frequency of heat waves. The severe drought in North-Central Texas exacerbated nighttime UHI in Dallas as shown by Winguth and Kelp (2013), who recorded a UHI of 5.4°C during severe drought and heat wave activity on July 2011. In the late morning, a UCI magnitude of 2.3°C was recorded due to lower soil moisture content in the rural regions. Of note is that the UHI combined with drought and climate change in the Southwest can degrade the quality of water through dust storm intrusions, and impact urban water supplies by accelerating the evaporation process (Earman et al., 2006; Reheis and Urban, 2011; Yates et al., 2013).

Alghannam and Al-Qahtnai (2012) examined T2m and relative humidity (RH) in the Al Hofuf region of Saudi Arabia. They argued that larger RH differences between urban and rural areas (ΔRH) can exhibit less UHI intensity from an outcome of more

vegetation coverage in the rural district. In the arid/semi-arid climate of Phoenix, Middel et al. (2012) investigated various LULC characteristics in the city during 2 summer days in 2005 using a Local-Scale Urban Meteorological Parameterization Scheme. They found that the LULC strongly influenced the time of negative sensible heat flux at night based on the surface heat storage. Impervious surfaces containing high heat storage capacities delayed positive-to-negative sensible heat transitions up to 3 hours, while vegetated areas accelerated them by 2 hours.

1.3 UHI and UCI Temporal Variability

The UHI intensity depends on the urban location, climate regime, synoptic patterns, and season (Kimura and Takahashi, 1991; Kim and Baik, 2005; Alghannam and Al-Qahtnai, 2012). UHI tends to be stronger during the summertime as larger amounts of solar radiation allows more heat to be absorbed and released by urban structures (Fast et al., 2005; Svoma and Brazel, 2010). The winter poses the opposite effect having less solar radiation and resulting in weaker UHI activity (Svoma and Brazel, 2010). Clear skies and light winds during high-pressure systems favor stronger UHIs and UCIs (Oke, 1987), while low-pressure systems associated with stronger winds, increased cloudiness, and precipitation act to suppress the UHI and UCI effects (Kim and Baik, 2005).

1.4 Observing the UHI and UCI

Hansen et al. (2001) analyzed global surface temperatures throughout the US using the Goddard Institute for Space Studies analysis and the U.S. Historical Climatology Network records. Since the start of the 20th century, they found warming from 1900-1940 and 1965-2000, while 1940-1965 corresponded as a cooling period.

They argued that aerosol forcing was at its highest during 1940-1965 due to massive amounts of fossil fuel burning. This could have contributed to the slight global cooling of -0.1°C (Hansen et al., 2001). When conducting analysis of the UHI, it is fundamental to examine and separate the trends in the records related to the local, regional, and global trends. On a global scale, it is argued that cities could have negligible effects (Hansen et al. 2001), but city temperature related trends are influence by regional and global trends. However, it is challenging to separate such influences due to the large variation of city LULC characteristics (Hansen et al., 2001; Cai and Kalnay, 2003).

The difficulties of studying urban climate are generally based on data quality and availability of sites that adequately represent in-city characteristics. Some observational networks lack rigorous quality assurance and quality control (QA/QC) protocols and are not adequately design to highly contrasting surface characteristics of city landscapes. The complex terrain inside and surrounding an urban structure further limits UHI characterization. Hence, adequate distinction of global and regional temperature trends (including interdecadal-to-decadal climate variation) from changes attributed to LULC and SEB alterations is a challenging task.

Remote sensing tools can be very valuable to characterize urban temperature environments. Jin (2012) used skin temperature from remote sensing platforms to measure the UHI in Beijing and New York. Her results showed diurnal and seasonal variations of maximum UHI in the daytime and during summer. Since this was based on skin temperature, these conclusions pertained more to the estimated heat storage of heterogeneous surfaces. Even though observations from remote sensing are more

accurate during clear sky conditions, they can be very valuable to characterize the highly contrasting thermal differences within the city.

Xian (2008) used Landsat satellite imagery to distinguish surface parameters for Seattle, Tampa Bay, and Las Vegas. Long-term climate observation records (50-years) measuring T2m were also examined to clarify regional climate conditions. Monthly data from these records showed a weak increase in mean temperatures (T_{mean}) and a moderate increase in minimum temperatures (T_{min}) for Tampa Bay and Seattle. Las Vegas showed the strongest increase for T_{min} at 0.69°C/decade with a moderate increase in T_{mean}. Landsat temperatures were separated into 4 categories of LULC based on the percentage of impervious surface per pixel. Urban-rural temperature differences showed warmer temperatures with greater percentages of impervious surface area. Las Vegas is the only city to show negative differences, which were evident for impervious pixels between 10-60%. Similar results of surface temperature in correlation with the amount of impervious surfaces are further discussed in Xian and Crane (2006) for the study areas of Las Vegas and Tampa Bay.

1.5 Urban Canopy Models

The urban canopy model (UCM) is arising as a fundamental tool for urban weather and climate studies. Typically, the UCM accounts for processes and city geometry, including: canyon orientations regarding the shading and radiative reflectivity inside the canyon; canopy layer wind profile; the heat transfer of roof, walls, and roads; diurnal changes of the solar azimuth angle oriented to the canyon; anthropogenic heat; and the thin bucket model for hydrological processes (Kusaka and Kimura, 2004). The

UCM coupled with the Weather Research and Forecasting (WRF) model and Noah Land Surface Model (LSM) takes into account the physics and dynamics of the urban structure.

UCMs have been used for many urban studies associated with large coastal cities such as Tokyo (Chen et al., 2011; Ikeda and Kusaka, 2010; Kusaka and Kimura, 2004), New York (Holt and Pullen, 2007), Houston (Chen et al., 2004; Lee et al., 2011), Beijing (Miao et al., 2009), and Taiwan (Lin et al., 2008) among several other urban areas. Kusaka et al (2001) showed that the UCM had a consistent diurnal energy budget for roofs, roads, and walls when compared against observations.

Two main UCM categories have been developments: the single-layer (Kusaka et al., 2001) and the multi-layer urban canopy (Ca et al., 1999; Kondo et al., 2005). The difference between the single- and multi-layer UCMs is the 2-dimensional and 3-dimensional urban canyon geometries, respectively (Kusaka et al., 2001). Although the urban geometry of buildings, streets, and walls have different dimensions, both models have a 3-dimensional radiation treatment due to the canyon orientation and the diurnal variations of the solar azimuth angle (Kusaka et al., 2001; Kusaka and Kimura, 2004). According to the previously mentioned studies, the UHI is well simulated by both UCMs. However, nighttime UHIs were generally better simulated than daytime UHIs (Holt and Pullen, 2007; Lin et al., 2008; Miao et al., 2009).

According to Kusaka et al. (2001) study in Tokyo, single- and multi-layer UCM sensitivity for heat storage differed a few hours after sunset and before sunrise by 20 and 29%, respectively. They found that the multi-layer UCM produced a greater heat storage capacity than the single-layer UCM. Miao et al. (2009) showed that UCM simulations for

the Beijing Valley adequately represented the main diurnal and spatial patterns associated with the UHI, even with the complex interactions of mountain-valley circulations. He concluded that canopy layer parameters (e.g., temperature and wind speed) for the UCM performed better than the surface parameters (e.g., T2m and 10 m wind speed). Lin et al. (2008) simulations for Taiwan showed underestimates of T2m by 1.7°C from 1100-1600 LST, while overestimates of 1.0°-1.3°C occurred between 0500-0700 LST for the single-layer UCM. Lee et al. (2011) conducted a sensitivity study using a three model configuration: the Noah-LSM, a modified LSM, and the single-layer UCM. When evaluating against the observations, the UCM performed better than the other two models. The Noah-LSM overestimated sensible heat up to 200 W m^{-2}, which not only affected the T2m warm-bias by ~3.6°C, but also the planetary boundary layer (PBL) conditions.

A few simulated studies have been performed in the semi-arid climate of Salt Lake City, Utah to evaluate and model anthropogenic activity (Tewari et al., 2011; Nehrkorn et al., 2013). Tewari et al. (2011) modeled the transport and dispersion of urban pollutants by coupling the WRF to the Noah/UCM and using WRF without UCM treatment. For T2m, the WRF and WRF-UCM displayed similar values except for in the industrial/commercial zone where WRF-UCM performed better. However, the models showed some disagreements from the observations which was theorized as a prelude to the urban parameterizations of the model. Similar conclusions were discussed in Nehrkorn et al. (2013) where they used WRF and WRF-UCM to simulate urban CO_2 on a local and mesoscale level. Error statistics were improved for CO_2 test sites when using

the WRF-UCM. The diurnal cycle of T2m was much more accurate during the nighttime and morning with the WRF-UCM. However, T_d exhibited a larger bias with WRF-UCM and provided inconclusive results. Although simulated RH was accurate against the observations, it was noted that the function of T2m had the strongest influence on these results. Therefore, the moisture simulations remained to show inaccuracies. The primary idea from these studies in Salt Lake City insist that adjusting the urban parameters would be needed to accurately depict the local flow, which can help decrease the biases of other meteorological variables to forecast realistic values.

1.6 Statement of Work

This work was funded by an NSF-EPSCoR research project aiming to initiate and explore methodologies for water vulnerability studies in the City of Las Vegas and surrounding areas under changing climate. An important task in this project was to characterize the Las Vegas current climate and observed trends. The goal of this thesis is to distinguish the Las Vegas climate and its relationship to urban growth, as well as to test new and alternative observational and modeling tools to address the following overarching research questions: i) Are there any observable and discernable differences between the urban temperature trends from those observed in the regional/global scale? ii) How are diurnal temperatures changing in response to a growing arid/semi-arid city?

To address these questions and to characterize the urban climate in Las Vegas we used different tools including surface stations (historical and from a specially design field campaign), high-resolution gridded data products (GDPs), and fine scale atmospheric modeling simulations with UCM treatment. Chapter 2 provides details of these tools and

the various methodologies of data analysis implemented throughout this study. Chapter 3 reports the results based on surface station observations, while Chapter 4 shows the analysis of the atmospheric modeling component using a single- and multi-layer UCM coupled with the WRF-LSM. The final section (Chapter 5) summarizes, integrates, and discusses the research findings and proposes future areas of research derived from this study.

2. Data and Methodology

2.1 Surface Station Networks

Significant efforts to collect surface station observations in the Las Vegas area was performed as part of this research. A total of 49 sites from six different networks were used for this study, which include: the Community Environmental Monitoring Program (CEMP; *www.wrcc.dri.edu*), National Weather Service (NWS; *www.ncdc.noaa.gov*), Nevada Climate-ecohydrological Assessment Network (NevCAN; *sensor.nevada.edu*), Weather Underground (WU; *www.wunderground.com*), the Remote Automated Weather Station network (RAWS; *raws.dri.edu*), and our own DRI-Urban Heat Island surface station network (DRI-UHI). General descriptions of these networks follow:

CEMP: The CEMP network is operated by the Desert Research Institute as part of a Department of Energy program designed to monitor regional environmental conditions, and radiation detection associated with desert nuclear test sites. Four stations from CEMP

were analyzed: three urban stations located in Las Vegas, Henderson, and Boulder City; and a fourth station located NNW outside of Las Vegas in the Indian Springs area.

NWS: The NWS network provides historical records for airport stations. McCarran Airport has records dating back to 1948. During QA/QC procedures it was noted that McCarran had most of the 1988 data missing from the records. The data was therefore reprimanded, and the year 1988 was completely removed from the McCarran analysis. Nellis Air Force Base has historical data to 1928, but records dated that far back were too inconsistent due to the large time gaps per measurement (up to 15 hours). In 2000, the Nellis station was moved ~2 km south and kept within the confines of the base. It was then moved back to the original location in 2005. The surface station at Henderson Executive Airport was established in 2004 before it was moved ~875 m north in 2006 where its current location still stands. The NWS network provides a few rural sites outside Las Vegas. However, Desert Rock Airport (located ~75 km NW of Las Vegas) is the only rural station that continues to collect data with a record over 30 years.

NevCAN: NevCAN is part of a climate project by the University of Nevada, Reno; University of Nevada, Las Vegas; and the Desert Research Institute in conjunction with land owner agencies on efforts for long-term climate assessments with regards to the impacts of ecological and hydrological processes (Mensing et al., 2013). There are two transects occupied by the NevCAN network, each are located on the Snake Range (along the western Utah border) and the Sheep Range (~35 km NNW of Las Vegas). Four stations were selected in the Sheep Range site for analysis. Although NevCAN stations

have only been recording for a few years (since October 2011), they have one of the most robust and consistent datasets available to the public.

WU: WU stations are self-installed by scientists and amateur weather enthusiasts with purchase from the company's website (*http://www.weatherunderground/personal-weather-station*). The WU network was created to provide meteorologists with more weather data outside of airports. WU has the world's largest network of personal weather stations that are monitored and updated continually on their website. From the data of 23 WU stations collected, only 12 were used for the analysis. WU stations were rejected due to insufficient values (e.g. inordinate amount of missing records), and several stations in the WU database were uploaded from other networks that were already chosen for this study. All WU stations chosen for this study are located in or around residential sites within the City of Las Vegas.

RAWS: RAWS stations are in conjunction with the Desert Research Institute and the Western Regional Climate Center (WRCC). The data is available to the public in which it is collected, stored, and forwarded to satellite before returning to the National Interagency Fire Center in Boise, Idaho. RAWS data is used by fire and environmental managers to monitor fuels and conditions and predict fire behavior. Four RAWS stations were analyzed for this study. Similar to the NevCAN network, all the RAWS stations were located outside the city.

DRI-UHI: For this study, we deployed a network of 20 low-cost T2m and RH HOBO sensors to improve the spatial coverage inside and outside the City of Las Vegas. Careful planning went into selecting the sites and setting up the network to improve the

spatial distribution of existing surface station networks, and to better characterize the UHI from under-sampled land use categories. Eleven stations were installed in the front and backyards of residencies employed by UNLV and DRI who volunteered to setup the sensors at their homes. Seven more sensors were installed in Clark County School District schools and school maintenance facilities. Two stations were installed in the middle of golf courses: Wildhorse Golf Course located in east-central Las Vegas and Summerlin Golf Course located in NE Las Vegas.

Table 1. Observational networks and recording time increments.

Network	Time Increments
DRI-UHI	15 minutes
CEMP	10 minutes
NWS	1 hour
NevCAN	1 minute
WU	5, 10, 15, 30 minutes
RAWS	1 hour

On July 2012 and following siting and setup recommendations, the DRI-UHI T2m/RH sensors were installed within a solar radiation shield to avoid direct sunlight (Appendix B). When possible, the sensors were placed in shaded areas to further avoid direct solar radiation in order to properly measure the temperature and RH of the ambient air. The methods for setting up the DRI-UHI stations followed Watts (2009) guidelines.

Since observations were recorded in each site by a data logger, the sampling time increments were set to 15 minutes to maximize recording sampling and to minimize visits to the sites. The DRI-UHI data was downloaded manually every six months, during 2 years. With every visit to these locations, we performed basic quality assurance protocols

along with maintenance and cleaning of equipment. Due to funding constrains, the sampling time increment was recently reset to hourly measurements. Depending on further resources, we hope to maintain the network for at least three more years. Data collected from this network is made available to the public and other scientific groups on the Nevada Climate Change Portal (*sensor.nevada.edu*).

Urban climate studies can be easily skewed due to stations located near impervious surfaces, influences of nearby equipment generating heat, moving/replacement of sites, technical changes in the sensors, and short and missing record periods (Watts, 2009). Thorough QA/QC protocols were carried out to clean the data from all surface station networks, and to create a robust and solid database for UHI characterization in time and space. Only sites with hourly or smaller time increments were kept for the analysis (Table 1). Also, metadata and LULC attributes and footprints of station sites were recorded to composite stations by their dominant footprint characteristics. Figure 2 shows a map of all the analyzed surface networks for this study, while *Appendix A* shows a summary of each station's characteristics.

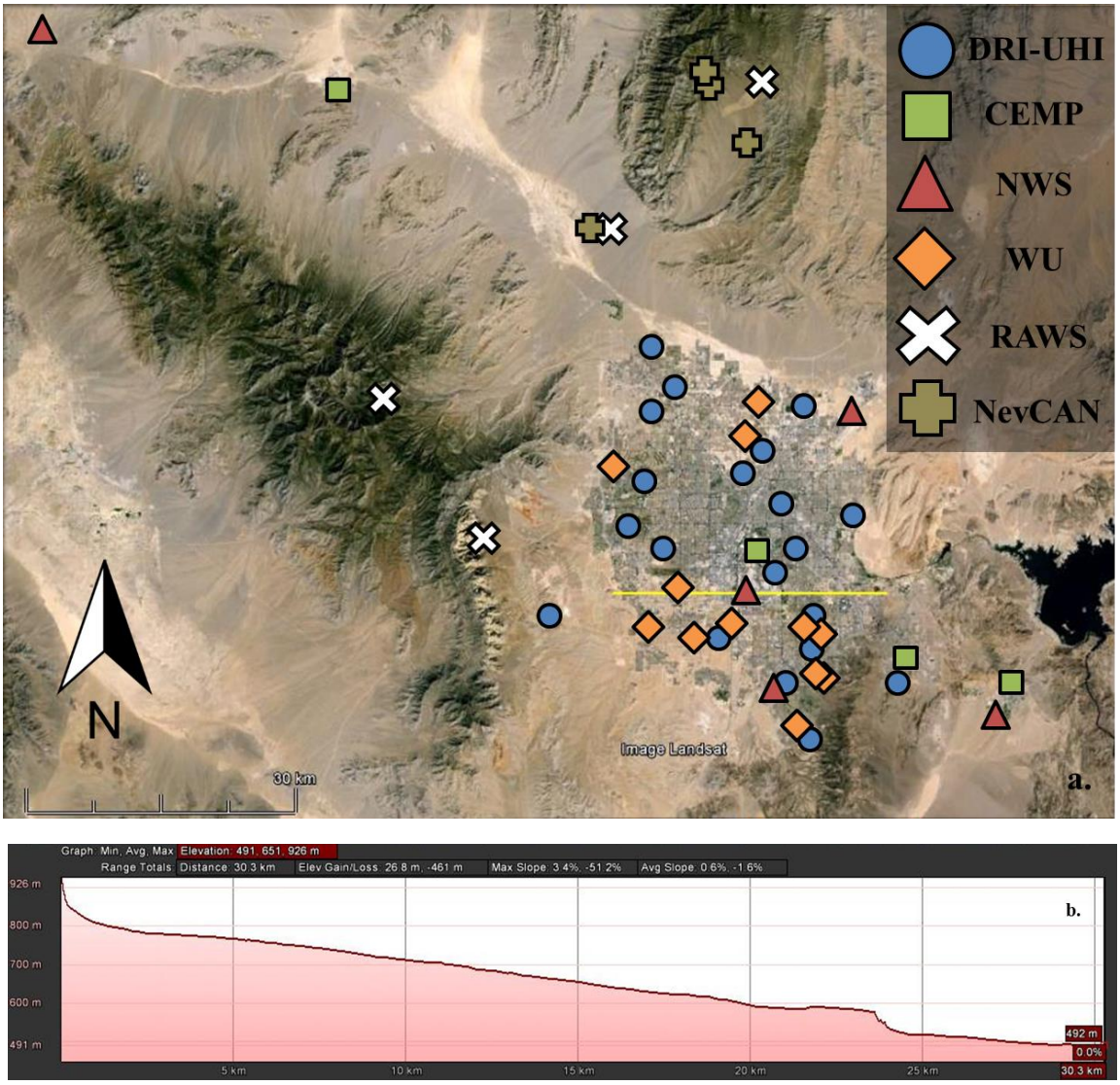

Fig. 2. (a) Spatial distribution of analyzed stations. Networks are classified by shapes and total 49 stations. (b) Elevation across the yellow line in (a) shows a 434 m east-west difference through Las Vegas. *Source: Google Earth.*

2.2 Gridded Data Products

Two climate GDPs were tested for spatial temperature analyses: The Parameter-elevation Regression on Independent Slopes Model with 800 m grid size of monthly data (PRISM 800 m; Daly et al., 2008) and Daymet 1 km grid size of daily data (Thornton et al., 1997). For the purpose of this thesis, Daymet daily data was aggregated to monthly

means. These gridded datasets integrate data assimilations/interpolation procedures with topography, temperature, and other meteorological variables (Scully, 2010). GDPs use surface station data that is weighted from regression analysis in which gridded values are determined by the distance from the analyzed grid cell (Daly, 2006). Hence, a few of the surface observation stations analyzed in this study (e.g. NWS and RAWS) are used in the GDPs interpolation methods. The goals were to evaluate whether PRISM 800 m and Daymet are useful in detecting urban signals, and if their spatial distribution adds value to urban climate studies.

Figure 3 displays a map with three regions of interest over and around the city to represent the Las Vegas Valley. The red rectangle is a representation of the dense downtown structure of Las Vegas while the green rectangle represents more suburban influence within the city. The blue rectangle is a representation of the rural region outside of Las Vegas. Of note is that Daymet data is available as far back as 1980, while PRISM 800 m had estimates back to 1895. Therefore, monthly trends from January 1980-December 2011 were analyzed for T_{max} and T_{min}. Residuals (i.e. UHI/UCI estimates) were calculated by averaging the output of T2m from the core (red box) and outer-core (green box) areas before subtracting by the output of the rural domain (blue box). Of note is that this analysis was not setup for the data of the customized domains to overlap each other. However, with the predetermined grid points provided by the GDPs, there may be small insignificant overlaps in the corner and edges of the domains.

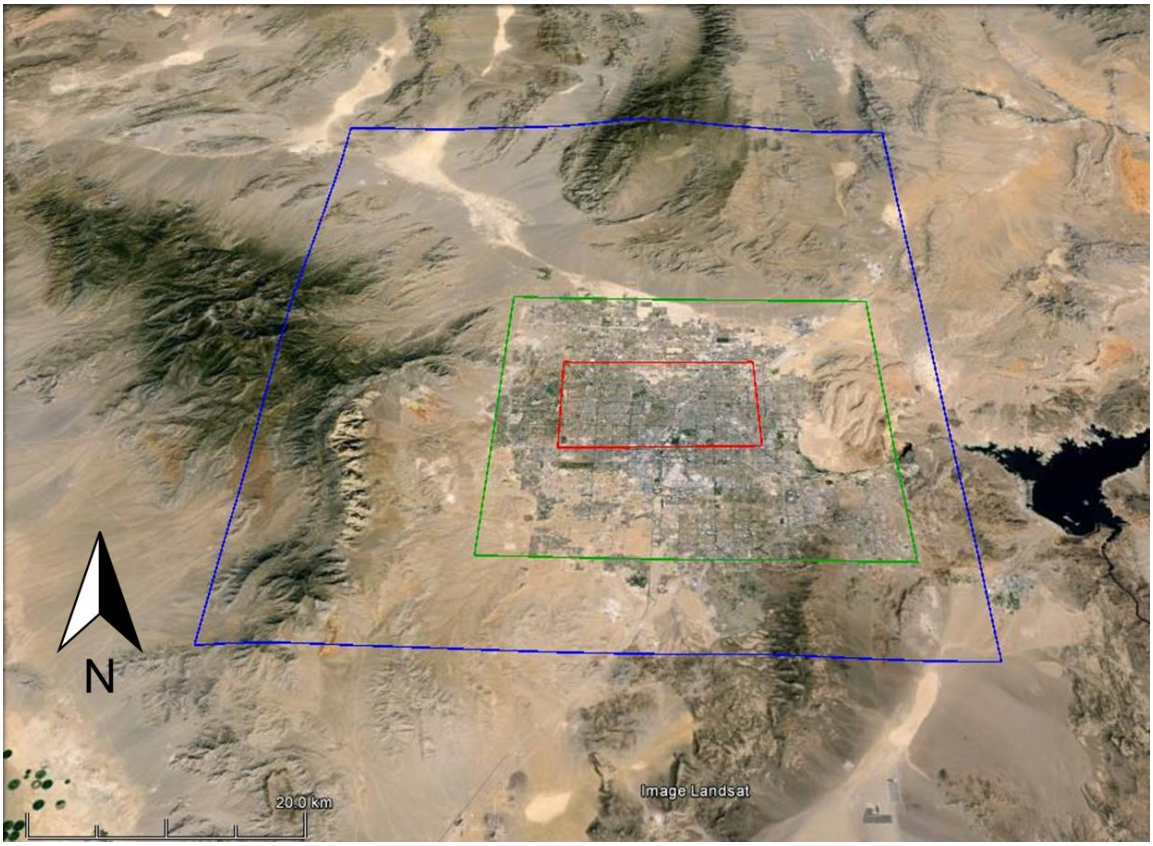

Fig. 3. A Landsat image of Las Vegas containing three rectangles covering the city core (red), outer-core (green), and rural (blue) boundaries for Daymet and PRISM 800 m analysis.

2.3 Long-Term Trend Detection

Las Vegas has been one of the fastest growing cities in the United States through the last decade taking in over 650,000 residencies since 2000 (source: *www.census.gov*; Figure 1) with the persistence of urban expansion. Figure 4 shows Landsat imagery highlighting the urban expansion of Las Vegas from 1973 through 2006 provided by the United Nations Environment Programme (UNEP, 2014). Note the spatial patterns of increased asphalt and vegetation.

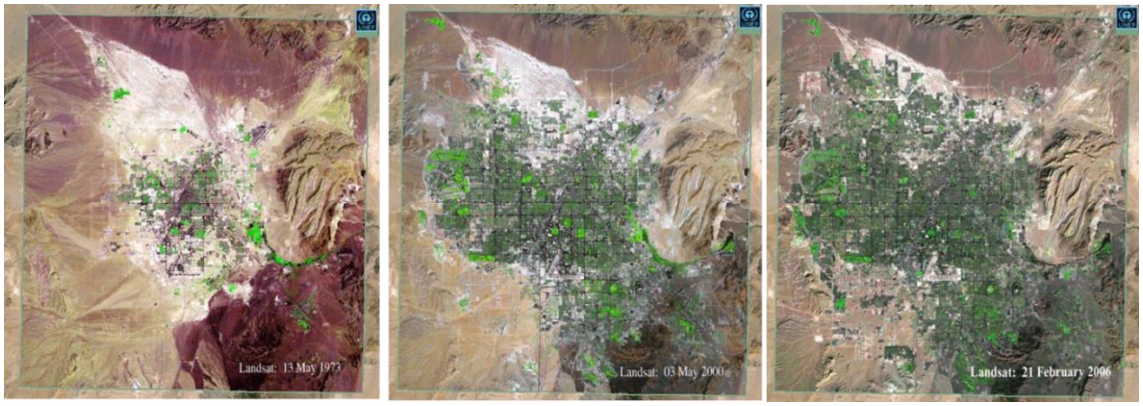

Fig. 4. Satellite composites of the expansion (urban footprint) of the City of Las Vegas. From left to right: 13 May 1973, 03 May 2000, and 21 February 2006. Vegetation is highlighted in green. This figure was adapted from UNEP (2014).

McCarran and Nellis airports have the best historical records available for Las Vegas (Appendix A). These two NWS sites are the only urban stations in Las Vegas that exceed a 30-year climatology record. Trends from December 1949-November 2011 for T_{max}, T_{mean}, and T_{min} were selected for long-term analyses. Additionally, 5- and 10-year moving averages were estimated to smooth out interdecadal-to-decadal variability. Seasonal analysis was performed by aggregating the months as follow: winter (DJF), spring (MAM), summer (JJA), and fall (SON). Monthly T2m anomalies were calculated as follow:

$$T_a = \mu_{ij} - \overline{X}_i \qquad \text{(Equation 1)},$$

where T_a is the temperature anomaly, μ is the temperature average, and $\overline{X}$ is the climatological average of temperature. The indices of i and j represent the year and month, respectively.

Changes in the diurnal cycle of temperature and humidity were also estimated using hourly records from McCarran and Nellis. Diurnal patterns have been used to characterize local changes in climate (Scheitlin and Dixon, 2010; Svoma and Brazel, 2010; Middel et al., 2012). Computing the diurnal cycle required averaging temperature data for each hour in a specified timeframe through a 24-hour period. To see how diurnal patterns were behaving through time, the cycles were separated into 10-year periods from 1950-2009. Hence, there were five decades of data analyzed for the stations of McCarran and Nellis to establish the occurring changes in nighttime and daytime patterns of temperature. Diurnal analyses were computed by season.

To remove regional climate trends from the local city-related trends, statewide averages for T_{max} and T_{min} were selected for Nevada (NV) and Arizona (AZ). Statewide data was obtained using Westmap (http://www.cefa.dri.edu/Westmap/) provided by the WRCC, where averages were computed from the PRISM 4 km data. T_{max} and T_{min} statewide trends were estimated by subtracting the decades of 2000-2009 minus 1950-1959 to represent the regional changes. For robustness and consistency, averages during intermediate decades were also evaluated. The average decadal differences between city-estimated trends and regional statewide trends were calculated to retrieve residuals. Thus, positive and negative city residuals were a representation of the UHI and UCI magnitude, respectively.

A similar approach was implemented while analyzing GDPs. However, instead of using statewide averages to compute a city residual, the rural boundary average (Fig. 3)

was subtracted from the average output between the city core and outer-core boundaries to retrieve a residual value. GDP residuals were estimated through the 1980-2011 period.

Moisture parameters of RH, T_d, dewpoint depression (K_o), vapor pressure (e_a), and vapor pressure deficit (VPD) were examined for long-term trends (December 1949-November 2011) from the McCarran and Nellis stations. These parameters were used to measure the near surface humidity and characterize the long-term interannual variability of wet and dry periods. More importantly, moisture variables drive UCI so it is of value to assess the behavior of these parameters.

RH is defined as a ratio of e_a over the saturation vapor pressure (e_s), and is a representation of the amount of moisture in the air versus the amount of moisture the air can have before saturation. Hence, if e_a and e_s were the same value, the RH would be 100% and the air would be completely saturated. K_o simply measures moisture by taking the difference between temperature and T_d (i.e. T2m - T_d). In other words, smaller K_o values signify greater moisture which in turn compliments larger RH. The e_a is a function of T_d and was calculated using the equation from Bolton (1980):

$$e_a = 6.11 \cdot 10^{7.5T_d / (T_d + 237.3)} \qquad \text{(Equation 2).}$$

VPD is the deficit between e_a and e_s (i.e. $e_s - e_a$) which is larger when RH and K_o are low. The VPD further implies how dry or moist the air is by larger or smaller differences in vapor pressure, respectively.

An advance drought index created by McEvoy et al. (2014) was used to examine the role of regional droughts relative to observed changes in Las Vegas surface

temperature and humidity parameters. The Evaporative Demand Drought Index (EDDI) follows the concepts of popular drought indices (e.g. Standardized Precipitation Index) while accounting for important parameters that affect evaporation and ET. For further validation of the EDDI, the interannual shifts of the Pacific Decadal Oscillation (PDO) and Lake Mead levels were also used to detect the severity of drought. The PDO detects warm and cold sea surface temperatures in the Pacific Ocean that impact the global climate. Warm (Positive) phases of the PDO are associated with above average precipitation, while cold (negative) phases permit below average precipitation in the Southwestern US. PDO data was collected from the Joint Institute for the Study of Atmospheric and Ocean website: *jisao.washington.edu*.

2.4 Land Use Land Cover (LULC)

Surface stations were classified by the surrounding land use using the 2006 National Land Cover Database (NLCD 2006) at 1 km grid size (Fig. 5). For each grid the dominant LULC category (i.e. the LULC category covering the largest percentage in a pixel) was selected as the characterizing LULC (Wickham et al., 2013). Appendix C shows the LULC categories for all analyzed sites. These categories were further evaluated and verified by using recent Landsat Imagery (Fig. 2), and by a direct survey made during the DRI-UHI field campaign.

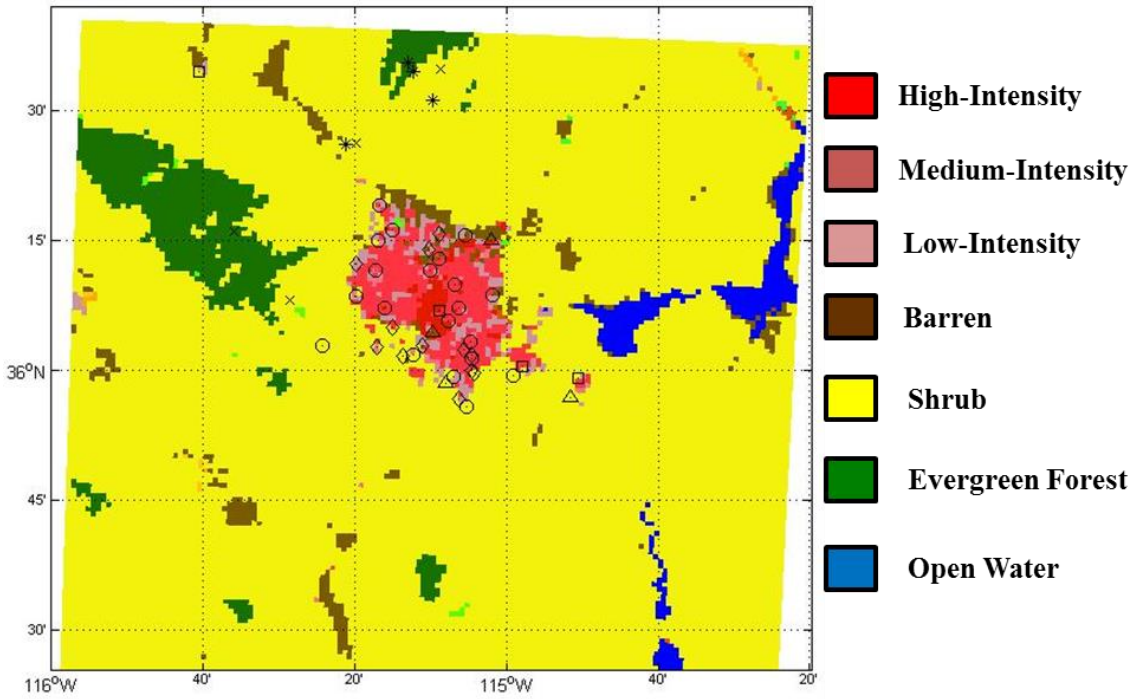

Fig. 5. LULC map of the Las Vegas region provided by the 2006 NLCD. Networks are classified by shapes: DRI-UHI (circle), NWS (triangle), CEMP (square), NevCAN (star), RAWS (x), and WU (diamond). The LULC are classified by the color grids with the major categories labeled in the legend.

High-, medium-, and low-intensity pixels are representations of the urban development containing impervious surfaces. The high-intensity areas are located in downtown Las Vegas along the strip and around McCarran Airport. Total impervious coverage for high-intensity areas approximate between 80-100% (Wickham et al., 2013). Medium- and low-intensity areas are primarily attributed to residential areas that contain some vegetation with 50-79% and 20-49% impervious coverage, respectively (Wickham et al., 2013). Barren areas are composed of bare desert surfaces that contain < 15% vegetation. There are barren sites that are associated with in-city stations primarily along the northern perimeter of Las Vegas. The shrub pixels make up most of the rural domain around Las Vegas and appear to have a slightly darker tint than the barren soil under

Landsat visible imagery (Fig. 3). Shrub areas contain moderately more vegetation than barren pixels according to the NLCD 2006 descriptions provided by Wickham et al. (2013). Evergreen forest pixels are located at higher elevations in the Spring Mountains and Sheep Range (Las Vegas study area described further in Chapter 2.5). These areas are governed by trees exceeding 5 m with canopy coverage greater than 20% (Wickham et al., 2013). Finally, the open water pixels highlight Lake Mead and are categorized to contain less than 25% coverage of vegetation or soil.

2.5 Surface Station Elevation Differences and Correction Factors

This section describes the efforts for temperature corrections due to elevation differences across the Las Vegas Valley. As displayed in Figure 2b, the elevation within the city varies ~400 m in the west-east direction. Las Vegas is part of the Mojave Desert and is surrounded by various mountain ranges. To the west are the Spring Mountains, which has a north-south transect that creates the southern boundary of the Great Basin. As mentioned before, the Sheep Range covers the range north of Las Vegas. The valley is also surrounded by the Frenchman Mountain located to the east, and the McCullough Range located to the south.

To adjust T2m from the complexity of the desert terrain for the purpose of estimating the UHI, the mean environmental lapse rate ($\Gamma_e = {}^{6°C}/_{1000\ m}$) was used to correct T2m to a reference level. The lowest elevated station amongst all networks was Las Vegas High School (534 m) from the DRI-UHI network. Las Vegas High School was used as a base station to adjust the higher elevated areas down to its elevation level. The

equation implemented for this method is termed the "correction factor" (CF). The equation for CF is as follows:

$$CF = (z_i - z) \cdot \Gamma_e \quad \text{(Equation 3)},$$

where z_i is the elevation of the observed station, z is the elevation of Las Vegas High School, and Γ_e is the environmental lapse rate. After the CF was calculated, it was added to the original temperature for each station, thus referencing the T2m at the altitude of Las Vegas High School. Once the new T2m values were established for each station, the UHI magnitude was calculated by averaging the station temperatures located in urban intensity sites in accordance to the updated LULC (Appendix C), thereafter subtracting them by the average temperature of the rural stations (i.e. stations with shrub LULC). Stations located in the evergreen forest were ignored in this process, as these sites do not represent the footprint of the shrub land that existed prior to urban development. The period analyzed for the CF method was from August 2012 to April 2013. This particular period was selected in order to implement the full temporal dataset collected from DRI-UHI. Further validity of this method was tested by observing the differences of UHI for colder months (January to February 2013) versus warmer months (March to April 2013). RH and other moisture variables were not measured in the CF analysis as they are more complex in their variation in space and altitude.

A second strategy was performed by estimating the standard z-scores as follow:

$$z = \frac{x - \mu}{\sigma} \quad \text{(Equation 4)},$$

where *x* is the monthly data, and μ and σ are the mean and standard deviation, respectively, for each month of the year. Monthly calculations for Equation 4 were done to reduce errors from the NWS station dataset by computing the standard deviations from the mean. Data was analyzed from January 1980-December 2011 for the in-city stations of McCarran and Nellis, and the rural site of Desert Rock. Linear regression was used to estimate T2m trend values in the z-score. In-city trends from McCarran and Nellis were subtracted by rural trends from Desert Rock to estimate the overall UHI/UCI at T_{max} and T_{min}. Furthermore, RH values were calculated from Equation 4 before using the ΔRH method from Alghannam and Al-Qahtnai (2012). As described in Chapter 1, this method was used as a reference to the behavior of RH under the circumstances of UHI and LULC influences. ΔRH is simply the urban RH minus the rural RH. RH_{max} and RH_{min} were used to test any correlated behavior of T_{min} and T_{max}, respectively. Further examination was done for e_a by subtracting the urban e_a from the rural e_a. This was referenced as Δe_a, and it is executed to remove the T2m impact and focus strictly on the moisture content. Of note is that Equation 4 was calculated for e_a prior to solving Δe_a, and further used for the GDP T2m analysis.

2.6 Urban Canopy Modeling

The WRF model is a numerical mesoscale model used for both operational forecasting and atmospheric research (Skamarock et al., 2005; NCAR, 2013). The UCM is a sub-model within WRF which parameterizes the energy of the urban canyon and water balances that are coupled to the WRF model. In other words, it accounts for radiation and hydrological principles of an urban setting (Kusaka and Kimura, 2004),

including: the shadowing and albedo from urban infrastructure; road orientation and diurnal changes from the solar azimuth angle; the exponential wind profile in the canopy layer; a multi-layer heat equation for the impermeable surfaces of roads, roofs, and walls; anthropogenic heat from urban energy consumption; and hydrological processes for soil properties and urban vegetation (Kusaka et al., 2001; Kusaka and Kimura, 2004; Holt and Pullen, 2007; Miao et al., 2009; Wang et al., 2013).

Five, one month-long hindcast (i.e. test) simulations for November 2012 were performed. This period was selected because no rain was recorded, allowing to isolate rather unreliable processes associated with precipitation (e.g. spatial/temporal variability and intensity) within WRF that carry on to affect other parameters (Coniglio et al., 2010; Zhang et al., 2013). The five simulations performed were: (i) using a Land Surface Model (LSM) called Noah Land Surface Model *without* UCM treatment, (ii) same as (i) with a single-layer UCM (UCM1), (iii) same as (i) with a multi-layer UCM (UCM2), (iv) removing the urban categories within the simulation and replacing them with the predominant shrub LULC (NC; Fig. 6), and (v) is the same as (ii) but considering the scenario of increasing the urban albedo. In terms of increasing the albedo for a simulated scenario, the surface albedo of rooftops were changed from 0.20 to 0.65 (Jacobson and Ten Hoeve, 2012). Additionally, we assume that the difference of T2m and e_a simulations from (i, ii, iii) minus (iv) represents the simulated effect of the urban environment.

A four-nested domain was adopted to downscale the initial and lateral large-scale atmospheric input from the NCEP Final Analyses (FNL; *rda.ucar.edu*) at 1-degree arc grid size (~100 km) to 27 km, 9 km, 3 km, and 1 km grid sizes (Fig. 7). However, only

the 1 km grid was evaluated as it reasonably considers the basic intra-city features (Fig. 5). Vertical grids contained 51 sigma levels from the surface to 50 hPa as the upper limit. The vertical resolution was greatest near the surface to better compliment active processes driven by topography and the PBL.

Other physics parameters implemented were: the Rapid Radiative Transfer Model (RRTM) scheme for longwave radiation; the Duhdia scheme for shortwave radiation; the Monin-Obukhov similarity theory modified by the Janjić scheme for the surface layer; the Mellor-Yamada-Janjić (MYJ) PBL scheme for the PBL physics; the Kain-Fritsch (KF) for convective parameterization only on the coarser domain (convection in the inner domains are treated explicitly); and Single-Moment 6-class (WSM6) scheme for the microphysics process. These schemes are standard for WRF which are commonly used in arid/semi-arid regions for research purposes (Castro et al., 2012; Tripathi and Dominguez, 2013).

Since WRF uses the U.S. Geological Survey (USGS 1993) as the default land use map, some modifications were necessary to upgrade the model to the NLCD 2006; which were also necessary for UCM parameterization schemes implemented by WRF. Table 2 lists all the configurations from the model.

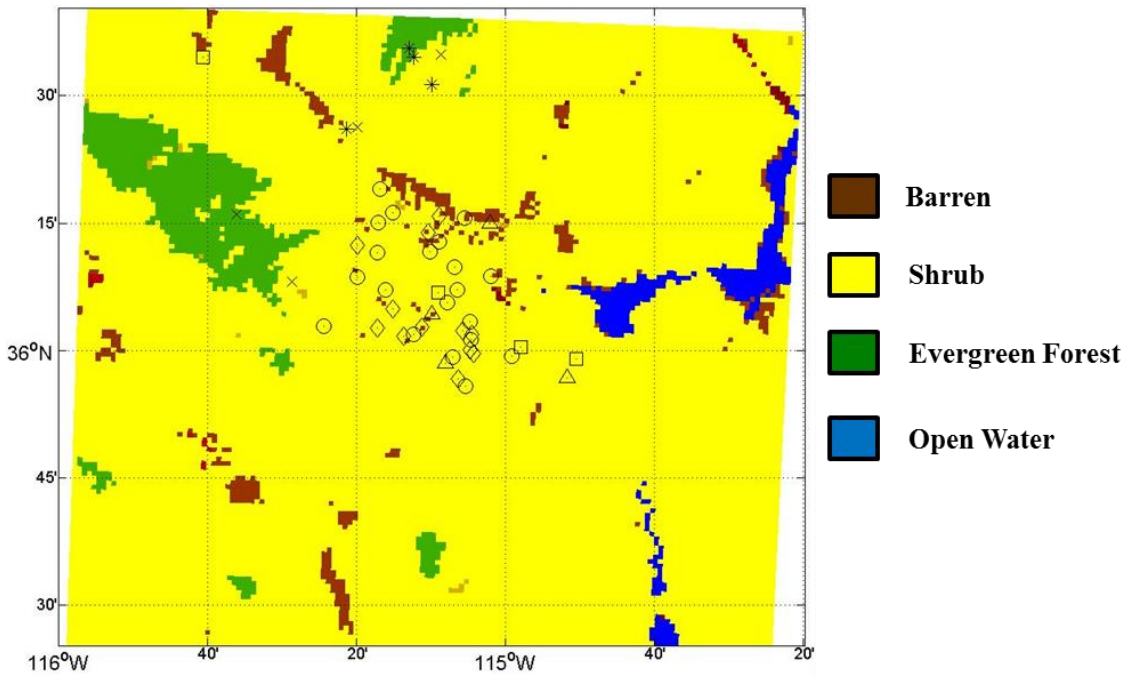

Fig. 6. Same as Figure 5 but removed the City of Las Vegas urban categories and replaced them with shrub.

The purpose of the LSM, UCM1, and UCM2 simulations are to assess the model output from the default urban settings and compare them with the surface observations. As mentioned in Chapter 1, the UCM has rarely been tested under non-coastal arid cities. Using default urban parameters will display the sensitivity of the models under idealized climate in the arid southwest. The sensitivity of the models were tested by implementing a time series for the entire month to characterize synoptic and diurnal variability against observations. Spatial sensitivity was also examined by subtracting domain 4 outputs between the LSM, UCM1, and UCM2.

Statistical methods used to help show confidence of the simulations against observations consisted of calculating the bias, root-mean-square error (RMSE), and the

correlation coefficient for T2m, RH, and e_a. The bias is simply the model output minus the observations. In connection with the bias, the RMSE is calculated as so:

$$\text{RMSE} = \sqrt{\frac{1}{n}\sum_{i=1}^{n}(\hat{y}_i - y_i)^2} \qquad \text{(Equation 5)},$$

where n is the sample size, i is the data index, $\hat{y}$ is the model output, and y is the observational data. The correlation coefficient is based off of Pearson's and is computed as:

$$\rho = \frac{n\sum \hat{y}_i y_i \sum \hat{y}_i \sum y_i}{\sqrt{n\sum \hat{y}_i^2 - (\sum \hat{y}_i)^2}\sqrt{n\sum y_i^2 - (\sum y_i)^2}} \qquad \text{(Equation 6)}.$$

The correlation coefficient measures the linear relationship between the model and observations with values between -1 and 1. In other words, values of 1 and -1 represents a perfect positive and negative linear relationship, respectively. When $\rho = 0$, then the relationship is uncorrelated.

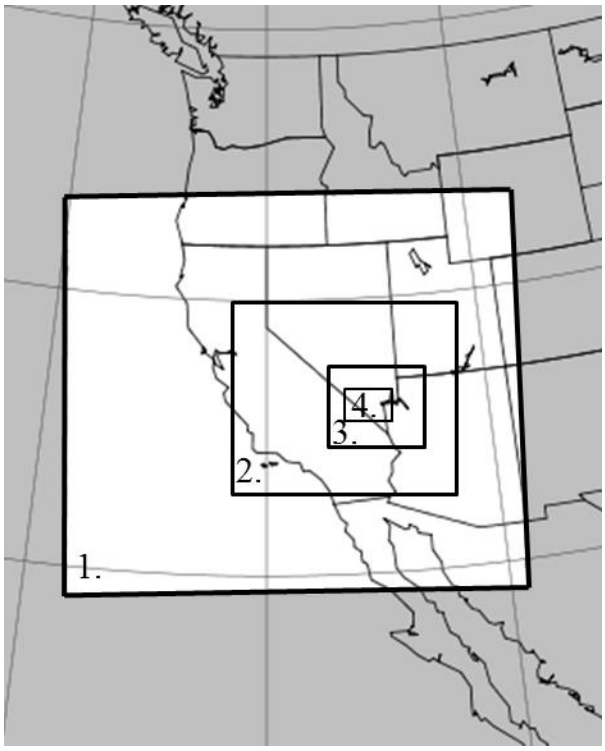

Fig. 7. The setup of the WRF model contains four-nested domains with grid sizes of (1.) 27 km, (2.) 9 km, (3.) 3 km, and (4.) 1 km.

Table 2. Model configuration.

Model	WRF Version 3.5.1
Simulation Period	1 November 00 LST to 29 November 23 LST
Horizontal Resolution	27 km, 9 km, 3 km, 1 km
Vertical Resolution	51 sigma levels to 50 hPa
Land Surface Scheme	Noah-LSM
Urban Scheme	Single-layer UCM and Multi-Layer UCM
Shortwave Radiation	Dudhia
Longwave Radiation	RRTM
Planetary Boundary Layer	YSU
Cumulus Physics	KF (Domain 1 only)
Cloud Microphysics	WSM6
Surface Physics	Monin-Obukov (Janjic Eta)
LULC Map	NLCD 2006 (40 Categories)

3. Results

3.1 Observed Temperature Trends

Figures 8 and 9 shows monthly surface temperature anomalies with 5- and 10-year moving averages highlighting the long-term trends through the period December 1949-November 2011 for McCarran and Nellis, respectively. Of note is that observed temperature changes include not only the local trends associated with LULC change, but also the regional and global trends. Though substantial interdecadal-to-decadal variability is observed, a warming trend is evident in T_{mean} and $T_{min,}$ with larger trends exhibited by McCarran T_{min} of ~0.68°C/decade. McCarran T_{max} trends of ~0.18°C/decade are less significant but still show a warming pattern. Nellis shows similar results but with slightly smaller warming trends with T_{min} increasing ~0.52°C/decade and T_{max} increasing ~0.05°C/decade.

Fig. 10 and 11 show statewide/regional temperature anomalies for Arizona (AZ) and Nevada (NV), respectively. Overall, regional temperature trends follow similar long-term trend patterns indicated at McCarran and Nellis. T_{max} in NV shows a slight warming of ~0.05°C/decade while AZ shows ~0.12°C/decade. T_{min} contributed to greater regional warming of ~0.28°C/decade and ~0.30°C/decade for NV and AZ, respectively.

During the last decade in this analysis, the local stations and statewide temperatures show a cooling trend. Such cooling trends have been related to global teleconnection patterns associated with the PDO (Mantua and Hare, 2002; Benson et al., 2003; McCabe et al., 2004; Schneider and Cornuelle, 2005) and their regional impact

over the West. Nevertheless, a striking result is that McCarran and Nellis exhibit larger warming relative to the regional trends that we argue are attributed to the UHI effect.

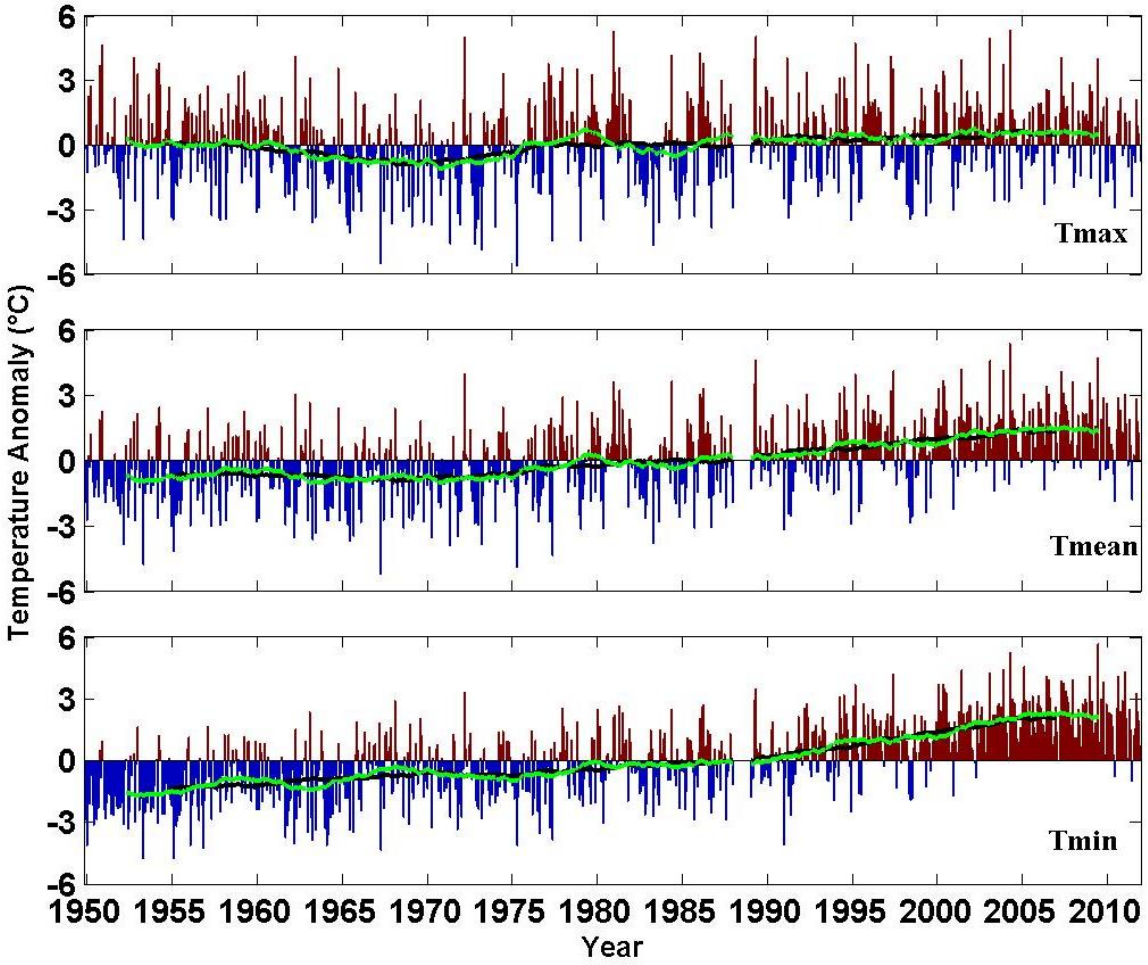

Fig. 8. McCarran monthly maximum (top panel), mean (mid panel) and minimum (lower panel) temperature anomalies. Red bars signify positive anomalous months, while blue bars present negative anomalous months from December 1949 to November 2011. A 5- (green) and 10-year (black) moving average is overplotted to highlight trends of the interannual variability. The 1988 data has been removed due to excessive data missing.

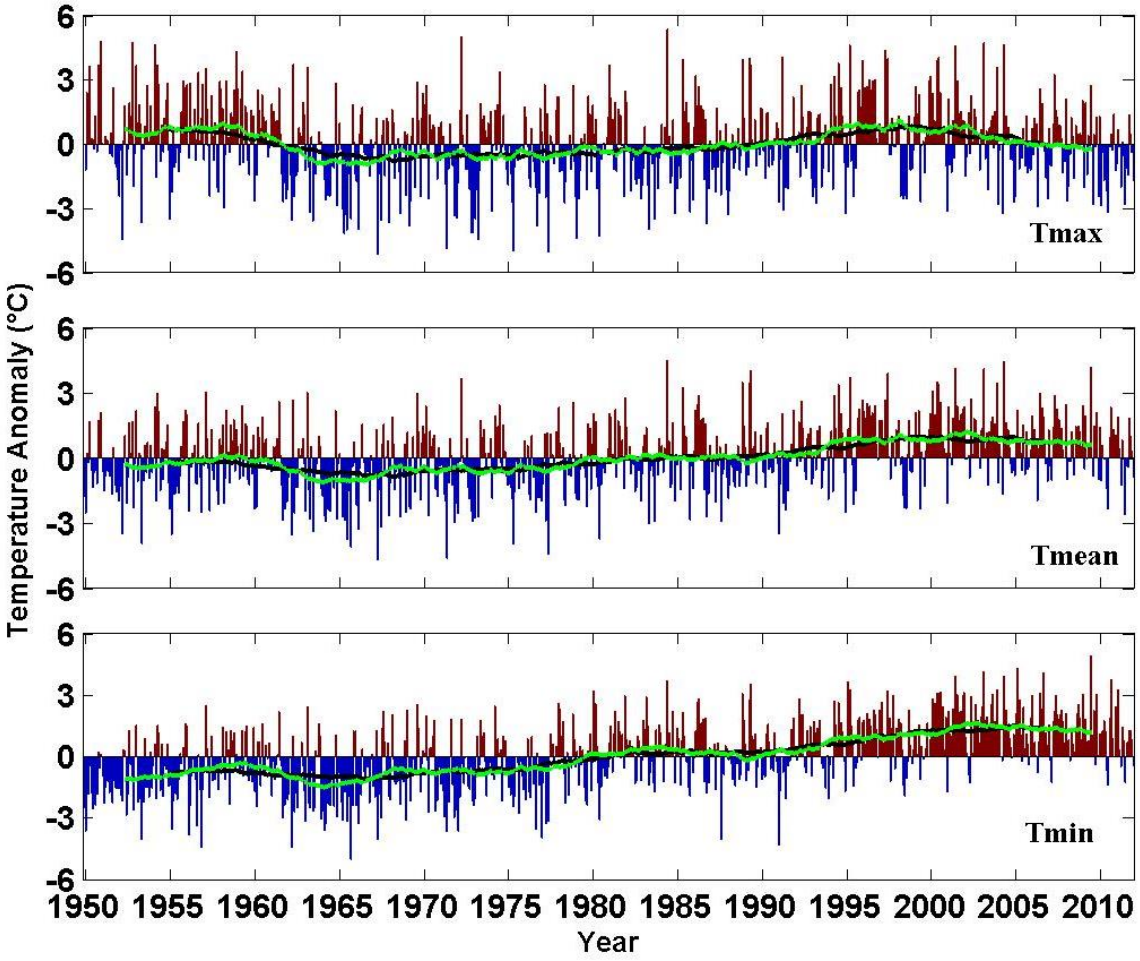

Fig. 9. Nellis monthly maximum (top panel), mean (middle panel), and minimum (lower panel) temperature anomalies. Red bars signify positive anomalous months, while blue bars present negative anomalous months from December 1949 to November 2011. A 5- (green) and 10-year (black) moving average is overplotted to highlight trends of the interannual variability. The station was moved on 1 Jan 2000, before moving back on 1 Jan 2005 to its original location.

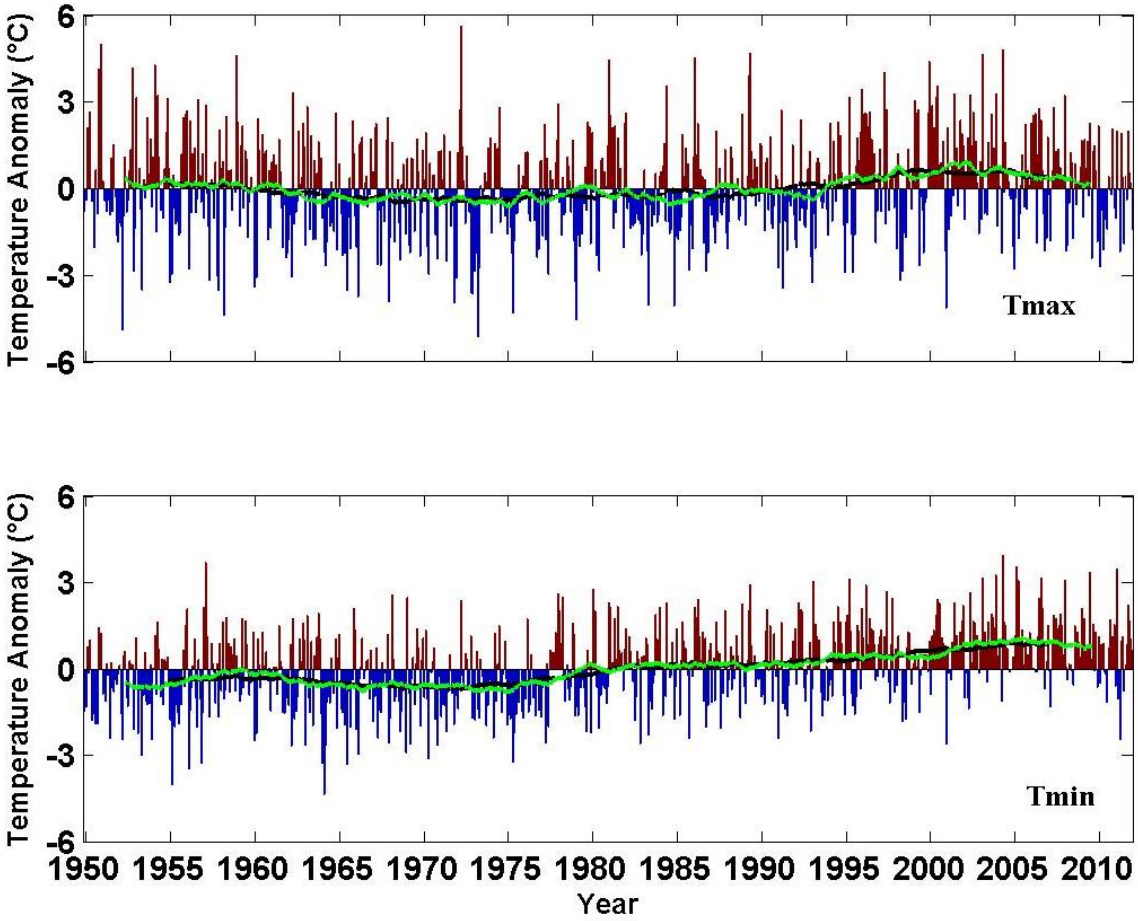

Fig. 10. Arizona monthly maximum (top panel) and minimum (bottom panel) temperature anomalies. Red bars signify positive anomalous months, while blue bars present negative anomalous months from December 1949 to November 2011. A 5- (green) and 10-year (black) moving average is overplotted to highlight trends of the interannual variability. *Source: Westmap.*

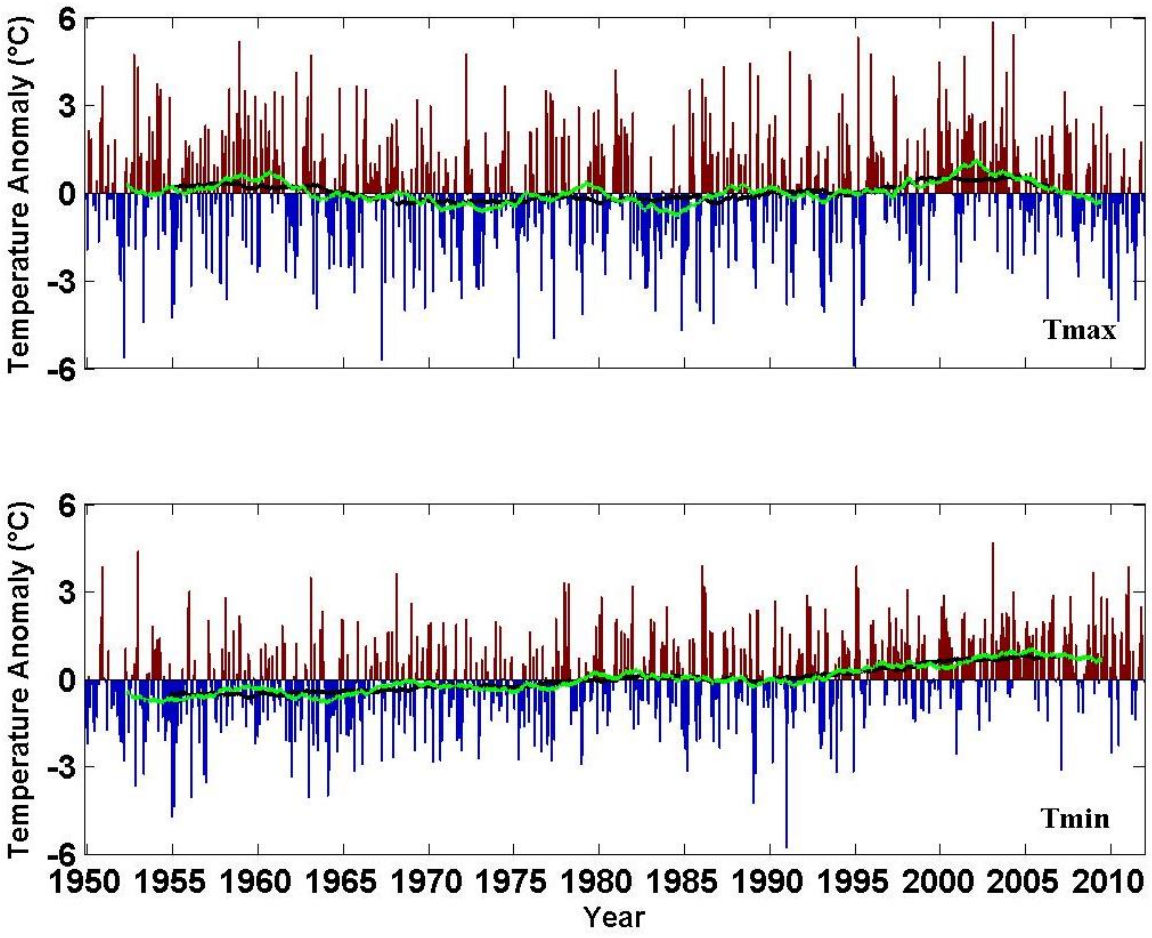

Fig. 11. Nevada monthly maximum (top panel) and minimum (bottom panel) temperature anomalies. Red bars signify positive anomalous months, while blue bars present negative anomalous months from December 1949 to November 2011. A 5- (green) and 10-year (black) moving average is overplotted to highlight trends of the interannual variability. *Source: Westmap*.

Seasonally, temperature anomalies of T_{max} and T_{min} exhibit similar interannual variability with consistent warming trends for T_{min} containing some variability, and smaller less consistent trends in T_{max} (Figs. 12-15). For example, T_{max} at McCarran (Fig. 12) shows a slight warming during all seasons, while Nellis (Fig. 14) shows a cooling trend for SON and DJF. Overall, seasonal results further show that in-city T_{min} is warming, regardless of the season.

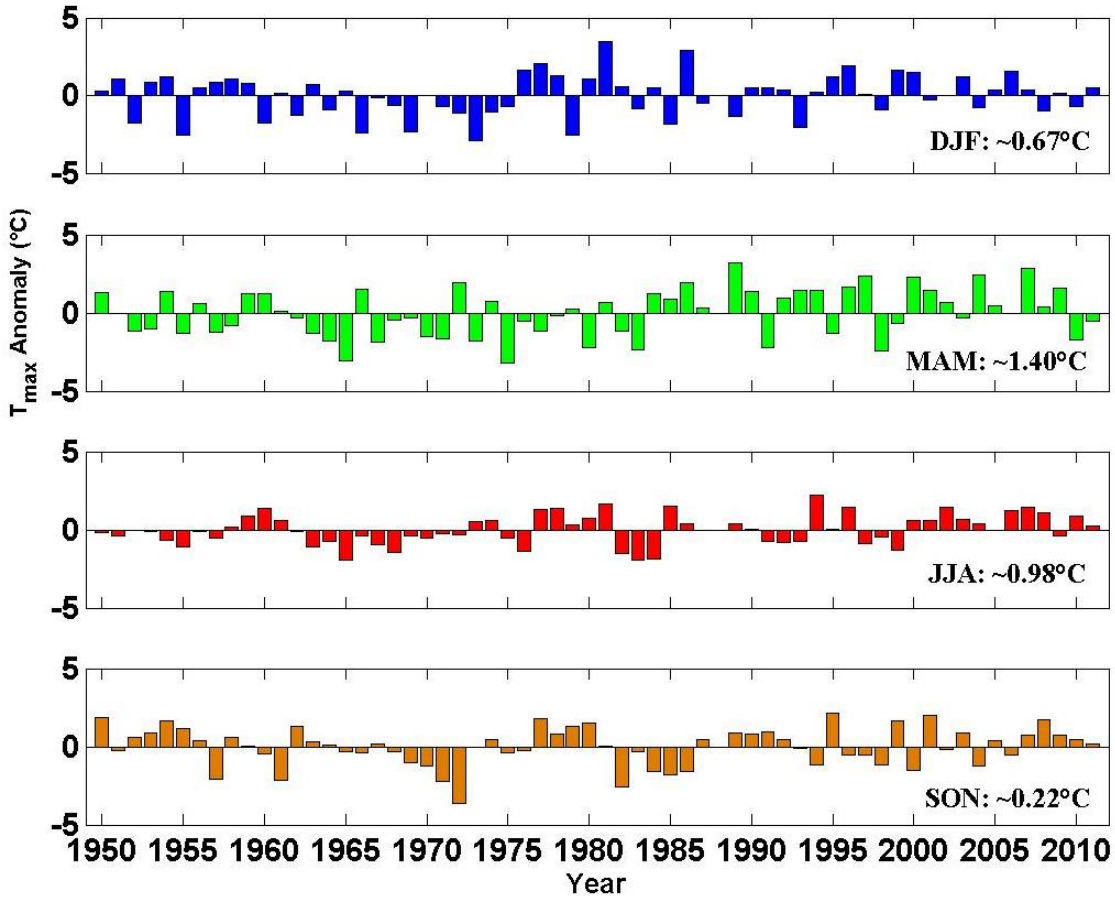

Fig. 12. Seasonal T_{max} anomalies at McCarran from 1950-2011. The bars represent seasonal anomalies of DJF (blue), MAM (green), JJA (red), and SON (orange). Overall seasonal values were computed using the slope of the best fit line. The 1988 data has been removed due to excessive missing data.

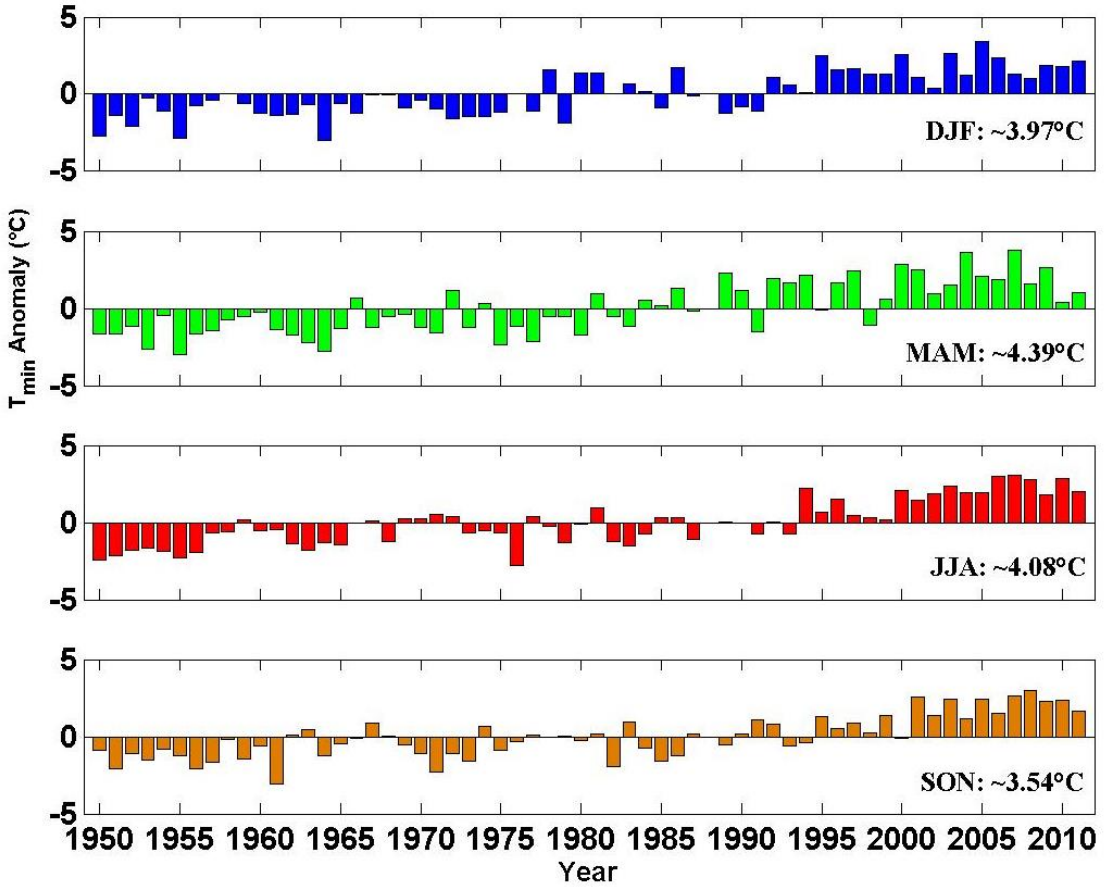

Fig. 13. Seasonal T_{min} anomalies at McCarran from 1950-2011. The bars represent seasonal anomalies of DJF (blue), MAM (green), JJA (red), and SON (orange). Overall seasonal values were computed using the slope of the best fit line. The 1988 data has been removed due to excessive missing data.

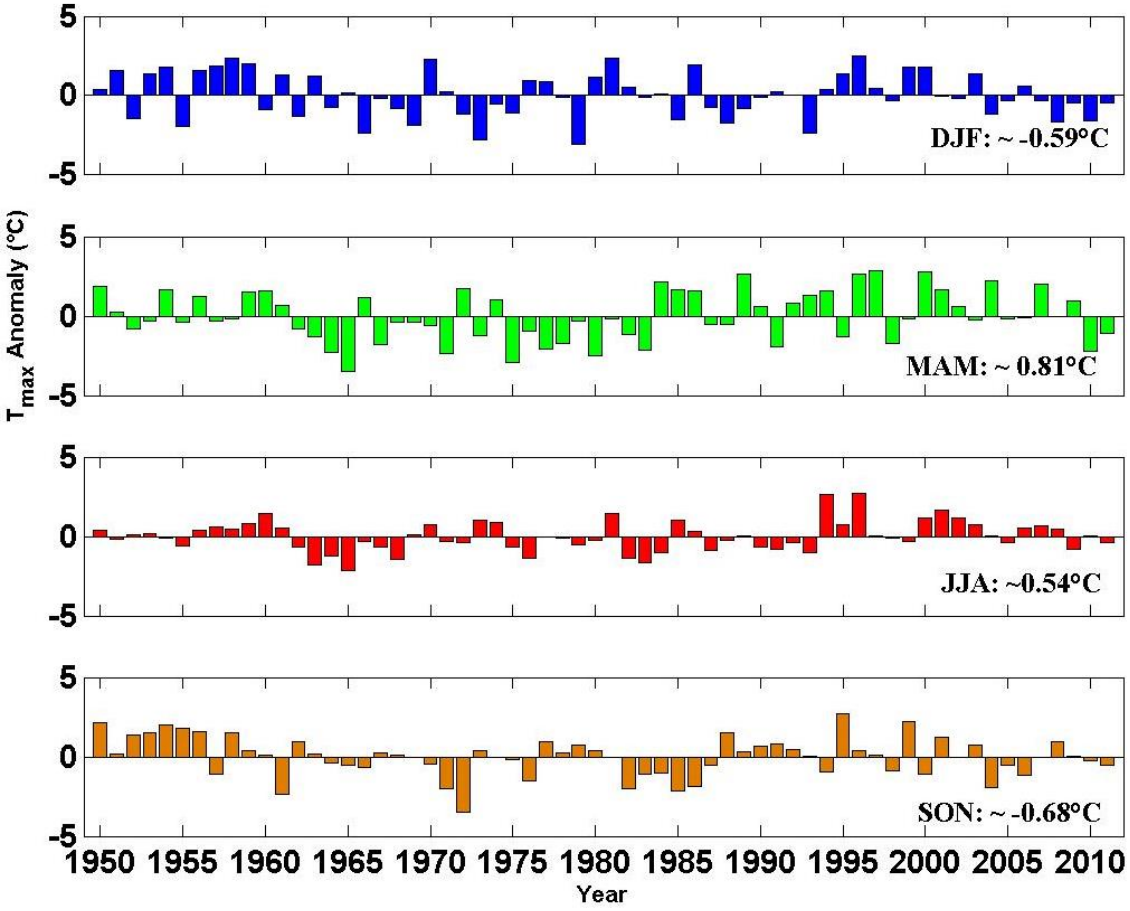

Fig. 14. Seasonal T_{max} anomalies at Nellis from 1950-2011. The bars represent seasonal anomalies of DJF (blue), MAM (green), JJA (red), and SON (orange). Overall seasonal values were computed using the slope of the best fit line. The station was moved on 1 Jan 2000, before moving back on 1 Jan 2005 to its original location.

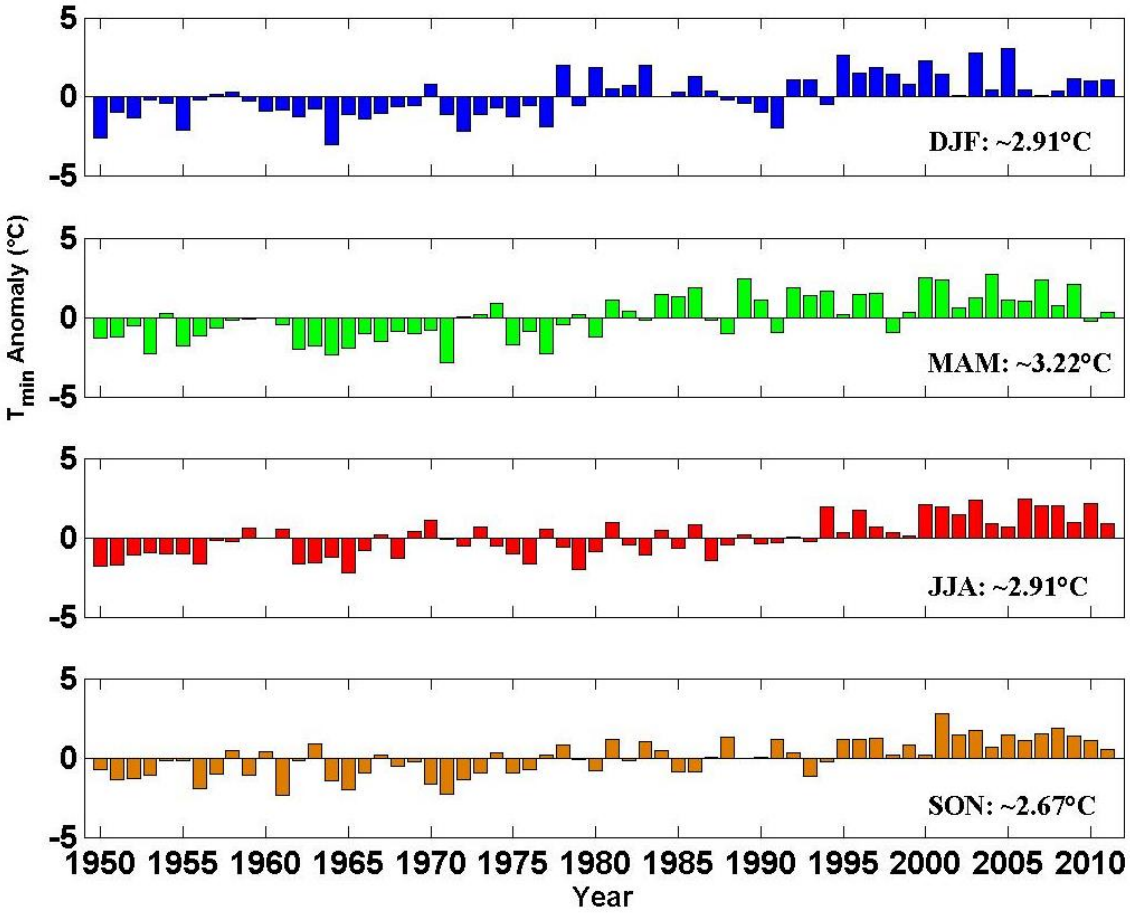

Fig. 15. Seasonal T_{min} anomalies at Nellis from 1950-2011. The bars represent seasonal anomalies of DJF (blue), MAM (green), JJA (red), and SON (orange). Overall seasonal values were computed using the slope of the best fit line. The station was moved on 1 Jan 2000, before moving back on 1 Jan 2005 to its original location.

3.2 Observed Changes in the Diurnal Cycle

Figure 16a shows a seasonal diurnal cycle for the decades of 1950-1959 and 2000-2009 at McCarran. The behavior of hourly T2m shows a diurnal evolution of increased nighttime/morning T2m with smaller daytime changes for all seasons, which supports findings from other UHI studies (Svoma and Brazel, 2010). During the daytime, warming is observed during MAM and JJA, while negligible cooling is observed at T_{max} time during DJF (~-0.13°C) and SON (~-0.26°C).

Nellis exhibits similar diurnal behavior to McCarran (Fig. 16b). However, Nellis shows a stronger cooling signal during daytime for DJF (~-1.48°C) and SON (~-1.33°C). Furthermore, observations show that T_{max} and T_{min} trends shifted ~1 hour earlier since the mid-20^{th} century. The T_{min} shift is evident at Nellis for JJA and SON; moving from 0500 to 0400 LST and 0600 to 0500 LST, respectively. Note the shifting for T_{max} at McCarran between 1400 and 1500 LST in DJF show similar T2m, and are to a lesser degree than the T_{min} shifts.

The diurnal cycle at McCarran and Nellis shows evidence of the diurnal temperature ranges (T_{amp}) decreasing with time. Results show a strong change in the diurnal regime that we argue is attributable to Las Vegas urban and population growth and their UHI effects (Emmanuel and Fernando, 2007).

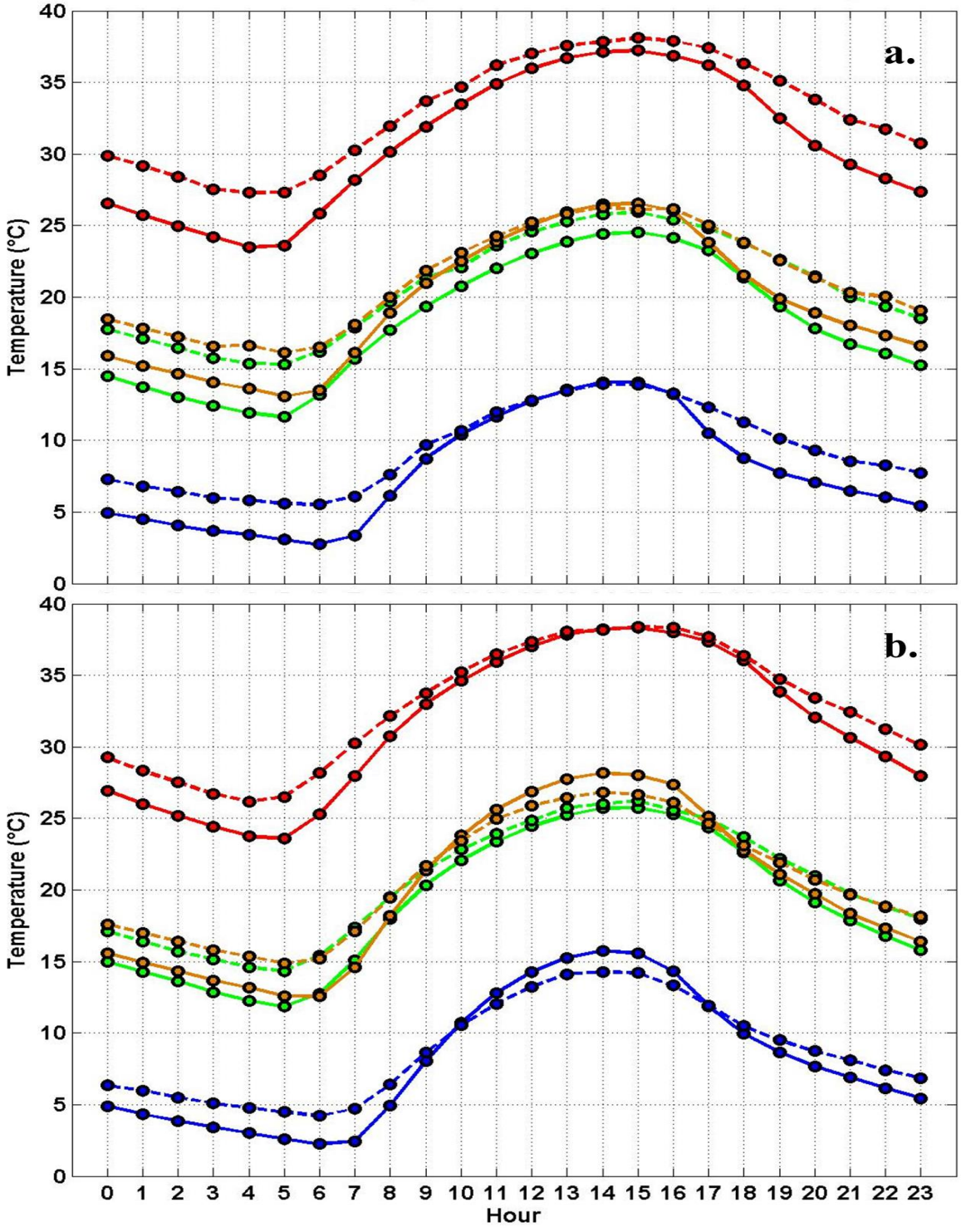

Fig. 16. Seasonal diurnal cycle in LST of T2m for (a) McCarran and (b) Nellis. Hourly temperature averages were determined for mid-20th century (1950-1959; solid lines) and early 21st century (2000-2009; dash lines) for DJF (blue), MAM (green), JJA (red), and SON (orange).

3.3 Local and Statewide/Regional Trend Differences

Figure 17 shows seasonal statewide decadal averages of recent (2000-2009) minus past (1950-1959) 10-year periods. A sensitivity test was performed by computing the differences with other past decades (e.g. 1960s, 1970s, 1980s, and 1990s) to evaluate the influence of decadal-to-interdecadal variability in this analysis, which indicated that differences monotonically increase as decadal averages were closer in time (figure not shown). NV and AZ show T2m differences that further highlight JJA and MAM exhibiting greater regional warming, while statewide T_{max} cooling for DJF and SON concurs with McCarran and Nellis daytime trends.

Figure 18 shows the in-city or "local" station differences between the 2000s and 1950s for McCarran and Nellis. Of note is that the local trends have larger seasonal T2m decadal differences when compared to the statewide trends. Thus further showing that T_{min} has increased most rapidly in the urban than in the regional environments (Hansen et al., 2001). Furthermore, T_{max} regional cooling trends have been locally identified, further expressing the response of the observed cooling shown by the diurnal cycle (Fig. 16).

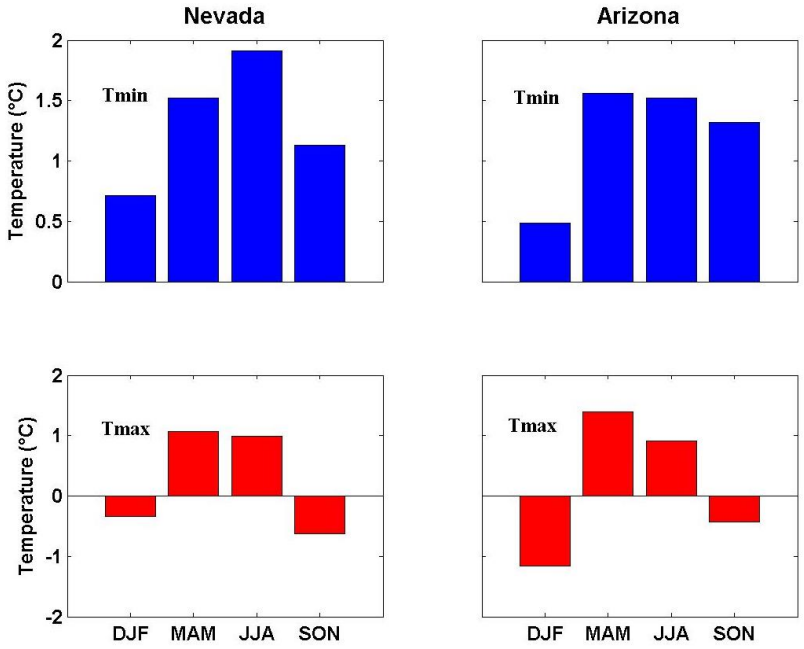

Fig. 17. Seasonal statewide T_{min} (top panels) and T_{max} (bottom panels) differences (2000-2009 average minus 1950-1959 average) for Nevada (left hand side panels) and Arizona (right hand side panels).

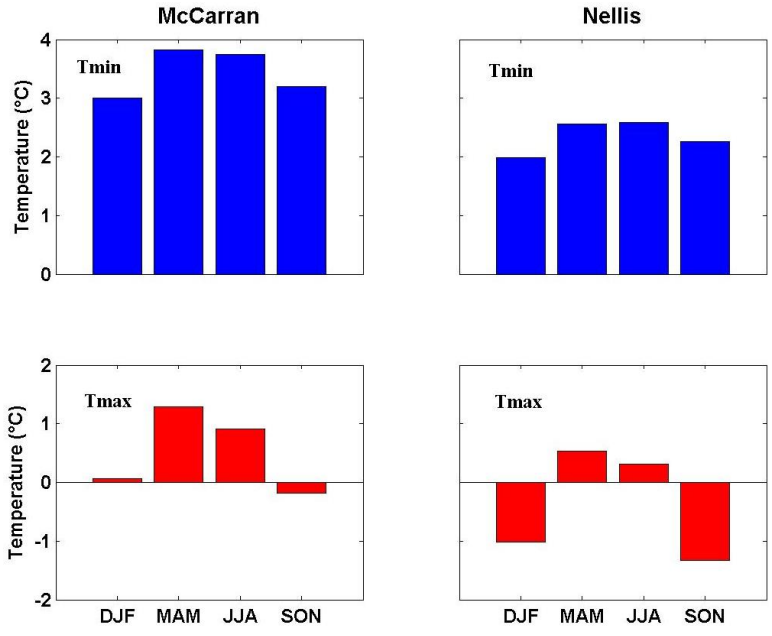

Fig. 18. In-city T_{min} (top panels) and T_{max} (bottom panels) differences (2000-2009 average minus 1950-1959 average) for McCarran (left hand side panels) and Nellis (right hand side panels).

Table 3 shows seasonal residuals (i.e. in-city minus statewide differences) for T_{max} and T_{min}. Statewide and in-city values are given by the average decadal differences shown in Figures 17 and 18, respectively. Overall, residuals in Table 3 are an estimation of the observed UHI (positive residuals) and UCI (negative residuals). Although MAM and JJA exhibited the strongest T2m warming, UHI intensity was greatest for DJF. Furthermore, DJF also showed a weak T_{max} UHI. T_{max} UHI is most evident at McCarran aside from a trivial UCI during JJA (~-0.03°C). Nellis exhibits UCI for T_{max} and a weaker T_{min} UHI effect than McCarran by 1.10°C. Stronger UCI intensities are evident for the seasons that had the largest warming trends (i.e. JJA and MAM).

It is recognized that local cooling can be established through the latent heat flux of ET from turf grass (Linden, 2011; Taha, 1997), and the introduction of an artificial open water surface in the city (Theeuwes et al. 2013). However, since Nellis is primarily barren soil it could simply be an artifact of using statewide trends rather than the influence from ET. Additionally, residuals slightly differed based on the statewide impacts. AZ had more of an overall warming trend than NV. Without AZ, the UHI was ~0.10°C cooler and the UCI was ~0.09°C warmer. However, for robustness we averaged all residuals to estimate the overall metric of the UHI and UCI influence for Las Vegas.

Table 3. T_{min} and T_{max} trends for in-city (McCarran and Nellis) and statewide (Arizona and Nevada) data in °C. The residuals define the local effect from removing regional trends. When residuals are positive (negative), we argue that the temperature trends are attributed to the UHI (UCI).

T_{min}	State wide trends			In city trends			Residuals				
	NV	AZ	Average	McCarran	Nellis	Average	McCarran - NV	McCarran - AZ	Nellis -NV	Nellis-AZ	Average
DJF	0.71	0.48	0.60	3.01	1.99	2.50	**2.30**	**2.53**	**1.28**	**1.51**	**1.91**
MAM	1.52	1.56	1.54	3.82	2.56	3.19	**2.30**	**2.26**	**1.04**	**1.00**	**1.65**
JJA	1.92	1.52	1.72	3.75	2.60	3.18	**1.83**	**2.23**	**0.68**	**1.08**	**1.46**
SON	1.13	1.32	1.23	3.20	2.25	2.73	**2.07**	**1.88**	**1.12**	**0.93**	**1.50**
Annual	1.32	1.22	1.27	3.45	2.35	2.90	**2.13**	**2.23**	**1.03**	**1.13**	**1.63**

T_{max}	State wide trends			In city trends			Residuals				
	NV	AZ	Average	McCarran	Nellis	Average	McCarran - NV	McCarran - AZ	Nellis -NV	Nellis-AZ	Average
DJF	-0.35	-1.16	-0.76	0.07	-1.02	-0.48	**0.42**	**1.23**	**-0.67**	**0.14**	**0.28**
MAM	1.07	1.40	1.24	1.29	0.53	0.91	**0.22**	**-0.11**	**-0.54**	**-0.87**	**-0.33**
JJA	0.99	0.91	0.95	0.92	0.31	0.62	**-0.07**	**0.01**	**-0.68**	**-0.60**	**-0.34**
SON	-0.63	-0.43	-0.53	-0.19	-1.33	-0.76	**0.44**	**0.24**	**-0.70**	**-0.90**	**-0.23**
Annual	0.27	0.18	0.23	0.52	-0.38	0.07	**0.25**	**0.34**	**-0.65**	**-0.56**	**-0.15**

Urban Heat Island effect **Urban Cool Island effect**

3.4 Moist Diurnal Cycle and Trends

In arid or semi-arid areas, adding vegetation (e.g., turf grass) can benefit the improvement of air quality, minimize runoff for flood control, and reduce other hazardous potentials driven by local climate change (Beard and Green, 1994). Adding turf grass can increase ET modulating the UHI/UCI within the city (Yu and Hien, 2006). The potential effect of ET on the UHI/UCI phenomenon is generally greater under arid and semi-arid regions (Kjelgren and Montague, 1998; Jonsson, 2004; Mueller and Day, 2005).

Figure 19a shows the RH diurnal cycle by seasons for McCarran averaged over for 1950-1959 and 2000-2009. In general, all seasons show a significant increase in daytime RH with JJA, DJF, and SON showing a decrease in RH during the nighttime/early morning hours. During the 2000s, relatively small spikes (< 5%) are

observed at 1500 LST, 2100 LST, and 0300 LST. Of note is that there is a lack of evidence containing these artifacts from other stations. In Nellis (Fig. 19b), DJF and SON show nighttime RH decreases with larger daytime increases. Nevertheless, both sites (McCarran and Nellis) show a decreasing trend in the amplitude of the RH diurnal cycle. Observations show a significant shift in RH_{min} of about one hour forward for SON and DJF at McCarran, whereas Nellis shows that RH_{max} shifted from 0400 to 0500 LST and decreased by ~5% during JJA. Not surprisingly, these results are consistent with the T_{min} shift presented earlier (Fig. 16b) as RH is a function of temperature.

To what extent the observed changes in RH are related only to moisture changes? We address this question by using moist parameters unrelated or less related to temperature, such as T_d, K_o, and VPD. Figure 20 shows the average T_d, K_o, and VPD trends for McCarran. In general T_d, K_o and VPD show similar trends to T_{mean} (Fig. 8), with the exception of the last 7 years (2005-2011). Note that long-term moisture trends at Nellis (Fig. 21) show similar trends to McCarran. Overall, McCarran shows a T_d increase of 0.64°C/decade, and Nellis increasing by 0.16°C/decade. The long-term trends of K_o and VPD were -0.17°C/decade and 0.03 kPa/decade, respectively at McCarran. K_o and VPD at Nellis were 0.14°C/decade and 0.03 kPa/decade, respectively.

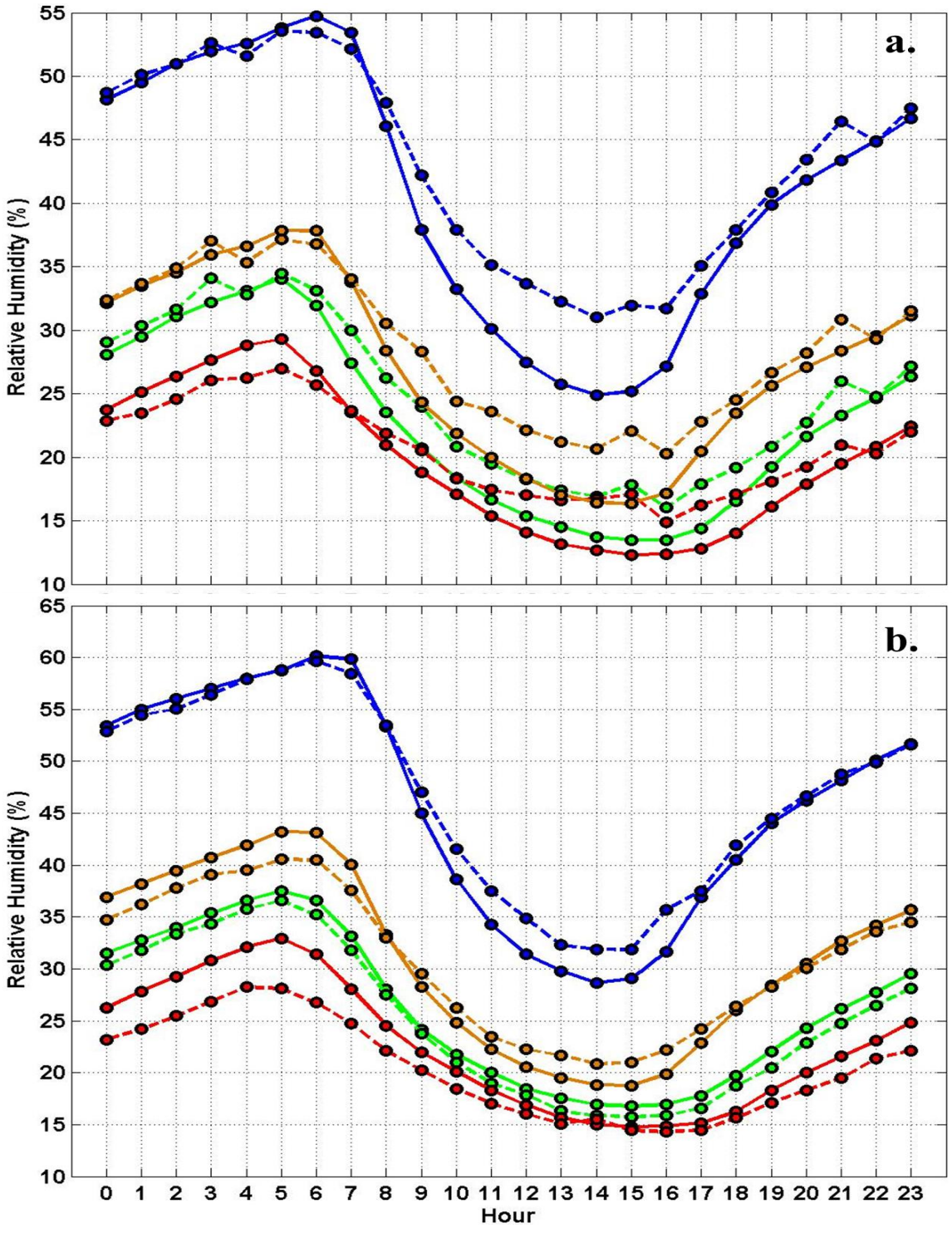

Fig. 19. Seasonal diurnal cycle in LST of RH for (a) McCarran and (b) Nellis. Hourly RH averages were determined for mid-20th century (1950-1959; solid lines) and early 21st century (2000-2009; dash lines) for DJF (blue), MAM (green), JJA (red), and SON (orange).

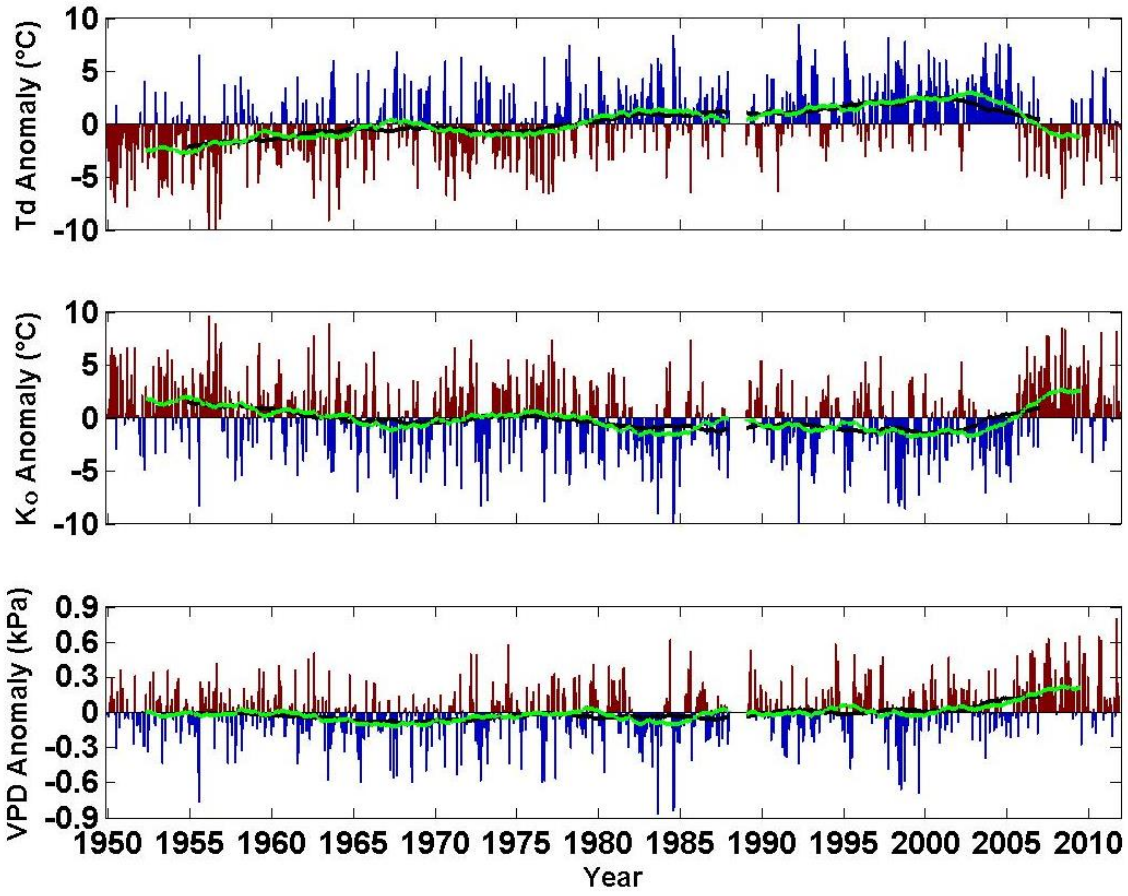

Fig. 20. Monthly mean T_d (top panel), K_o (middle panel), and VPD (bottom panel) anomalies for McCarran. The 5- (green) and 10-year (black) moving averages were added to highlight trends of the interannual variability. Time period is from December 1949 to November 2011. The red bars signify dry anomalous months, while the blue bars signify moist anomalous months. The 1988 data has been removed due to excessive data missing.

From 2000-2011, the Southwest regional droughts may have affected Las Vegas moist and temperature trends (Holdren and Turner, 2010; US Drought Monitor:*droughtmonitor.unl.edu*). Since 2000, the Southwestern US has experience severe-to-extreme droughts from March 2002-December 2005 followed by another

severe drought from June 2007-December 2007. Moderate drought and abnormal dry spells continued after 2007. McCabe et al. (2004) found that the most intense droughts in the Southwest typically occur during positive phases of the Atlantic Multidecadal Oscillation (AMO; Enfield et al., 2001) mixed with negative phases of the PDO (Mantua and Hare, 2002). These global teleconnection relationships could have also influenced the regional and Las Vegas drying trends. It is speculated in this study that daytime UCI is related to Las Vegas lawns and open water surfaces leading to the increase of e_a. However, a recent buy-out of Las Vegas residencies beginning in 2003 aimed to remove lawn turf grass to replace it with more natural/xeric landscapes. These water conservation methods could have been partially related to the observed changes in e_a.

Figure 22 shows T_{min} and e_a monthly mean anomalies for the period 1949-2012, contrasting in-city and rural temperature and moisture trends. The in-city T_{min} warming trend relative to the rural sites is yet further striking evidence of the UHI effect. In-city and rural e_a show similar interannual variability as both regions are influence by the same wet/drying regional patterns. However, McCarran e_a shows a distinct increase from 1950-2004 as the Las Vegas urban area expanded. There is a noticeable difference in trends between McCarran e_a and rural/Nellis e_a after 1995, with McCarran e_a increasing ~1 kPa likely related to the rapid rise in population (Fig. 1). After 2004, e_a experiences a drastic drop, most notably in McCarran which is arguably related to the implementation of water conservation strategies (Southern Nevada Water Authority, personal communication). As this occurs, the T_{min} positive trends at McCarran became neutral. After 2005, both in-city and rural e_a patterns start showing similar values once again.

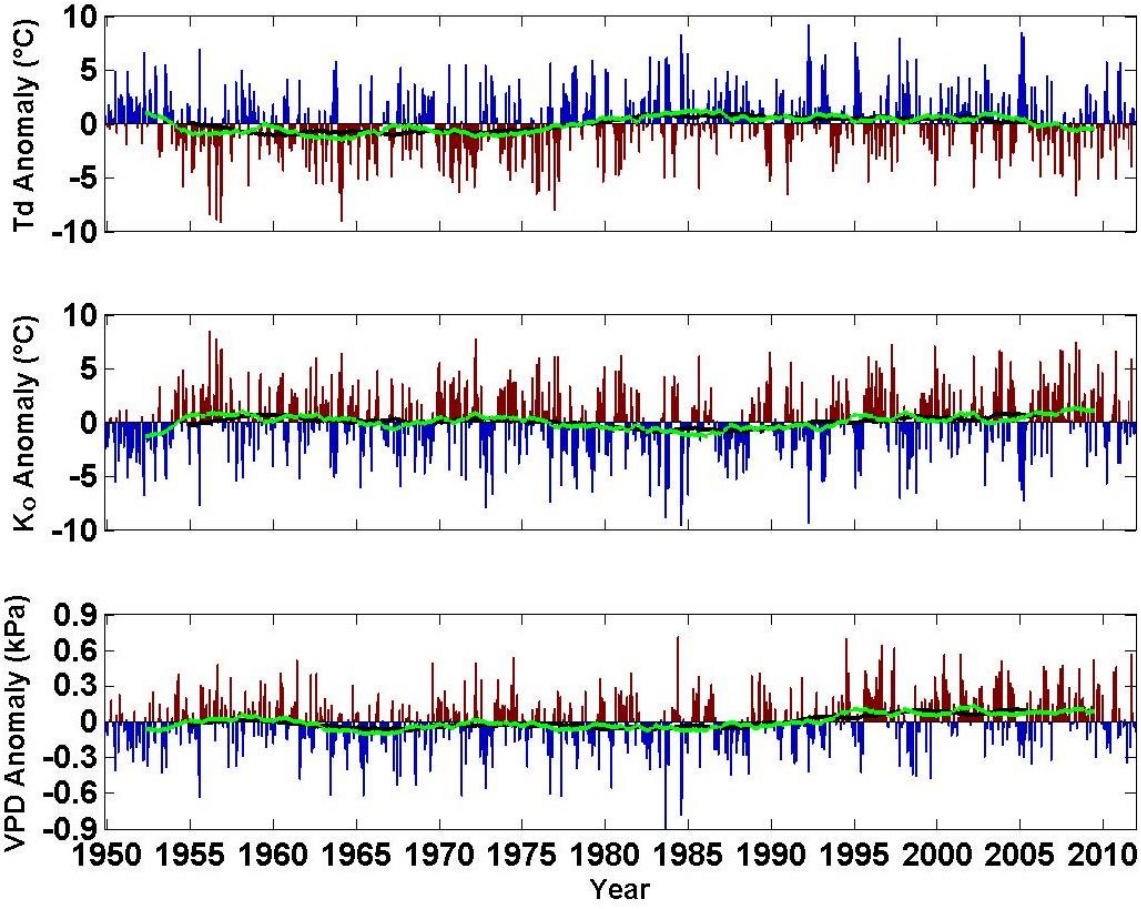

Fig. 21. Monthly mean T_d (top panel) K_o (middle panel), and VPD (bottom panel) anomalies for Nellis. The 5- (green) and 10-year (black) moving averages were added to highlight trends of the interannual variability. Time period is from December 1949 to November 2011. The red bars signify dry anomalous months, while the blue bars signify moist anomalous months. The station was moved on 1 Jan 2000, before moving back on 1 Jan 2005 to its original location.

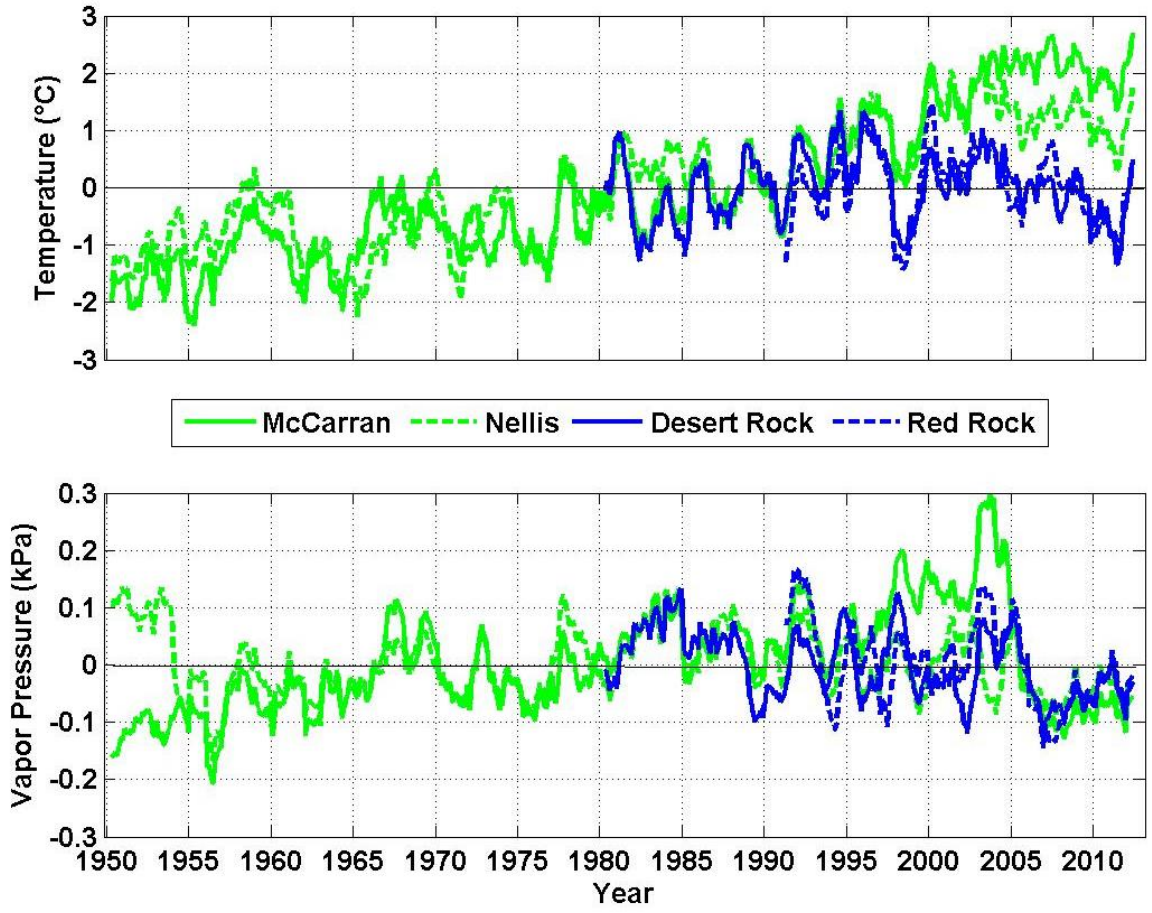

Fig. 22. T_{min} (top panel) and e_a (bottom panel) 1-year moving averages for in-city (McCarran and Nellis) and rural (Desert Rock and Red Rock) stations. Positive e_a values signify wetter than normal months, while negative e_a values signify drier than normal months. The 1988 data has been removed for McCarran due to excessive data missing. The Nellis station was moved on 1 Jan 2000, before moving back on 1 Jan 2005 to its original location.

Separation of regional climate trends from those associated with local influences (i.e. UHI/UCI) is challenging. In the Southwest, other changes could have contributed partly to the observed trends shown in Fig. 22. For example, Figure 23 shows Lake Mead water levels, the Evaporative Demand Drought Index (EDDI), and the PDO as proxies for regional climate variability in the region. The EDDI was analyzed for the Las Vegas

region and incorporates e_a along with other parameters related to the drivers of ET (McEvoy et al., 2014). Other factors to lake levels lowering water levels should be noted as the watershed contains five other states: Colorado, Wyoming, Utah, New Mexico, and Arizona. Lake Mead receives most of its inflow from the Colorado River which depends on snowmelt and rainfall in the Rocky Mountains (Holdren and Turner, 2010). Hence, watershed population and regional climate in the Rocky Mountains are also a factor. After 2010 the levels increased by ~10 m. However, current analysis suggests that lake levels are at their lowest in 2014 (Holthaus, 2014). During 1999-2010, lake levels dropped and primarily coincided with negative phases of the PDO. Between 1965 and 1988 the negative phases were less extreme and had smaller effects on the sinks of the lake level. After 2000, lake levels were decreasing rapidly with the majority of PDO variability in the negative phases. Positive values for the EDDI represent dry periods that are most discernable after 2000. Overall, the EDDI wet and dry periods are strongly correlated to PDO variability ($\rho = 0.42$). Of note is that the last decade involved frequencies of negative PDO with positive AMO activity, which have been argued to be related to regional droughts in the Southwestern US (McCabe et al., 2004). The constant decline from 2000-2010 of Lake Mead are also the effect of water demand (Holdren and Turner, 2010). Although there were some positive PDO activity and increases in e_a during severe lake level drop, the Las Vegas population and urban expansion were growing at an alarming rate during the early stages of a prolonged drought.

The slope of best fit line showed that in-city e_a has increased by 0.06 kPa while rural e_a has decreased by 0.09 kPa since 1991. This equates to a positive residual of 0.15

kPa that estimates the in-city local effect of e_a increasing from 1991-2012. Meanwhile, Lake Mead levels have dropped by 33.02 m during that time span. There is a solid pattern that relates lake levels increasing with positive e_a and sinking with negative e_a when comparing Figures 22 and 23 (primarily before 2000). In addition, T_{min} has been at least 1°C above average during the current depression of Lake Mead. Therefore, recent activity affecting water demand are linked to the prolong drought, negative PDO activity, and can partly explain some of the observed warming trends in T_{min}.

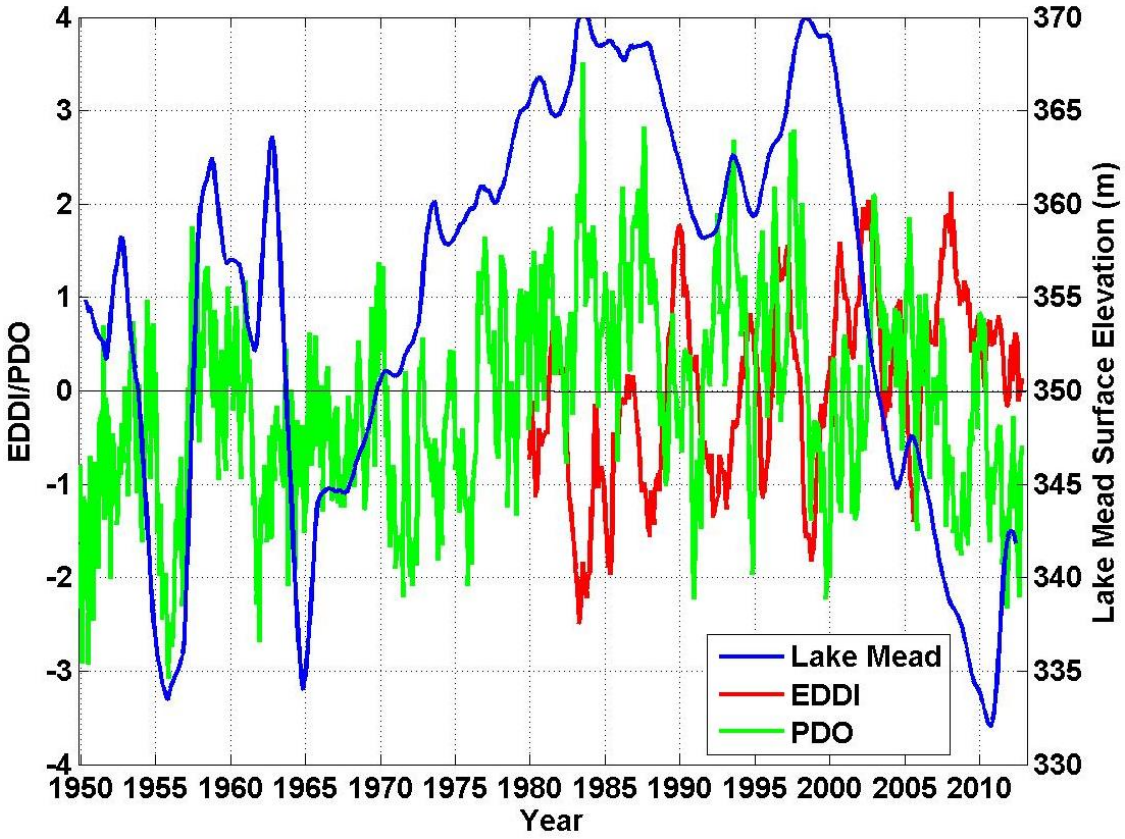

Fig. 23. Lake Mead surface elevation 1-year moving averages with EDDI and PDO anomalies. Positive and negative PDO values are associated with wetter and drier than normal periods in the Southwest US, respectively. Positive and negative indices of the EDDI represent drier and wetter periods, respectively.

3.5 CF Results

The CF (Equation 3) was used to reduce the T2m (dry adiabatically) of urban and rural stations at the reference elevation, in our case the lowest station within the city. The DRI-UHI network recording period of August 2012-April 2013 was used in this method to maximize the number of stations in the analysis. Table 4 shows a summary of T2m and the UHI determined by the average difference of in-city stations minus rural stations after CF calculations, per land use category. To no surprise, T_{min} accentuated greater UHI intensity than T_{max}. The smallest magnitudes of UHI were exhibited during the cooler period from January-February, 2013. However, March-April 2013 showed the lowest UHI range (T_{min} UHI minus T_{max} UHI). This may have been the result of the CF method overanalyzing T_{max} as there was no evidence of UCI present in the overall analysis.

T_{amp} values were smaller for urban sites than for rural shrub stations (~1°C) further showing evidence of an urban signal. However, there were no strong T2m significances between the urban LULC, with the exception of smaller T_{max} values in the barren and medium-intensity areas during the cooler period. Medium- and low-intensity areas are generally residential sites conformed mostly by lawns, parks, and golf courses (Appendix C). Hence, this cool/wet season may have resulted in a smaller UHI value for January-February 2013. Of note is that some low-intensity sites are conformed of little vegetation and xeric landscaping. This may have affected T_{max} averages to be warmer than high-intensity areas. High-intensity LULC had the warmest relative T_{min} during January-February 2013 (> 1°C) and March-April 2013 (< 1°C). These particular areas are known to absorb and trap most of the heat resulting in the largest in-city T2m and UHI

intensity (Grossman-Clarke et al., 2010). This was confirmed with the long-term trends in Las Vegas (Chapter 3.3; Table 3) by the McCarran station. Hence, this method does portray some effect of urban signals related to UHI. However, it may be less effective as elevation becomes more complex and with orographic induced circulations affecting T2m.

Table 4. LULC T2m averages and UHI detection based on the CF method (Chapter 2.5). The CF method uses Γ_e to bring T2m to the reference level of the Las Vegas High School station (534 m ASL). The number of stations (N_Stations) is shown for each LULC composite category. The UHI is estimated by the adjusted temperature differences between average composited LULC in-city categories minus the shrub category.

Aug 2012-Apr 2013				
LULC	**N_Stations**	**T_{max} Avg**	**T_{min} Avg**	**T_{amp} Avg**
Low Intensity	15	26.22	13.99	12.23
Medium Intensity	13	25.08	13.01	12.07
High Intensity	2	25.75	13.98	11.77
Barren	3	24.88	13.32	11.56
Shrub	11	25.01	12.11	12.90
UHI		**0.47**	**1.46**	-0.99
Jan-Feb 2013				
Low Intensity	15	16.32	4.45	11.87
Medium Intensity	13	14.54	4.04	10.50
High Intensity	2	16.07	4.76	11.31
Barren	3	15.12	3.50	11.62
Shrub	11	15.65	3.45	12.20
UHI		**0.23**	**0.77**	-0.54
Mar-Apr 2013				
Low Intensity	15	26.76	13.62	13.14
Medium Intensity	13	26.68	13.50	13.18
High Intensity	2	26.98	14.62	12.36
Barren	3	26.02	13.16	12.86
Shrub	11	25.74	12.32	13.42
UHI		**0.93**	**1.27**	-0.34

3.6 Normalized Observed Results

The normalized T2m calculated in Equation 4 showed a significant UHI for T_{min} (Table 5). McCarran shows a stronger UHI effect than Nellis as both sites appear to warm much faster than Desert Rock. Furthermore, T_{min} rates for McCarran and Nellis were significant at the 95% confidence level, which reflects indication of UHI activity via increased city warming. These results agree with our earlier findings summarized in Table 3. T_{max} yearly trends increased at slower rates for in-city sites, which is argued to be partially related to the UCI effect. Desert Rock T_{max} rates increased almost twice that of McCarran and three times more than Nellis. It is established that dry deserts have low thermal inertia, making the surface susceptible to heat and cool quickly during daylight and night hours, respectively (Titus et al., 2013).

Table 5. Yearly rates of normalized trends, and residuals for T_{max} and T_{min} from January 1980-December 2011. Residuals are the overall in-city trends (i.e. McCarran and Nellis) minus the overall trends at Desert Rock. Positive residuals represent the UHI effect. When residuals are negative, it is argued that the temperature trends are attributed to the UCI. McCarran was calculated as a 31-year period due to the absence of 1988 data.

Station	T_{max} [°C/yr]	T_{min} [°C/yr]	T_{max} Residuals [°C]	T_{min} Residuals [°C]
McCarran	$1.2x10^{-2}$	$5.9x10^{-2}$	-0.26	1.80
Nellis	$5.6x10^{-3}$	$3.2x10^{-2}$	-0.43	1.00
Desert Rock	$1.9x10^{-2}$	$1.1x10^{-3}$	***	***

Table 6 shows decreases in RH for the three NWS stations examined. However, when considering the urban minus the rural residual, Nellis shows the largest increase in ΔRH_{max}. Not surprisingly, ΔRH exhibits an inverse relation to temperature trends. Particularly, McCarran ΔRH behavior is in agreement with Alghannam and Al-Qahtnai (2012). Their argument was that increasing vegetation outside the city would help

suppress UHI activity by showing an inverse correspondence to ΔRH. However, since Desert Rock is without foreign vegetated surfaces; the results could be due to the addition of impervious material in the McCarran area. The inverse relation holds up to both maximum and minimum residuals at McCarran. In contrast, urban vegetation is increasing nearby Nellis as parks and other cool urban patches from golf courses and residencies may correspond to increasing RH by reducing both nighttime radiative cooling and thermal comfort (Spronken-Smith and Oke, 1999; Theeuwes et al. 2013). Although development nearby Nellis has been occurring, it is difficult to say whether ΔRH has a rapport with the UHI and UCI effects in this area.

Table 6. Yearly rates of normalized trends, and ΔRH for RH_{max} and RH_{min} from January 1980-December 2011. ΔRH is the overall in-city trends (i.e. McCarran and Nellis) minus the overall trends at Desert Rock. ΔRH represents an RH reference to UHI. McCarran was calculated as a 31-year period due to the absence of 1988 data.

Station	RH_{max} [%/yr]	RH_{min} [%/yr]	ΔRH_{max} [%]	ΔRH_{min} [%]
McCarran	$-2.5x10^{-2}$	$-1.8x10^{-2}$	-0.11	0.30
Nellis	$-3.8x10^{-3}$	$-2.5x10^{-2}$	0.57	0.04
Desert Rock	$-2.2x10^{-2}$	$-2.6x10^{-2}$	***	***

To get a better understanding of the Las Vegas moisture trends, Δe_a was calculated (Table 7). Instead of using maximum and minimum values, Δe_a was separated into daytime (Δe_{a_day}) and nighttime/morning (Δe_{a_nm}) hours of the day. The nighttime/morning e_a covers the hourly period of 1700-0900 LST. Daytime e_a covers the hourly period of 1000-1600 LST. Results show greater Δe_{a_day} for McCarran where there is an exceptional amount of residential (i.e. medium- and low-intensity) sites nearby compared to Nellis. Δe_{a_nm} have similar values at McCarran and Nellis. Low Δe_{a_day} at Nellis are due to the similar yearly rates as Desert Rock which shows both sites getting

dryer. Although residencies have expanded closer to Nellis, the station still lies on light colored barren soil which may be influencing less solar intake due to a larger albedo. It is known in arid/semi-arid regions that surface albedo decreases when soil moisture increases (Liu et al., 2008; Guan et al., 2009). Hence, the high albedo at Nellis may be partial to low Δe_{a_day} due to a lack of soil moisture. Larger Δe_{a_nm} may be influenced by atmospheric stability as moisture from upper levels (e.g. evergreen forest in the mountains and vegetation at upper elevated residencies) sink into the valley during the night.

Table 7. Yearly rates of normalized trends, and Δe_a for e_{a_day} and e_{a_night} from January 1980-December 2011. Δe_a is the overall in-city trends (i.e. McCarran and Nellis) minus the overall trends at Desert Rock. McCarran was calculated as a 31-year period due to the absence of 1988 data.

Station	e_{a_day} [kPa/yr]	e_{a_nm} [kPa/yr]	Δe_{a_day} [kPa]	Δe_{a_nm} [kPa]
McCarran	$1.6\text{x}10^{-2}$	$-5.5\text{x}10^{-3}$	1.23	0.50
Nellis	$-2.3\text{x}10^{-2}$	$-4.6\text{x}10^{-3}$	0.04	0.55
Desert Rock	$-2.4\text{x}10^{-2}$	$-2.3\text{x}10^{-2}$	***	***

3.7 GDP Long-Term Trends

The GDP datasets of Daymet and PRISM 800 m were analyzed from January 1980-December 2011. As previously mentioned for the customized domains in Figure 3, the core (red box) represents a more dense urban structure than the outer-core (green box). In regards to the analyzed observation sites, McCarran represents the core while Nellis represents the outer-core of Las Vegas. The rural domain (blue box) is located outside the Las Vegas metropolitan area.

Figure 24 shows the T_{max} and T_{min} trends of the customized domains for the GDPs in the format of 5-year moving averages. Warming trends were labeled for each product, and calculated by linear regression after T2m was normalized by Equation 4. Trends show that Daymet suggests greater T_{max} warming than PRISM 800 m, while T_{min} is warming more for PRISM 800 m. Residuals calculated from the average of the in-city domains (red box and green box average) minus the rural domain show small negative values for T_{max} with larger T_{min} positive residuals. Positive residuals suggested a UHI of ~1.03°C and ~0.69°C for Daymet and PRISM 800 m, respectively for the 32-year period. Negative residuals showed a UCI of ~-0.04°C and ~-0.11°C for Daymet and PRISM 800 m, respectively. Of note is that the rural domain contains more complexities of topography, and T2m gathered from this domain will provide greater differences from the different interpolation methods used by the GDPs which will overall affect residuals. In comparison to observations the GDPs undersample UHI and UCI (i.e. observations show larger residuals for UHI and UCI). The core presents the most activity in the trends as it suggests the most warming and cooling for T_{min} and T_{max}, respectively.

The downward trend shown for anomalous trends in Chapter 3.1 bares evidence under the 32-year time period displayed by the GDPs. T_{max} showed the greatest effect with an anomalous decline of ~1.5°C and ~1.25°C from 2006-2011 for PRISM 800 m and Daymet, respectively. Furthermore, the evolution of T_{min} trends show in-city warming exceeding rural T2m just prior to the millennium. An interesting artifact is the rural T_{min} trend increasing significantly for PRISM 800 m during the downward trend

effect, matching the outer-core values and possibly somehow influenced by the T_{max} cooling. Daymet does not show as strong of an effect for T_{min} in the rural domain.

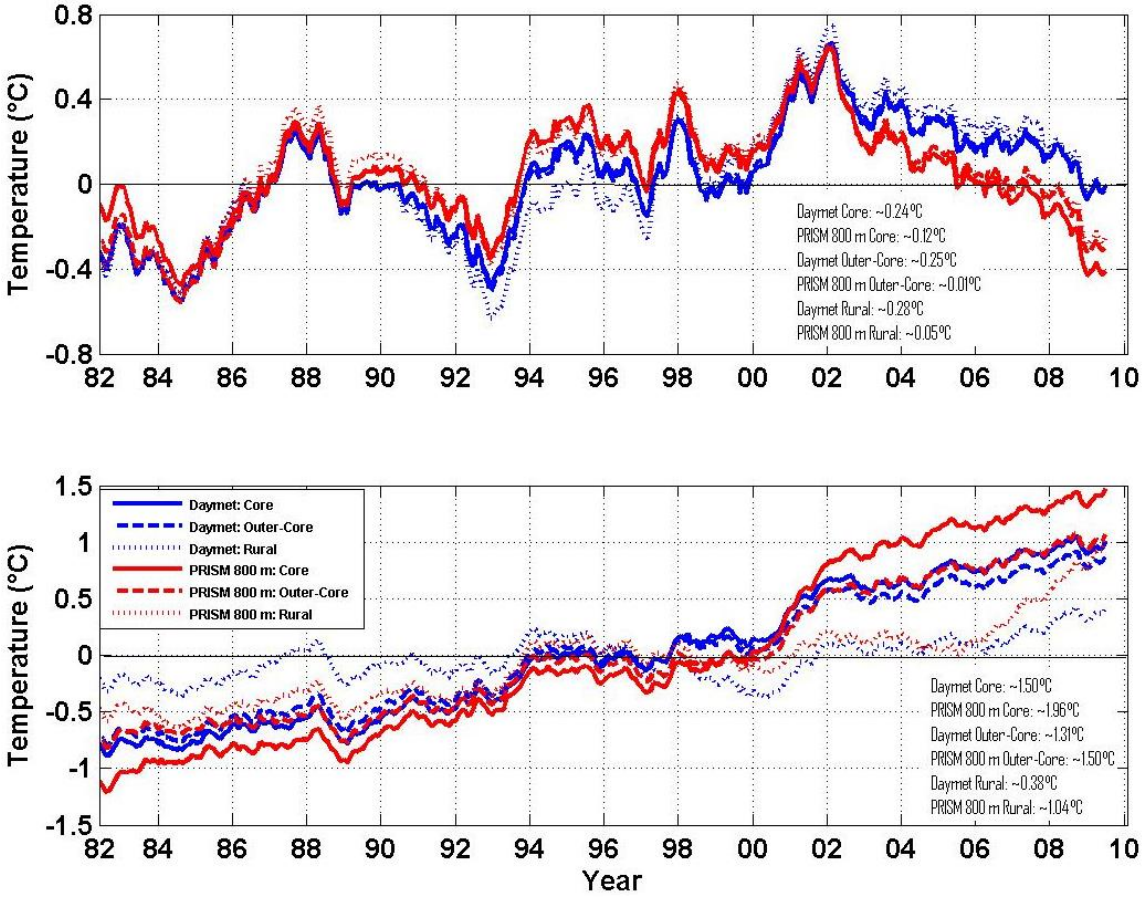

Fig. 24. T_{max} (top panel) and T_{min} (bottom panel) 5-year moving averages for the customized domains of the urban core (solid lines), urban outer-core (dashed lines), and rural area (dotted lines) of Daymet (blue) and PRISM 800 m (red) from January 1980 to December 2011.

3.8 UHI from Gridded Data Products

For a direct comparison between the station locations and GDPs, the nearest neighbor method was used. Figures 25 and 26 are annual time series of T_{max} and T_{min}, respectively, from 1980-2011 for three stations: McCarran, Nellis, and Desert Rock. In general, all products capture year-to-year variability quite well. The GDPs resemble the observations best for T_{max} with overall differences < 0.25°C. A greater separation exists for T_{min}. PRISM 800 m does a better job at tracking year-to-year trends, especially at Desert Rock. Daymet shows to be less certain at Desert Rock, which questions Daymet's ability at pristine locations and higher elevations. For in-city stations, T_{min} for Daymet and PRISM 800 m have differences of ~1.88°C and ~0.92°C, respectively. PRISM 800 m best highlights the observations at Desert Rock than for the in-city stations, and provides better analysis than Daymet.

Figure 27 shows seasonal biases of the GDPs and McCarran for T_{max} and T_{min} during the period of December 1981-November 2011. Since the earliest Daymet data available was January 1980, seasonal analysis had to start in December 1981 to fully capture seasonal trends in the dataset. Furthermore, since 1988 is missing from McCarran that year has been removed from the GDPs as well. The GDPs agree well with T_{max} as each season has a bias within ~0.6°C. Both evaluated GDPs show similar biases during DJF and SON, with PRISM 800 m having a cold (negative) bias for all seasons. T_{max} for the GDPs agree most with McCarran observations during JJA. On the other hand, T_{min} has a significant systematic cool bias all year (< -1°C). Daymet T_{min} shows colder biases than PRISM 800 m for every season over 1°C except for DJF.

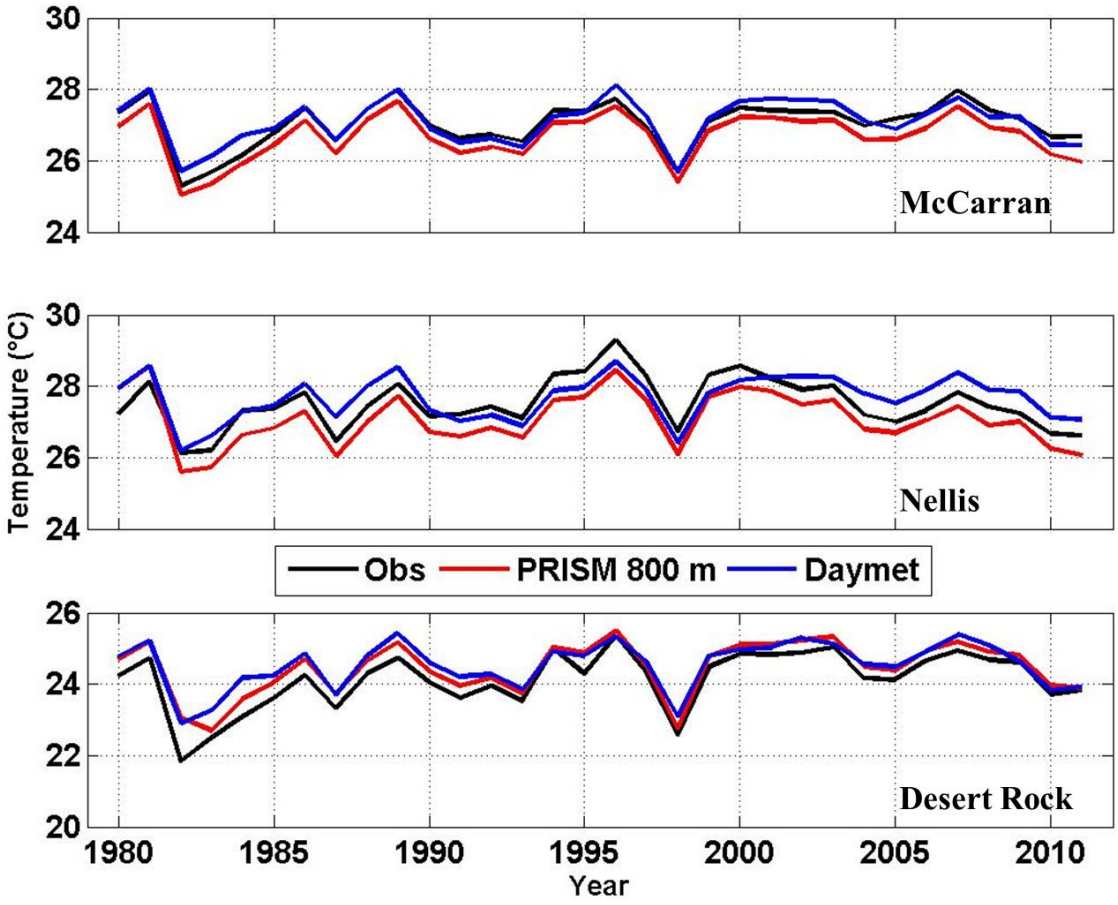

Fig. 25. Temperature trends of T_{max} for NWS surface stations and gridded products from 1980 to 2011. The gridded products of PRISM 800 m (red line) and Daymet (blue line) were retrieved for the nearest point to the observational sites (black line) for: McCarran (top panel), Nellis (middle panel), and Desert Rock (bottom panel). Note that biases are constant.

Figure 30 shows the seasonal biases at Desert Rock. For T_{max}, the GDPs slightly overpredict the observations. SON has the largest T_{max} biases and the greatest difference between Daymet and PRISM 800 m. PRISM 800 m has excellent performance against Desert Rock observations for T_{min} with negative biases under -0.5°C. However, Daymet biases for Desert Rock are about as unfavorable as McCarran (< -2°C). Hence, PRISM 800 m has a better representation of T_{min} outside the city while Daymet shows little

difference against in-city and rural observations. The magnitude of these biases will have important implications on how GDPs characterize in-city temperature environments as describe below.

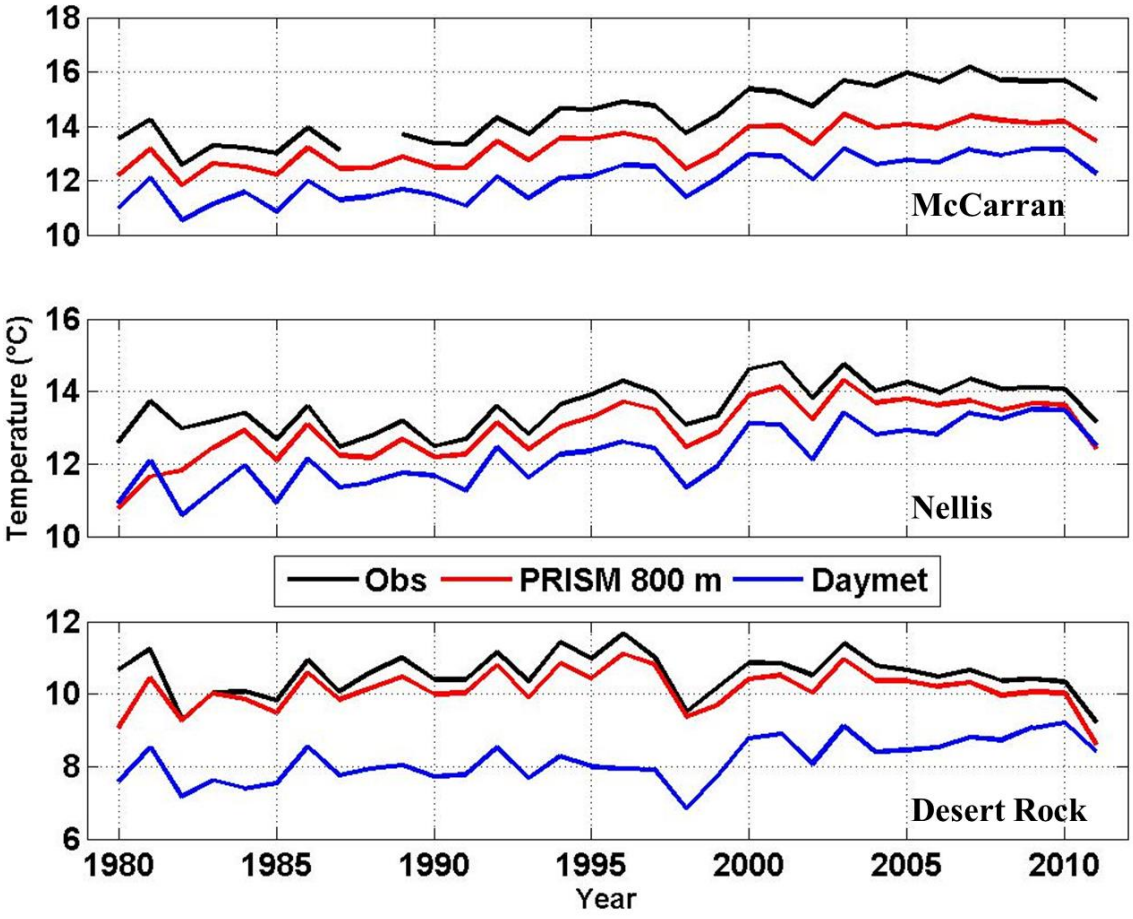

Fig. 26. Temperature trends of T_{min} for NWS surface stations and gridded products from 1980 to 2011. The gridded products of PRISM 800 m (red line) and Daymet (blue line) are to the nearest point to the location of the observational sites (black line) for: McCarran (top panel), Nellis (middle panel), and Desert Rock (bottom panel). Note that biases are constant.

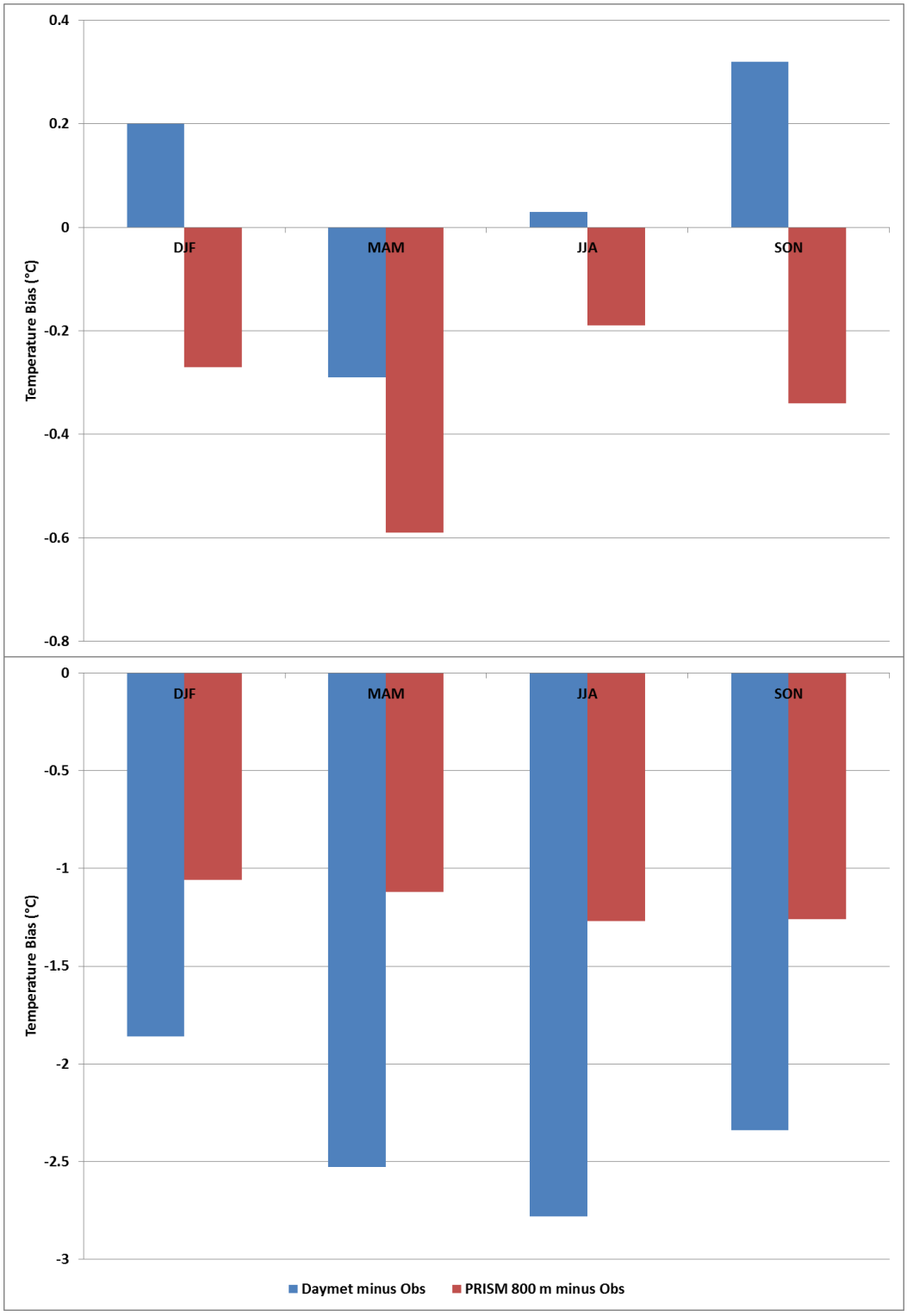

Fig. 27. T_{max} (top panel) and T_{min} (bottom panel) seasonal GDP biases from December 1981 to November 2011 for McCarran. The 1988 data was removed from the GDPs and McCarran due to excessive missing data from the observations.

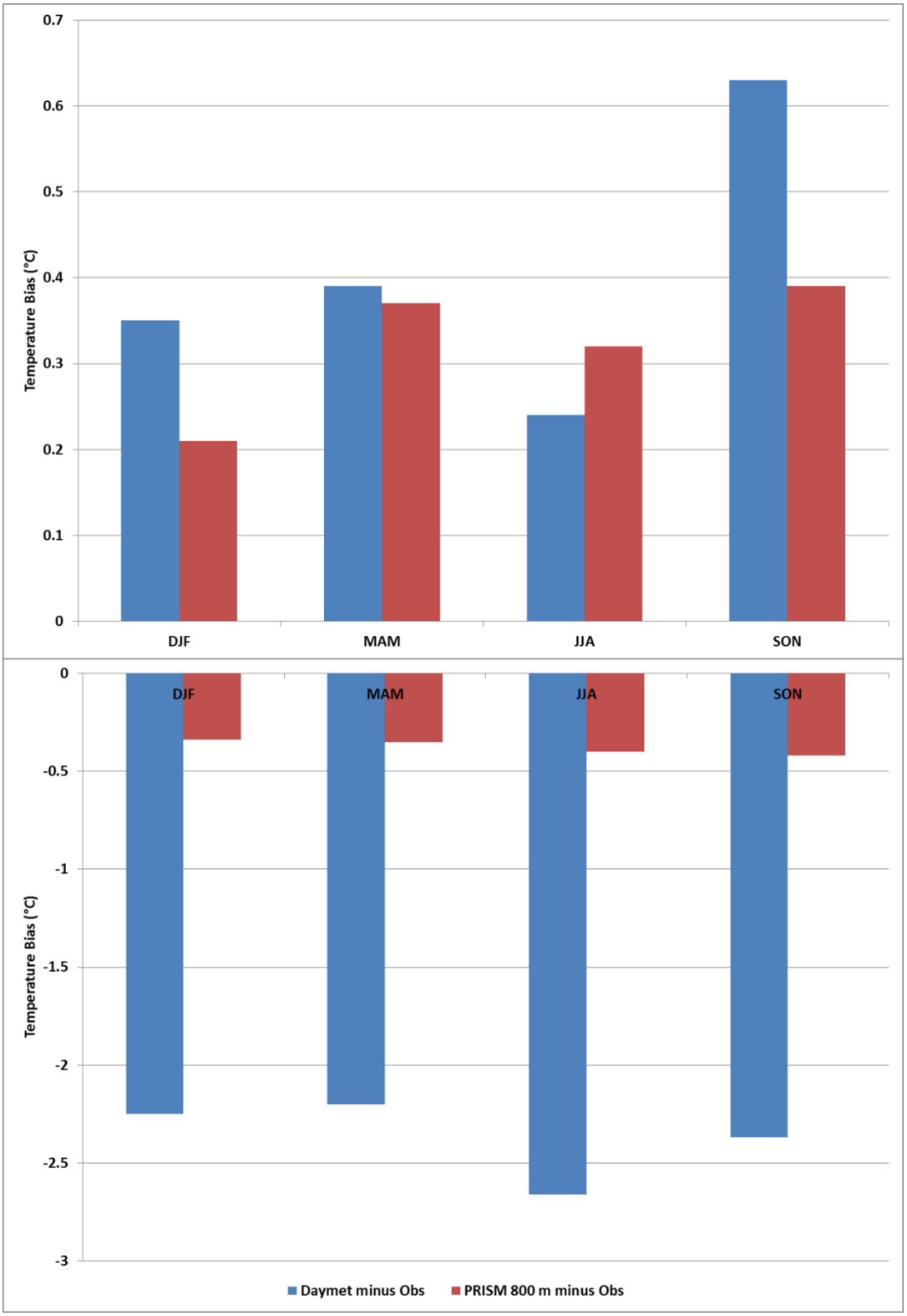

Fig. 28. T_{max} (top panel) and T_{min} (bottom panel) seasonal GDP biases from December 1981 to November 2011 for Desert Rock.

3.9 GDP Spatial Analysis

Figure 29a and 29b shows Daymet and PRISM 800 m T_{max} spatial differences for the 2000s minus 1980s decades, respectively in the Las Vegas region. In light of the observed interannual-to-decadal variability observed in Figure 24, it is reasonable to assume that these spatial differences can be used to characterize long-term trends. There are some surprising and striking differences between the GDPs. For example, PRISM 800 m shows more contrast in the urban footprint as North Las Vegas has cooled while the core and southern areas have warmed for T_{max}. In contrast, Daymet shows homogenous warming patterns in the metropolitan. North Las Vegas has transitioned from barren land to a more developed urban landscape with residencies and recreational areas (i.e. parks and golf courses), which may be a reason PRISM 800 m is interpolating a cooling signal that appears to be more accentuated in that area. Recall, however, that GDP biases shown earlier in Figure 27 suggest that GDP uncertainty to depict in-city spatial patterns in T_{max} is not statistically significant. Outside the city, Daymet shows a significant and interesting cooling pattern over the Spring Mountains and Sheep Range (~3°-4°C). This could be related to the deficiency that Daly (2006) acknowledged about Daymet's inability to produce nonlinear and non-monotonic elevation relationships.

Figure 29c and 29d T_{min} spatial trend distributions show urban warming in the metropolitan on the order of ~1°C for Daymet and ~2°-4°C for PRISM 800 m, respectively. In contrast to the North Las Vegas T_{max} cooling; PRISM 800 m shows an in-city warming, arguably significant (Fig. 29d), depicting a UHI that is more apparent in the northern half of the city. Once again, the temperature in the city is homogenous for

Daymet, as well as features outside the city. It is known that small-scale forcings that have an effect on larger scales (i.e. LULC) are generally not accounted for in the GDPs (Daly, 2006). Hence, the UHI/UCI magnitude and core locations may be erroneous.

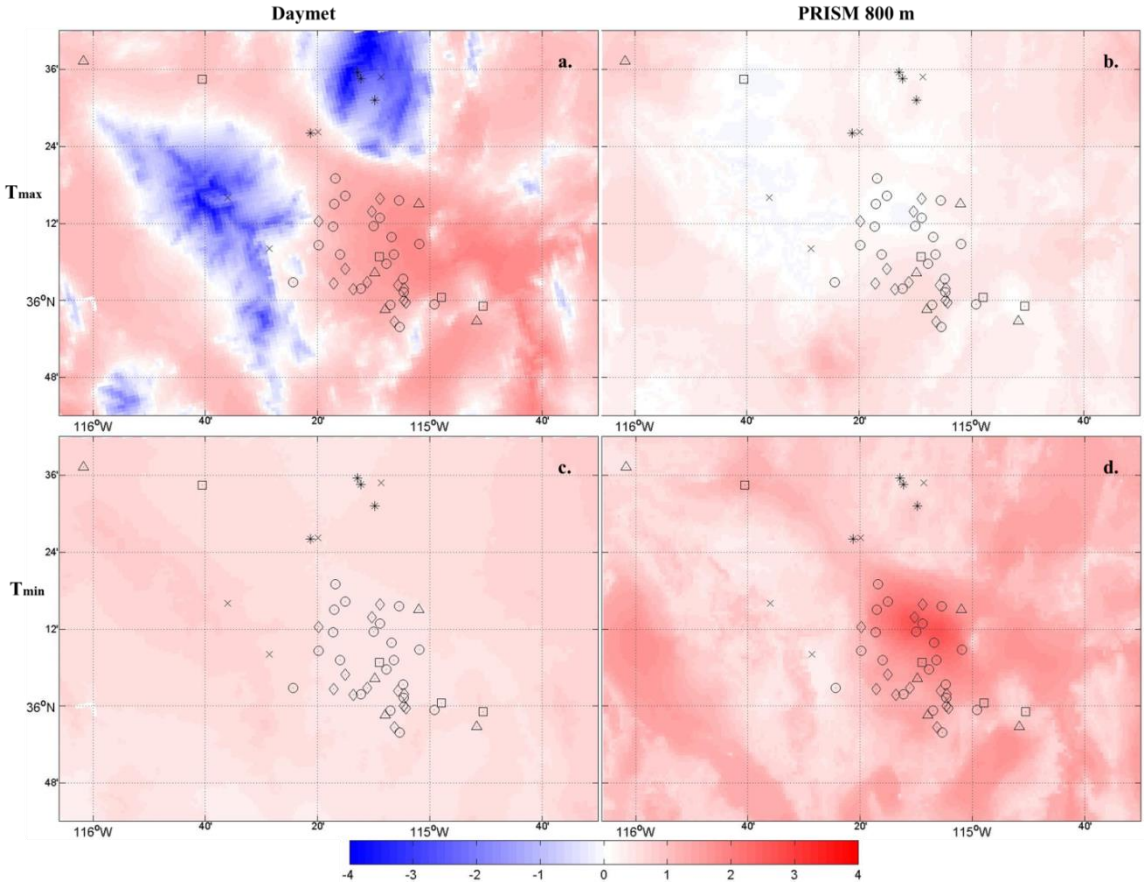

Fig. 29. T_{max} and T_{min} decadal differences (2000s minus 1980s) for (a, c) Daymet and (b, d) PRISM 800 m. The symbols show observed network locations for: DRI-UHI (circle), NWS (triangle), CEMP (square), NevCAN (star), RAWS (x), and WU (diamond).

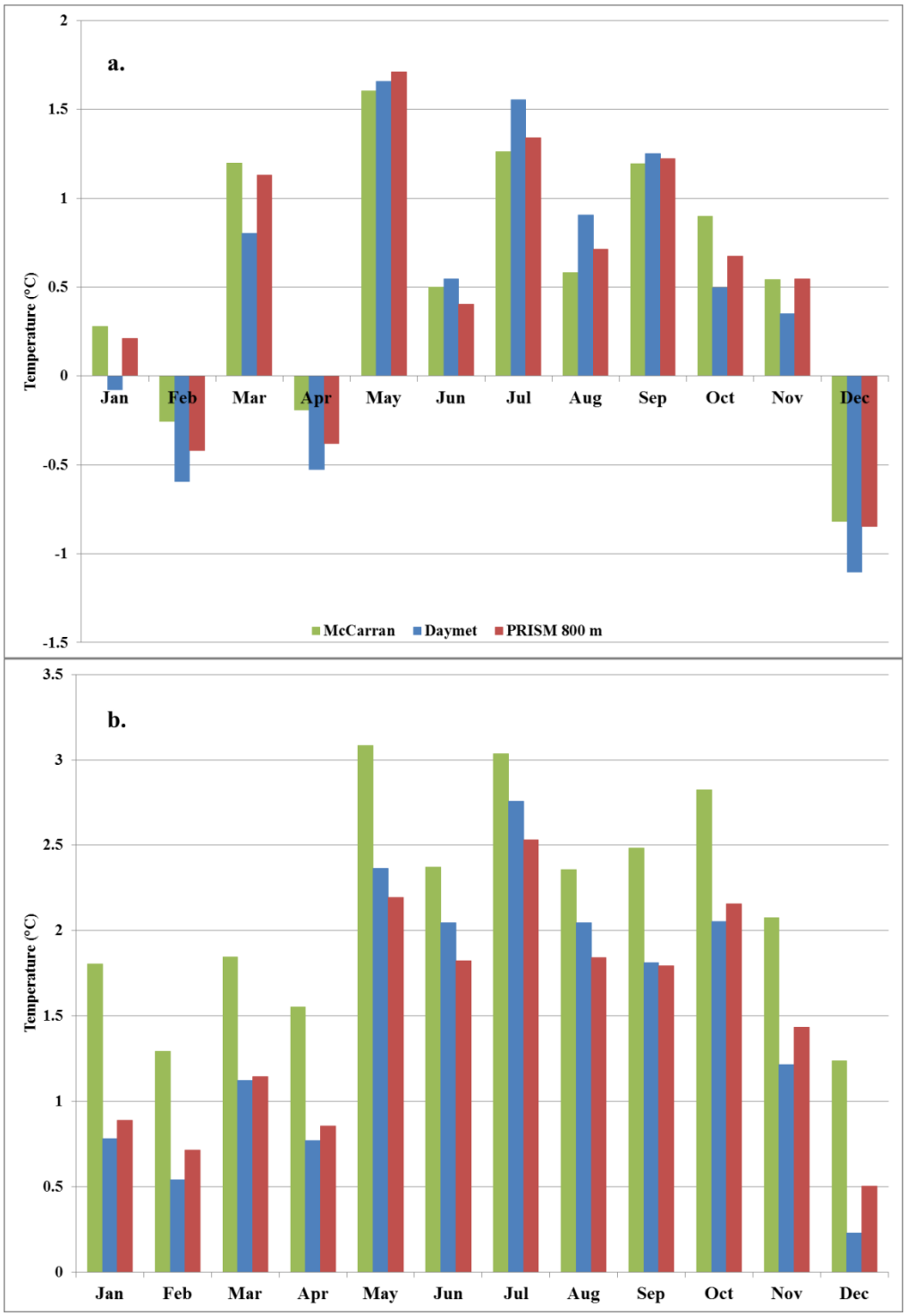

Fig. 30. 2000s minus 1980s (a) T_{max} and (b) T_{min} for McCarran (green bars), Daymet (blue bars), and PRISM 800 m (red bars). The 1988 data was removed from the GDPs and McCarran due to excessive missing data from the observations.

GDP annual in-city (city core, Fig. 3) long-term trends are presented in Figure 30. Overall, the sign and magnitude of the decadal differences (2000s minus 1980s) agree between McCarran and the GDPs. T_{max} shows cooling for February, April, and December. The GDPs and observations agree most in May and September. T_{min} (Figure 30b), however, highlights May-October with the largest trends, presumably associated to the UHI effect (Table 3; Fig. 30). Despite the biases and interpolation scheme uncertainties, there is moderate confidence when characterizing overall and seasonal UHI/UCI from the evaluated GDPs.

4. Urban Canopy Modeling

4.1 Control Run

The control run involves a simulation of the WRF-LSM without the UCM treatment. Figures 31-34 shows the observed and LSM in-city T2m and e_a diurnal and synoptic evolution during the month-long simulated experiment (November, 2012). In general, the model shows difficulties in simulating the urban diurnal cycle, which consistently overestimates nighttime and morning T2m (Fig. 31). These features hold true when evaluating against rural sites as well (Fig. 32). By contrast, e_a (Fig. 33) for urban stations show some deficiencies in simulating magnitudes by underpredicting most of the month. The e_a is most accurate during times of significant moisture increases as seen on days 8, 17-18, and 29. Of note is the model lags on day 16 predicting an early increase in e_a. For pristine rural stations (Fig. 34b-c), however, the e_a exhibits more skill. Overall, the LSM adequately simulates the synoptic patterns throughout the month. An example is the cold/wet spell occurring November 8-10 that was simulated very well for T2m and e_a. To

some extent this is not surprising as FNL global analysis updates boundary conditions every 6 hours.

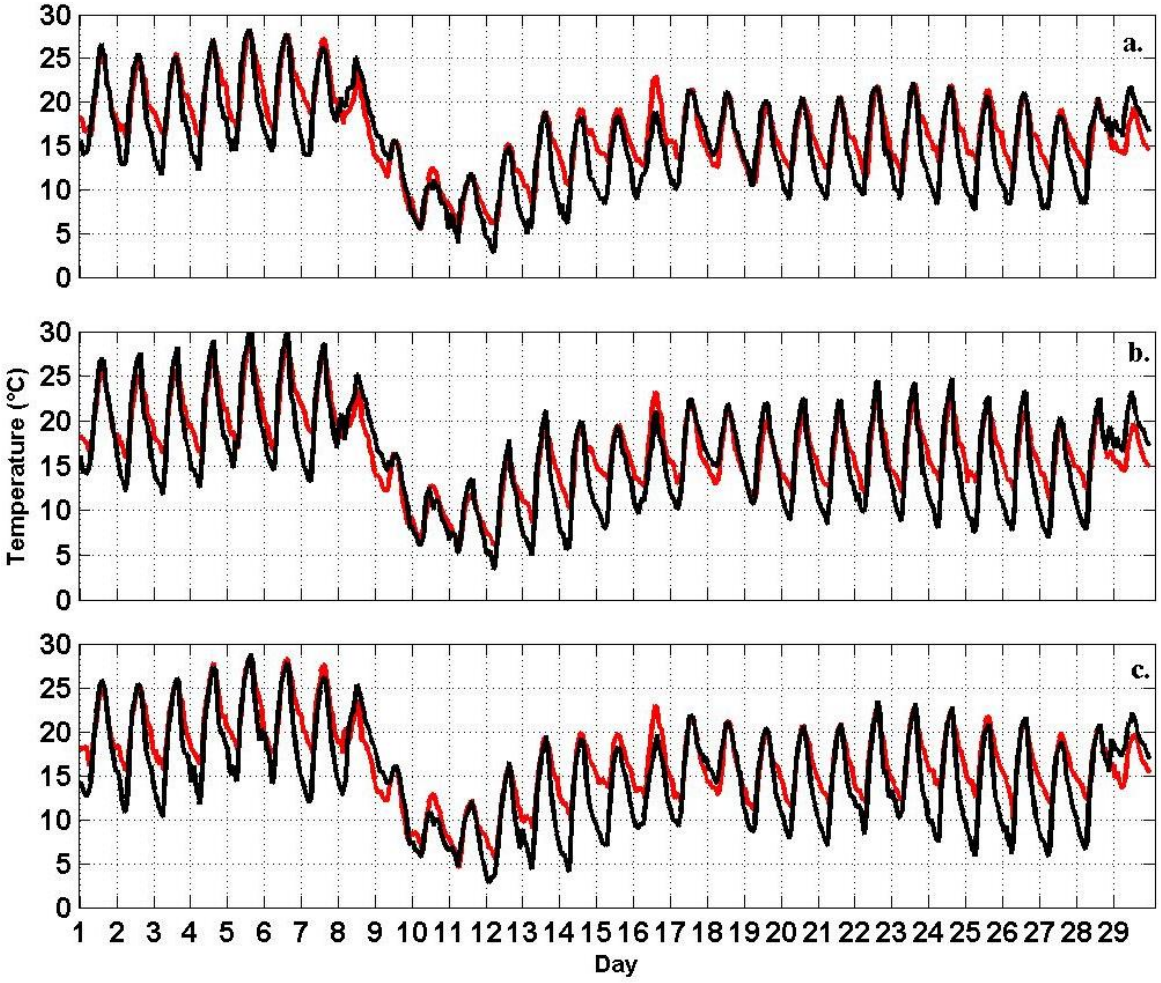

Fig. 31. Observed (black) and LSM (red) time series of T2m for November 2012 at the urban site locations (Appendix A) of (a) McCarran, (b) Las Vegas, and (c) West. Daily tick marks on the x-axis represent 00 LST.

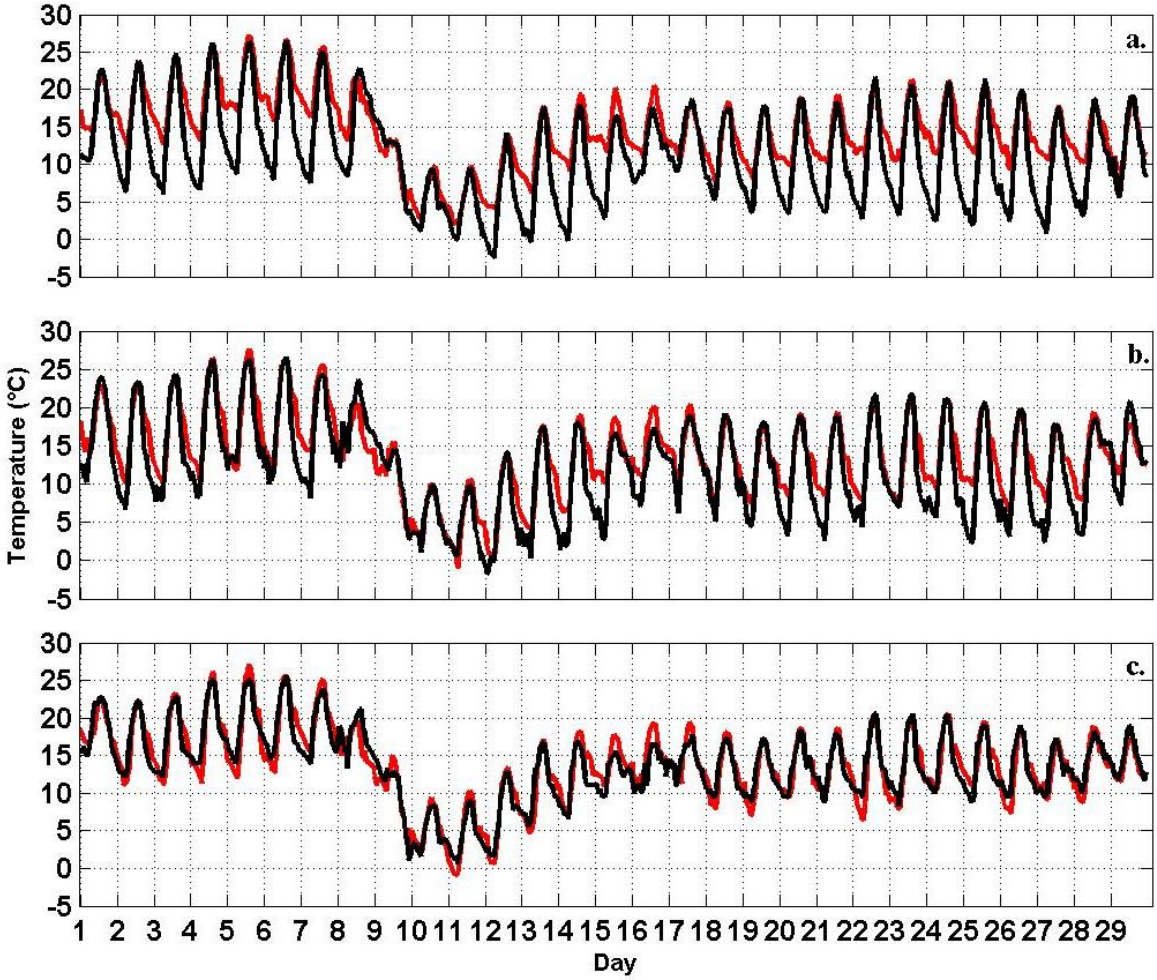

Fig. 32. Observed (black) and LSM (red) time series of T2m for November 2012 at rural site locations (Appendix A) of (a) Indian Springs, (b) Mojave Desert Shrub, and (c) Yucca Gap. Daily tick marks on the x-axis represent 00 LST.

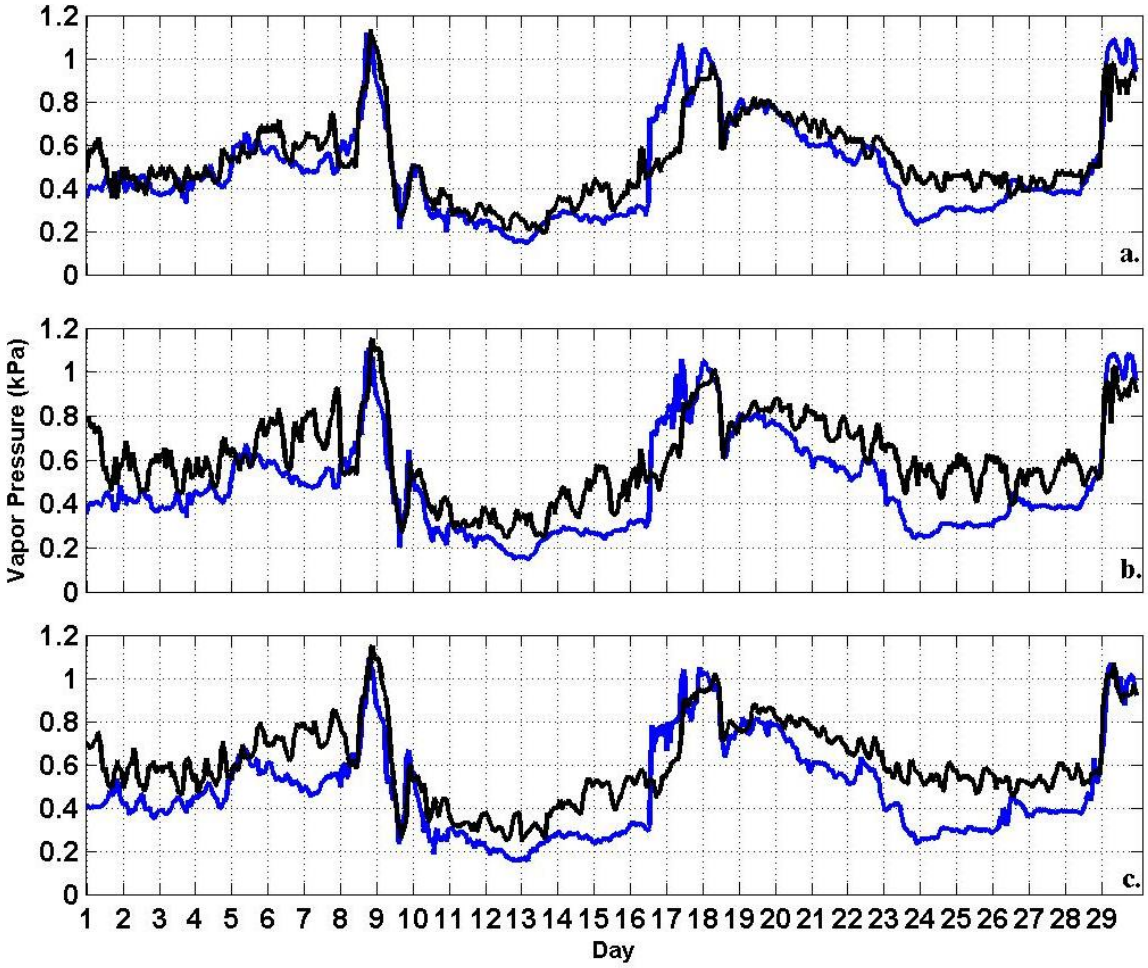

Fig. 33. Observed (black) and LSM (blue) time series of e_a for November 2012 at the urban site locations (Appendix A) of (a) McCarran, (b) Las Vegas, and (c) West. Daily tick marks on the x-axis represent 00 LST.

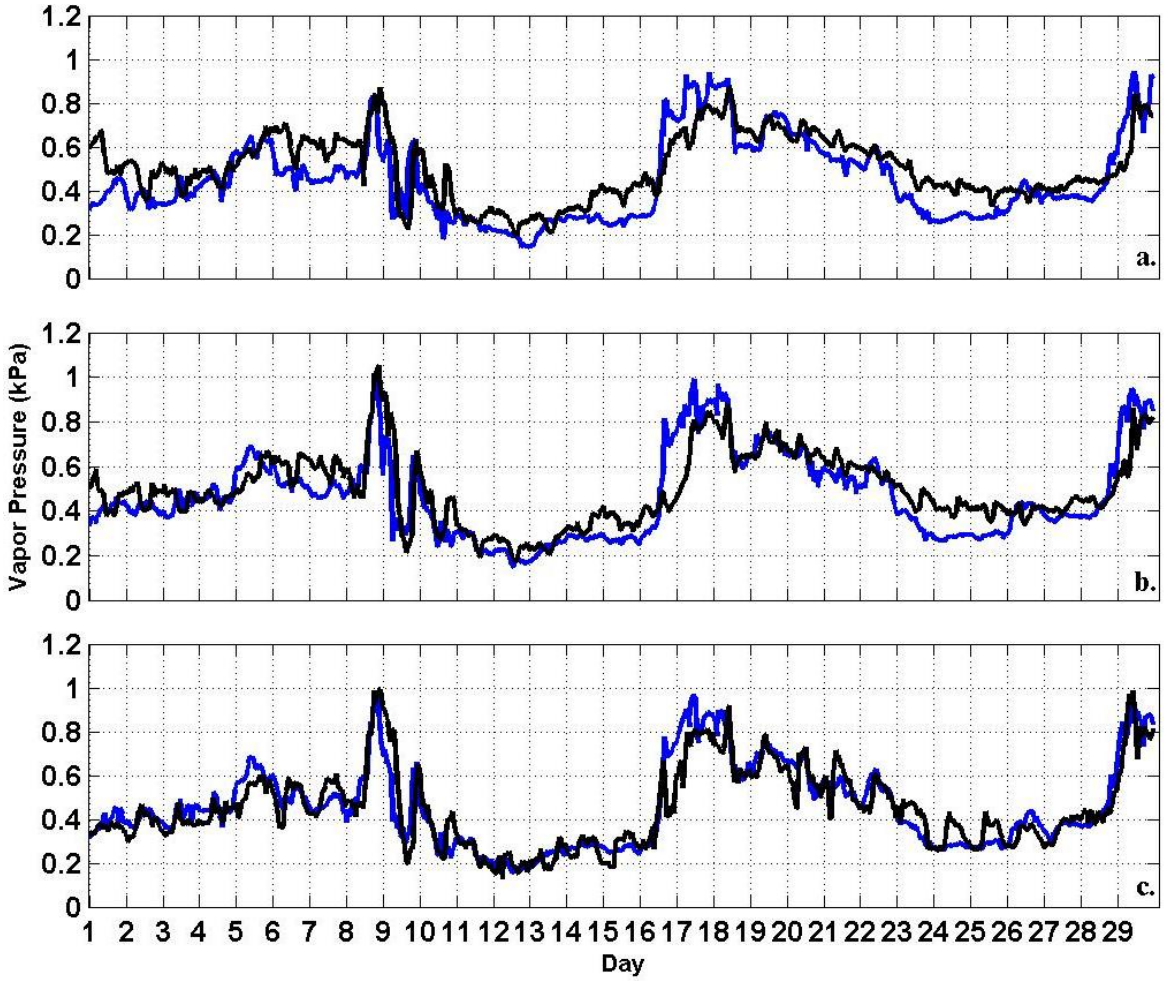

Fig. 34. Observed (black) and LSM (blue) time series of e_a for November 2012 at the rural site locations (Appendix A) of (a) Indian Springs, (b) Mojave Desert Shrub, and (c) Yucca Gap. Daily tick marks on the x-axis represent 00 LST.

4.2 Single-Layer and Multi-Layer UCMs

Simulated T2m biases of urban stations for LSM, UCM1, and UCM2 are shown in Figure 35. In general, all simulations behave similarly, with the models underestimating the amplitude of the diurnal cycle showing warm biases during the nighttime and cold biases during the day. Rural simulations in Figure 36 show similar biases with the exception of Indian Springs (Fig. 36a) influenced by a small urban

community nearby. Of note is that bias patterns are somehow controlled by the synoptic conditions, with warmer biases occurring during dry days and less warm or even cold biases during the wet spells (cloudy conditions).

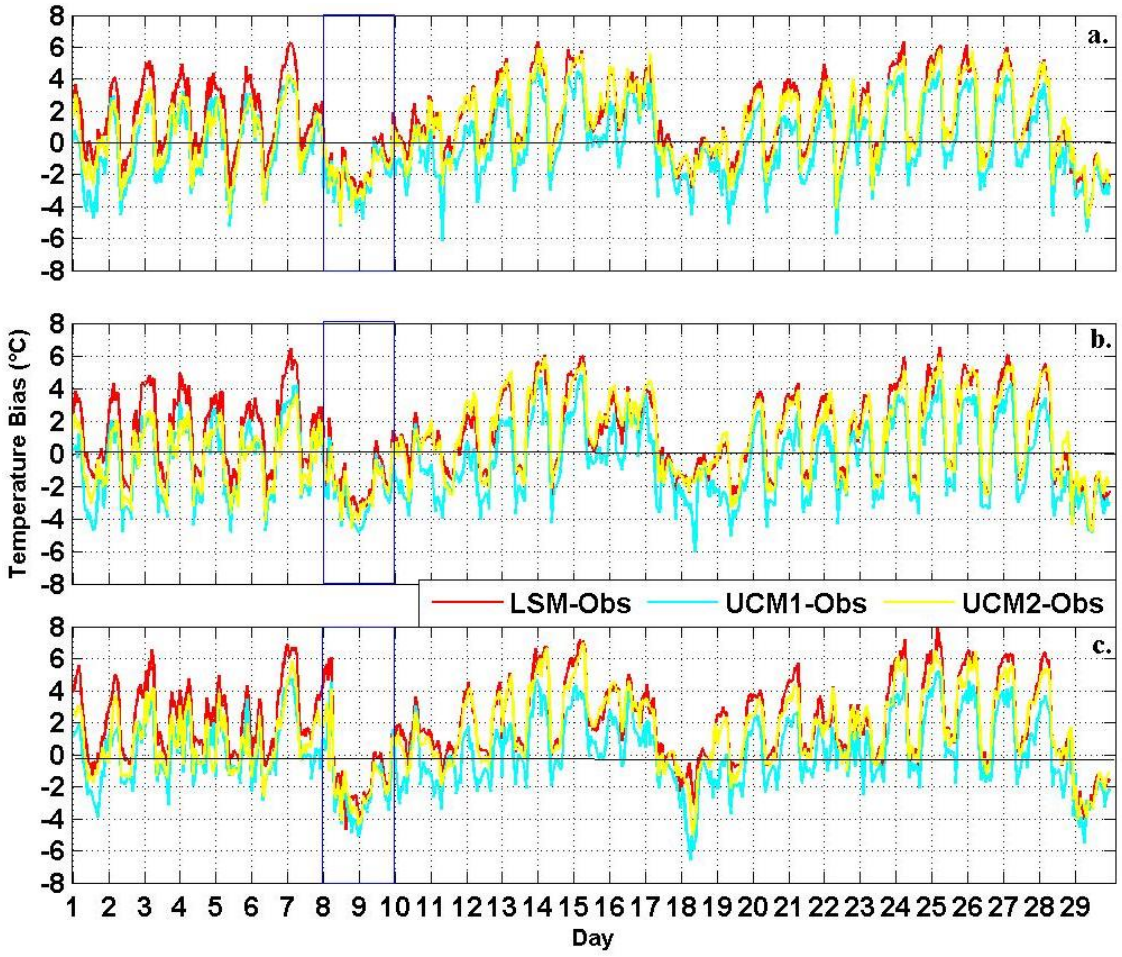

Fig. 35. Time series of T2m biases for November 2012 at the urban site locations (Appendix A) of (a) McCarran, (b) Las Vegas, and (c) West. The blue rectangle represents the time of the cold sink.

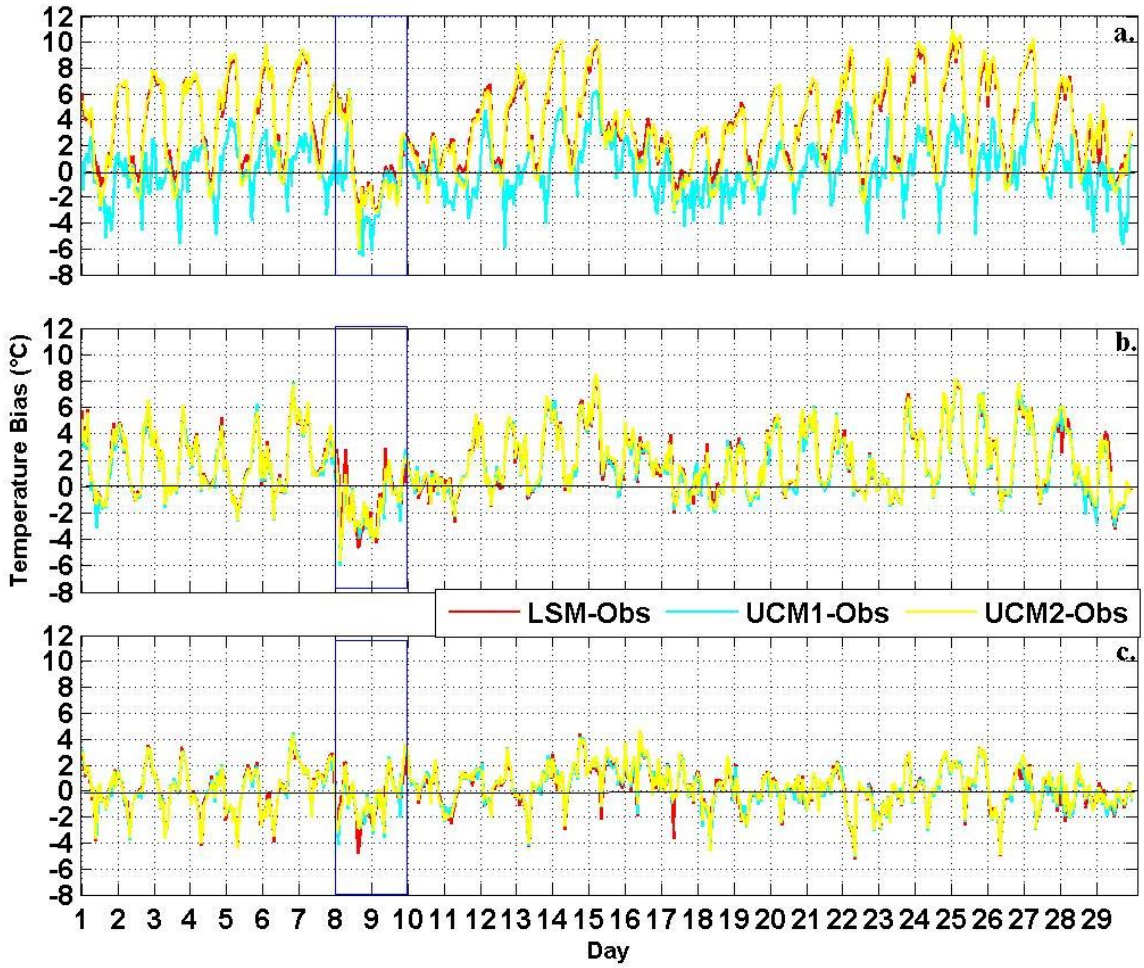

Fig. 36. Time series of T2m biases for November 2012 at the rural site locations (Appendix A) of (a) Indian Springs, (b) Mojave Desert Shrub, and (c) Yucca Gap. The blue rectangle represents the time of the cold sink.

Figure 37 shows the T_{max} and T_{min} spatial differences between LSM, UCM1, and UCM2 simulated outputs. Not surprisingly, the largest differences are located over urban LULC categories, while the smallest differences are outside the city. Of note is that for grid points marked as non-urban, all model configurations follow the same LSM procedure (Noah model). However, all differences in rural regions are associated with the propagation of differences on the outlined urban treatments. In general, results show that the LSM tends to simulate warmer urban T2m with T_{min} more sensitive across the models

relative to T_{max}. These results agree with Kusaka et al. (2001) who showed that different UCM treatments on urban radiation fluxes tend to diverge during the nighttime. The largest differences appear to be related to low-intensity urban categories.

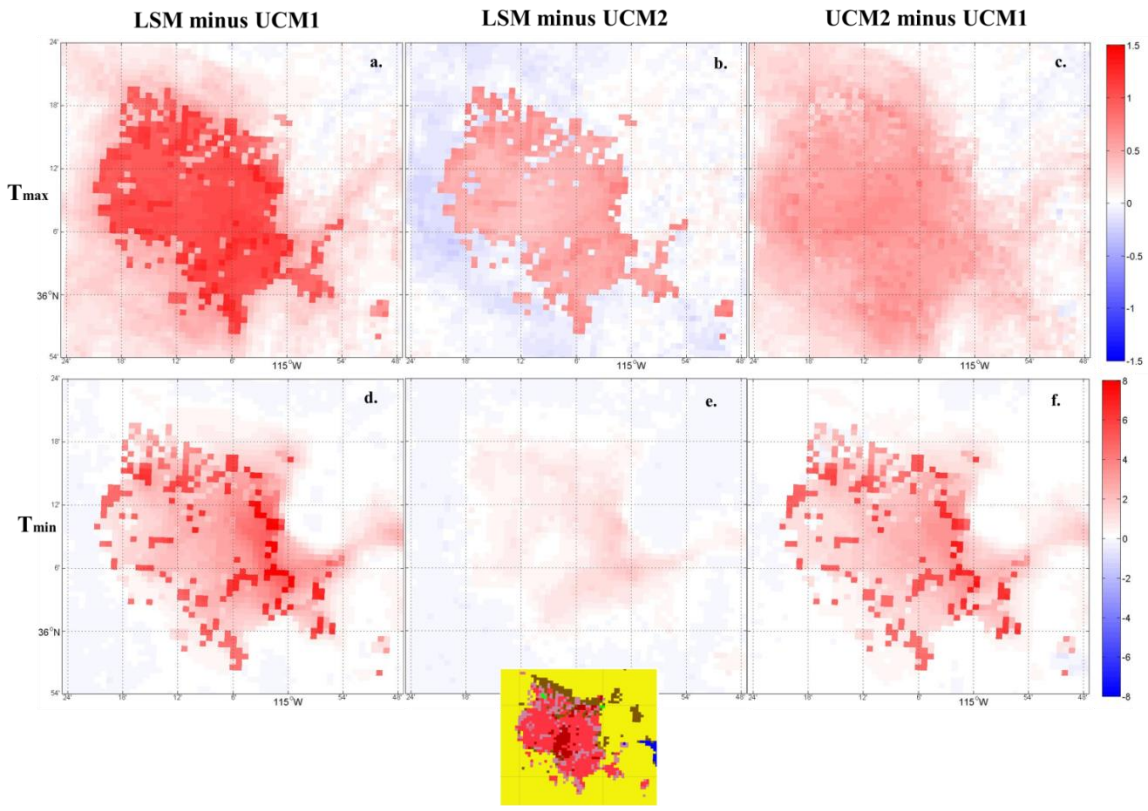

Fig. 37. Simulated outputs for T_{max} (top row) and T_{min} (bottom row) pertaining to the differences of (a, d) LSM minus UCM1, (b, e) LSM minus UCM2, and (c, f) UCM2 minus UCM1. The inset map shows the urban LULC based on Figure 5.

4.3 No City (NC) Simulation and Simulated UHI/UCI (UHI_{sim}/UCI_{sim})

The ability of the models to simulate a UHI/UCI (hereafter defined UHI_{sim}/UCI_{sim}) is categorized by the difference of LSM, UCM1, and UCM2 minus the NC simulation. Figure 38 shows the spatial T_{max} and T_{min} of the UHI_{sim}/UCI_{sim}. Again, it

is expected that the largest differences fall within the city boundaries. In general, LSM shows very little to no difference for T_{max}, while both UCM1 and UCM2 show an UCI_{sim} over most of Las Vegas. According to the UCM1 and UCM2, the strongest UCI_{sim} effect appears to be related to the low-intensity urban development. For T_{min}, all models show an UHI_{sim}. However, the UCM1 simulation shows strong cool patches over the low residential areas with little sensitivity, relative to LSM and UCM2 elsewhere. Recalling Table 3, the UCM2 simulations match up quite well and compliment the high-intensity space against McCarran observations for SON with a UHI and UCI bias of ~-0.5°C and ~-0.35°C, respectively.

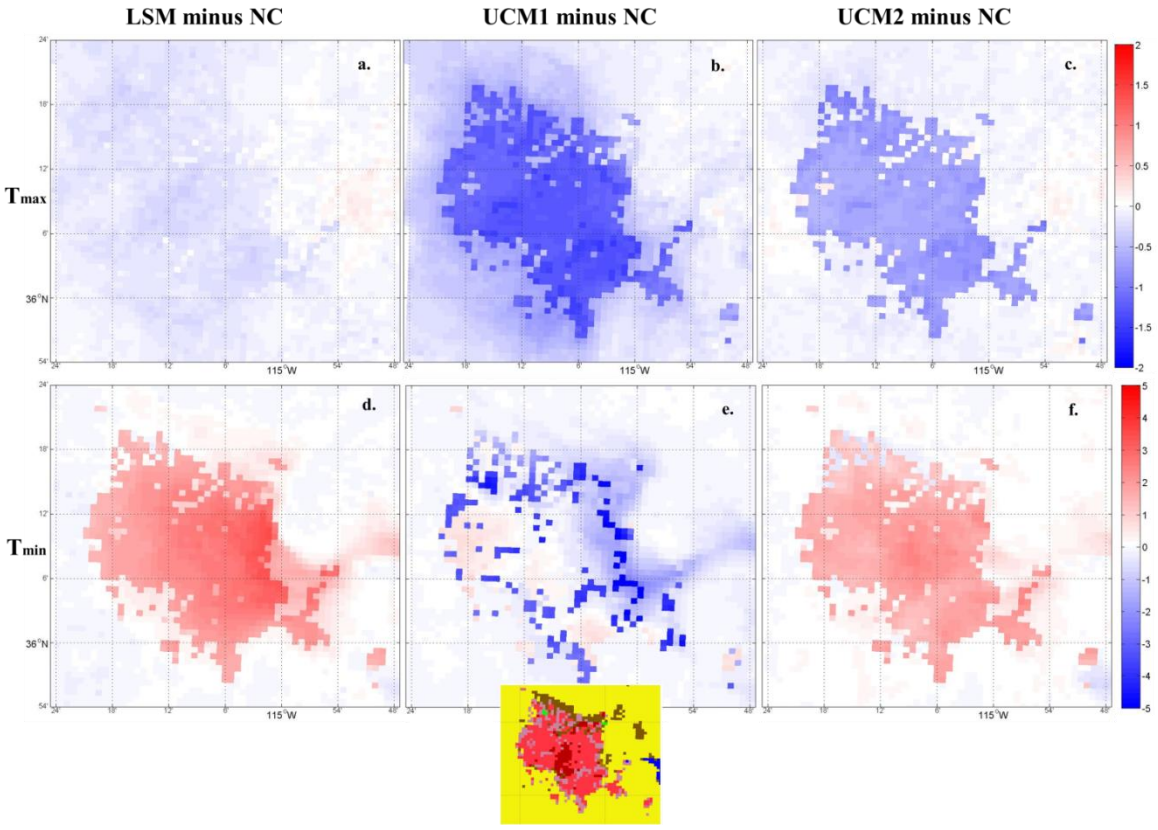

Fig. 38. Simulated outputs for T_{max} (top row) and T_{min} (bottom row) pertaining to the differences of (a, d) LSM minus NC, (b, e) UCM1 minus NC, and (c, f) UCM2 minus NC. The inset map shows the urban LULC based on Figure 5.

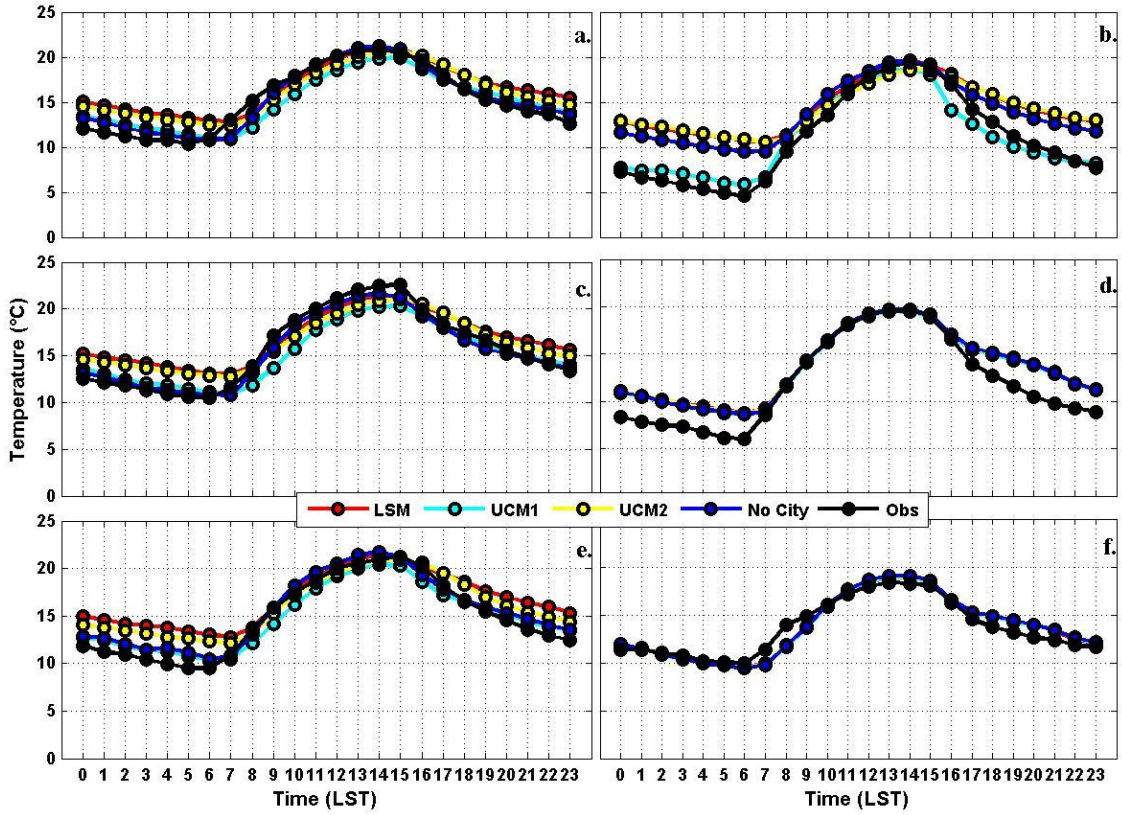

Fig. 39. T2m diurnal cycle for November 2012 of observations (black) and simulations. Model outputs include the LSM (red), UCM1 (cyan), UCM2 (yellow), and NC (blue). Site locations (Appendix A) in the figure are: (a) McCarran, (b) Indian Springs, (c) Las Vegas, (d) Mojave Desert Shrub, (e) West, and (f) Yucca Gap.

Figure 39 show both observed and simulated T2m diurnal cycles. In general, the simulations have close resemblances to the observed diurnal cycles over urban areas, with UCM1 having the most accurate simulations among the urban modeling. Simulations of the diurnal cycle accommodates similar results to Lin et al. (2008), with underestimates during daytime and overestimates during the early morning for T2m. Simulations over rural sites follow similar T2m diurnal patterns due to the rural grid points following the Noah-LSM procedures as previously mentioned. NC simulations

have the largest range among urban simulations clarifying the impact the urban environment has over rural desert land as it suppresses the diurnal range. Additionally, NC simulations for urban sites show a slight change for T_{min} which appears to occur one hour later relative to observations.

4.4 Moisture Parameters and UHI_{sim}/UCI_{sim}

4.4.1 Moisture Results from the LSM and UCMs

Figure 40 shows the month-long bias patterns of simulated e_a for urban stations. For urban sites, the models had a tendency to underestimate e_a for most of the month. Day-to-day variability associated with synoptic activity, for example the 8-11 November cold front, was simulated well. In contrast, the rural sites (Fig. 41) have the largest biases in e_a during the same cold front, showing that there was minor delay in the models during that moisture surge. Of note are the simulated e_a anomalies on November 14, 24, and 25 at Indian Springs for UCM1 simulations (Fig. 41a). These artifacts occur at 1500 LST and on days that do not show significant moisture surges. The e_a anomalies are associated with the T2m drop from 1500 to1600 LST (Fig. 39b). Among the three anomalous days, the T2m drops 5.58°C on average between 1500 and 1600 LST for the UCM1 simulations.

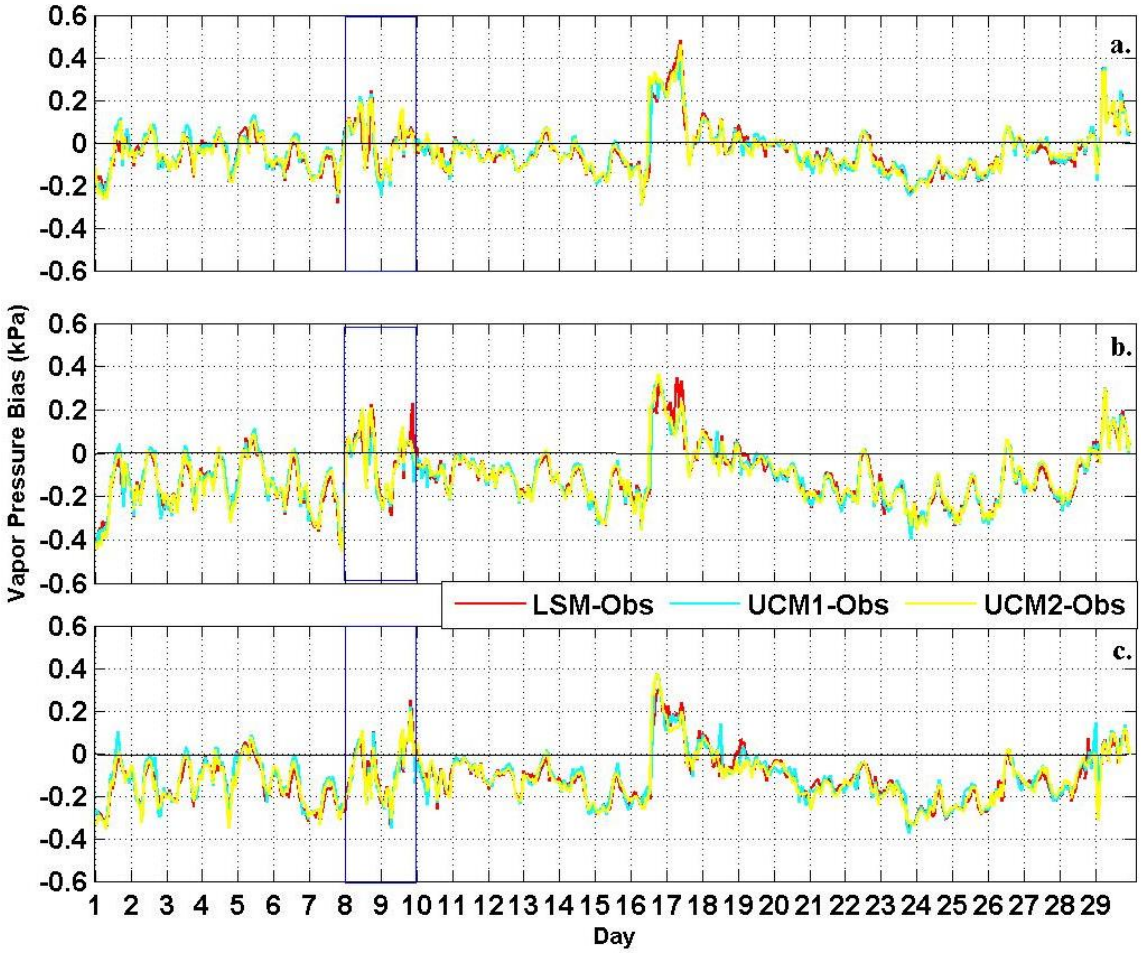

Fig. 40. Time series of e_a biases for November 2012 at the urban site locations (Appendix A) of (a) McCarran, (b) Las Vegas, and (c) West. The blue rectangle represents the time of the cold spell shown in Figure 35.

Figure 42 shows the RH mean diurnal cycle for the month of November 2012. The RH is best simulated during 1000-1600 LST. Nighttime/morning RH is underpredicted at urban sites along with Indian Springs and Mojave Desert Shrub, which is consistent with the overprediction in T2m. Given the same amount of moisture, warm nighttime biases would consistently simulate low RH. Rural simulations had different results in regards to simulating observations. The Indian Springs (Fig. 42b) simulated artifact at 0700 LST is surprising, however RH from UCM1 has been producing more

anomalous features (e.g. noise) than the LSM and UCM2. Over urban sites, the simulated RH_{max} offsets 1-2 hours earlier, while the daytime RH_{min} is accurately simulated by all models. Of note is that nighttime NC and UCM1 simulations agree better with observations. Yucca Gap has the closest agreement to observations, and slightly over predicts RH in the nighttime/morning hours. It is difficult to argue that rural sites generally have more skill in surface parameters compared to urban. However, the addition of the UCMs or LULC associated with urban areas appears to be in detrimental to the statistical results presented here. As expected the RH diurnal cycle inversely follows the diurnal cycle for T2m in Figure 39, which validates their relationship to be robust when simulated.

Simulated differences of e_{a_day} and e_{a_nm} between LSM, UCM1, and UCM2 are shown in Figure 43. As mentioned earlier, grid points marked as rural sites follow the same LSM procedure (Noah model) and any differences between models over rural areas are presumed to be related to the propagation effect of the urban environment cascading into the region. T2m results presented in Figure 37 have a few similar features to e_a outputs regarding the spatial activity. UCM1 simulates the most moisture for urban e_{a_day} values with significant differences between urban categories. Low-intensity urban categories show the largest (wettest) simulated values for UCM1. Other than the low-intensity urban pixels, there is not much difference in other urban categories when comparing the models for e_{a_day}. Aside from a few miscellaneous pixels, there is no strong significance of e_{a_nm} between the models as well.

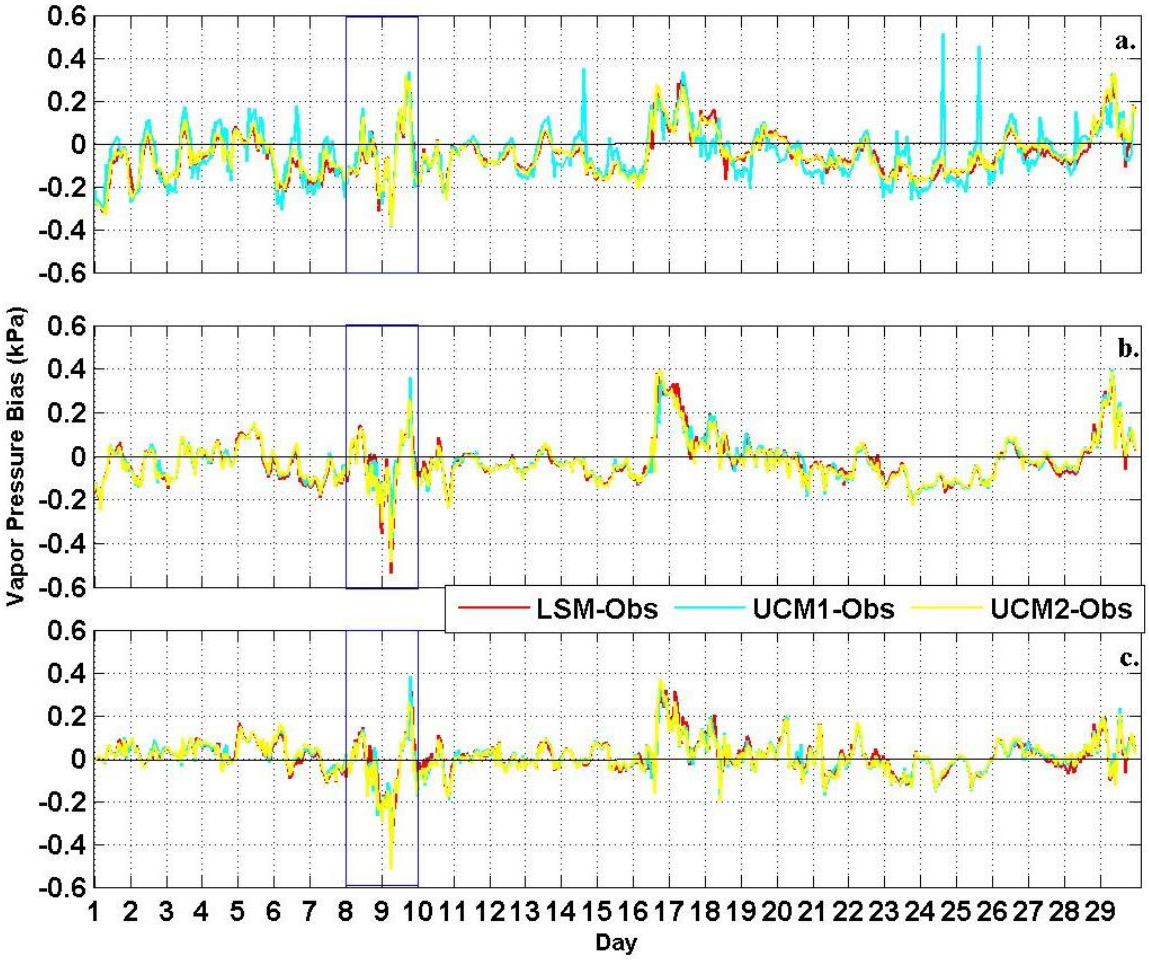

Fig. 41. Time series of e_a biases for November 2012 at the rural site locations (Appendix A) of (a) Indian Springs, (b) Mojave Desert Shrub, and (c) Yucca Gap. The blue rectangle represents the time of the cold spell shown in Figure 36.

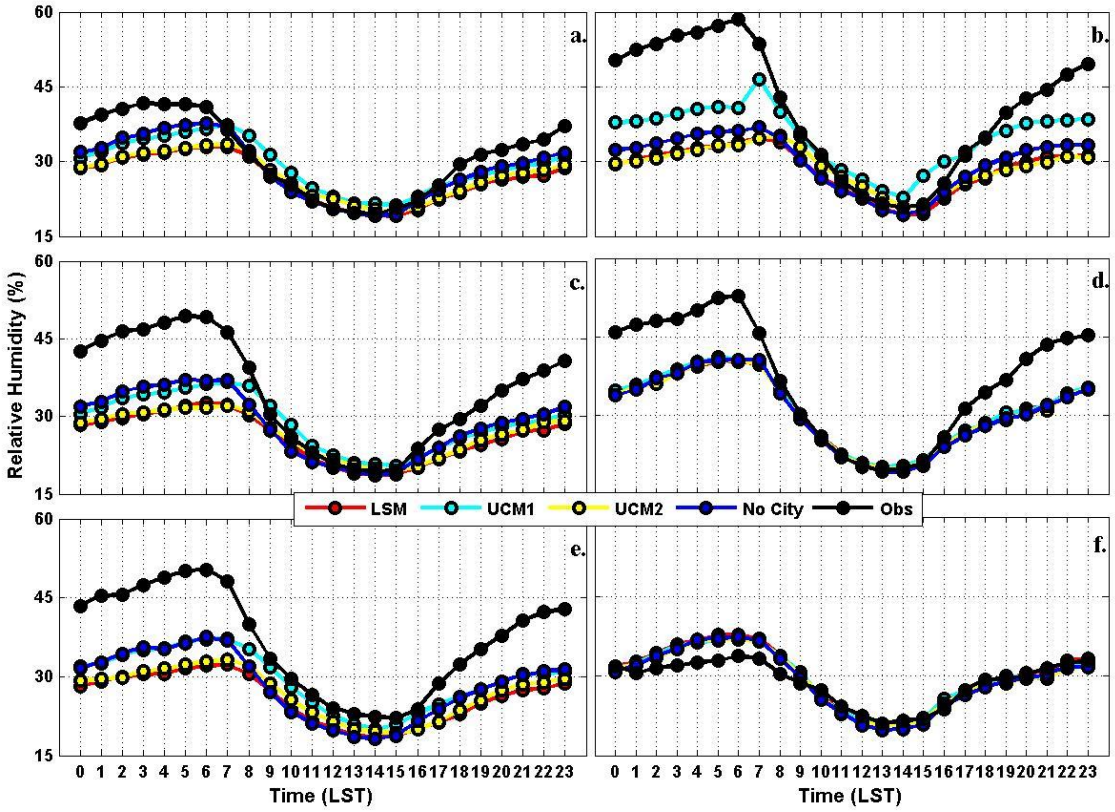

Fig. 42. RH diurnal cycle for November 2012 of observations (black) and simulations. Model outputs include the LSM (red), UCM1 (cyan), UCM2 (yellow), and NC (blue). Site locations (Appendix A) in the figure are: (a) McCarran, (b) Indian Springs, (c) Las Vegas, (d) Mojave Desert Shrub, (e) West, and (f) Yucca Gap.

Figure 44 shows the spatially simulated e_{a_day} and e_{a_nm} minus NC simulations. UCM1 best highlights the features of e_a as downtown Las Vegas and high intensity sites have the driest simulations. The LSM shows minimal e_{a_day} effects, and is about as insignificant as the UCI_{sim}. UCM2 highlights the similar activity as UCM1, however the spatial features are not as strong as there is smaller differences against the NC simulation. Smaller differences throughout the city are shown for e_{a_nm} which are mostly negligible towards the LULC classifications. In general, the spatial effects show specifics of the

Δe_{a_day} McCarran results (specifically UCM1) with UHI_{sim} intensity leading to drier mornings.

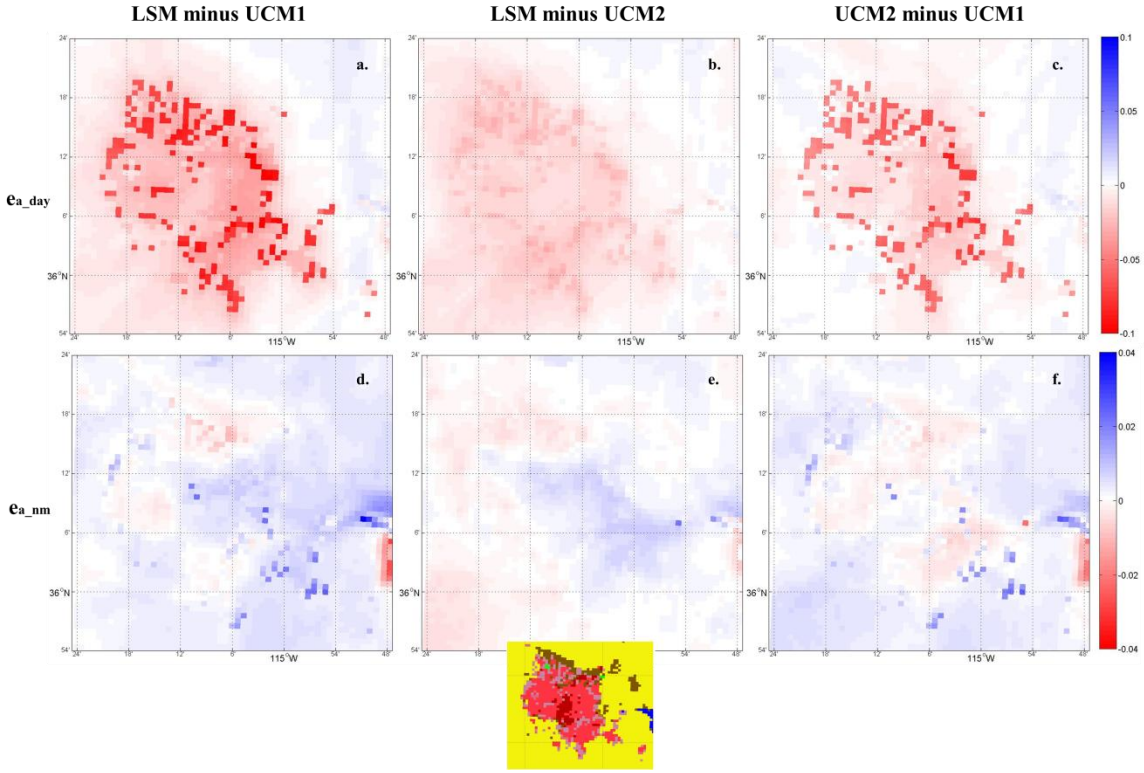

Fig. 43. Simulated outputs for e_{a_day} (top row) and e_{a_nm} (bottom row) pertaining to the differences of (a, d) LSM minus UCM1, (b, e) LSM minus UCM2, and (c, f) UCM2 minus UCM1. The inset map represents the urban LULC from Figure 5.

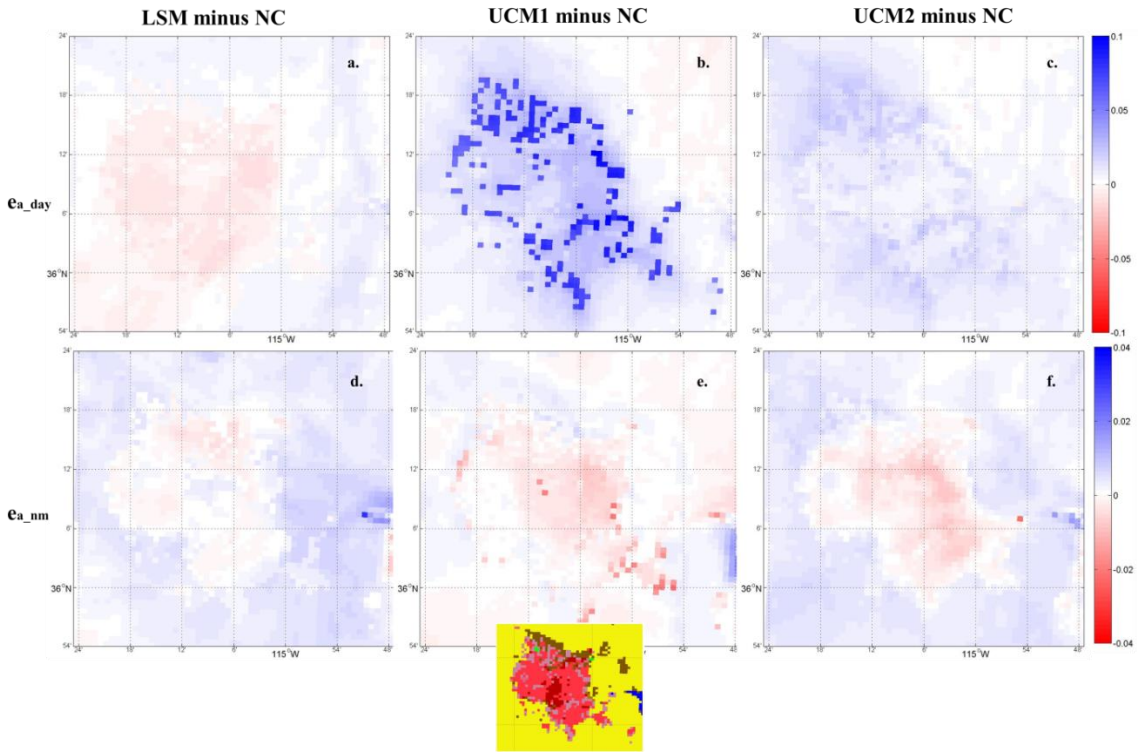

Fig. 44. Simulated outputs for e_{a_day} (top row) and e_{a_nm} (bottom row) pertaining to the differences of (a, d) LSM minus NC, (b, e) UCM1 minus NC, and (c, f) UCM2 minus NC. The inset map shows the urban LULC based on Figure 5.

4.4.2 UHI_{sim} and UCI_{sim} at McCarran

Figure 45 shows the November 2012 UHI_{sim} and UCI_{sim}, simulated RH, simulated zonal (U) winds, and observed cloud coverage for McCarran. McCarran was chosen as UCM1 and UCM2 showed the warmest activity in the core of Las Vegas during T_{min} when subtracted from NC. Periods with relatively less simulated cloud coverage was determined as clear sky (0-1/10th coverage), scattered (1/10th-5/10th coverage), broken (5/10th-9/10th coverage), and overcast (full coverage). The U wind is positive moving eastward and negative when moving westward. Daily results of cloud coverage with UHI_{sim} and UCI_{sim} are available in Appendix D.

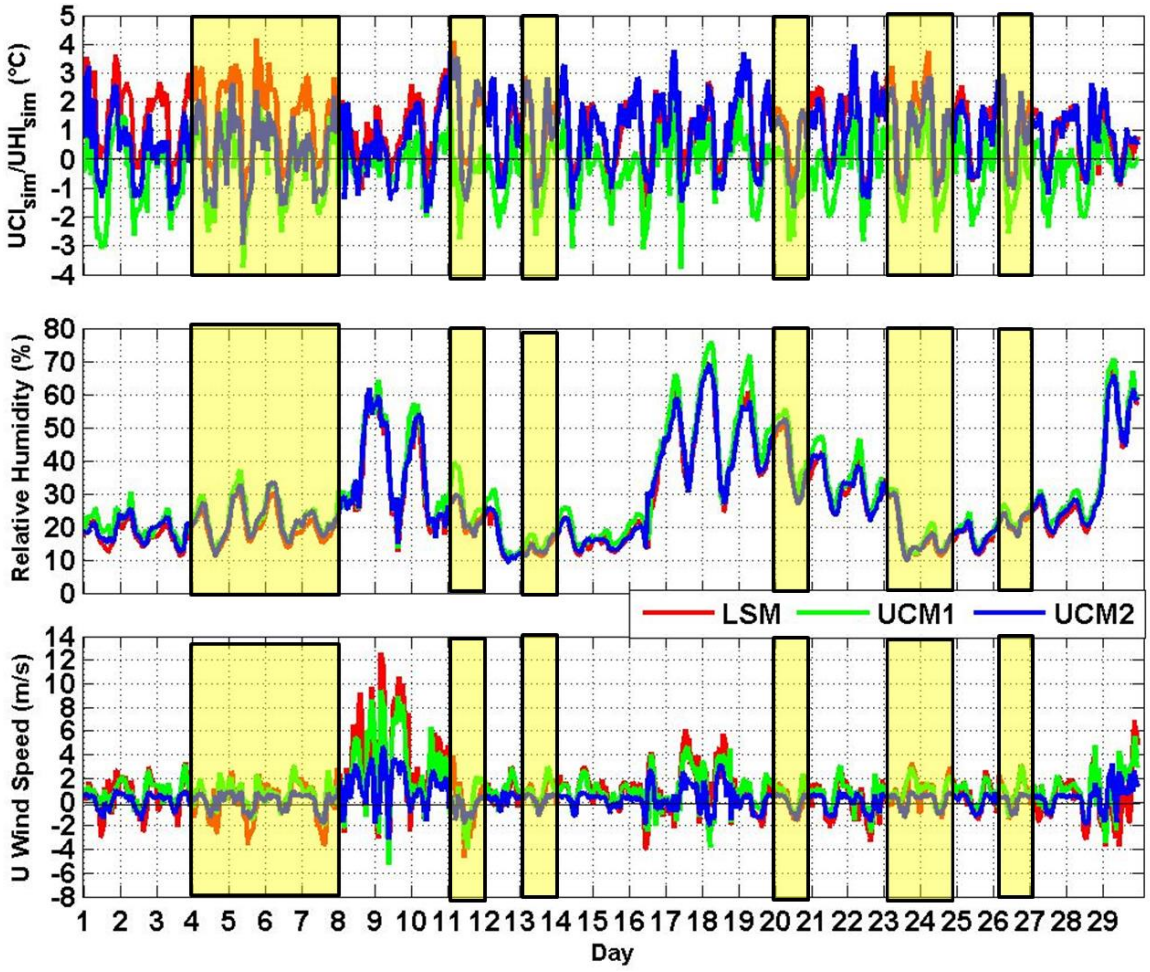

Fig. 45. The simulated November, 2012 evolution of UHI_{sim} (positive values) and UCI_{sim} (negative values) or [LSM, UCM1, and UCM2] minus NC (top panel), RH (middle panel), and U wind component (bottom panel). Simulated outputs include the LSM (red), UCM1 (green), and UCM2 (blue). The yellow shaded boxes show the days with dominant clear skies.

UHI_{sim}/UCI_{sim} appears to be stronger during days of clear skies, light winds, and low RH (Figure 45). The LSM shows more intense UHI_{sim} activity while the UCM1 shows the strongest UCI_{sim} activity throughout the month. All the simulations show weaker UHI_{sim} and UCI_{sim} activity during the cold front passage (November 8-9) that

highlighted enhanced westerly winds and RH. Cloud coverage was mostly scattered and broken with a slight period of overcast during this cold spell (Appendix D).

UCM2 had the strongest UHI_{sim} intensity during the RH surge from November 17-19. UHI intensity can increase when outgoing radiation becomes trapped from atmospheric water vapor (Neelin, 2011). Winds slightly increased during that period to 6 m s^{-1}. Though there is not a clear relationship of UHI_{sim} and winds, results show that UHI_{sim} tends to decrease only for days with significantly stronger winds. These results agree with the observations of Fast et al. (2005) who argued that the UHI in downtown Phoenix was not significantly modulated for winds under 7 m s^{-1}.

4.5 Statistical Results of the Models

In this section the confidence of the models is evaluated by using the bias, root-mean-square error (RMSE), and the correlation coefficient of T2m, RH, and e_a parameters. An evaluation is performed using all surface stations available (Chapter 2.1) that are composited by major rural and urban LULC categories.

Table 8, 9 and 10 show the results by model configuration and by LULC categories for the bias, RSME, and correlation coefficient ("error") statistics, respectively. Overall, UCM1 stands out as the model with better error statistics across the various LULC categories and parameters. Interestingly, UCM1 was relatively weak on simulating RH for stations with barren LULC. This may largely be due to the observed error from a WU station (NORTH6) where simulations had RH biases over 10%. The other barren sites had a 4-7% less bias RH difference.

Table 8. T2m (RH) [e_a] biases for LSM, UCM1, UCM2, and NC categorized by LULC.

LULC	LSM	UCM1	UCM2	NC
High Intensity	1.14°C (-6.87%) [-0.08 kPa]	-0.42°C (-4.05%) [-0.07 kPa]	0.73°C (-6.23%) [-0.08 kPa]	-0.07°C (-4.52%) [-0.08 kPa]
Medium Intensity	2.04°C (-12.35%) [-0.14 kPa]	0.50°C (-9.45%) [-0.14 kPa]	1.66°C (-11.72%) [-0.14 kPa]	1.07°C (-10.55%) [-0.14 kPa]
Low Intensity	1.35°C (-6.86%) [-0.07 kPa]	-0.35°C (-3.47%) [-0.06 kPa]	1.10°C (-6.25%) [-0.07 kPa]	0.64°C (-5.55%) [-0.07 kPa]
Barren	1.14°C (-0.60%) [0.02 kPa]	0.12°C (1.32%) [0.02 kPa]	0.83°C (0.02%) [0.02 kPa]	0.87°C (-0.14%) [0.02 kPa]
Shrub	1.29°C (-5.15%) [-0.03 kPa]	0.87°C (-5.23%) [-0.03 kPa]	1.30°C (-6.04%) [-0.03 kPa]	1.26°C (-6.17%) [-0.04 kPa]
Evergreen Forest	-0.19°C (-3.57%) [-0.04 kPa]	-0.16°C (-3.92%) [-0.04 kPa]	-0.17°C (-3.76%) [-0.04 kPa]	-0.15°C (-4.07%) [-0.04 kPa]
Average	**1.13°C** **(-5.90%)** **[-0.06 kPa]**	**0.09°C** **(-4.13%)** **[-0.05 kPa]**	**0.91°C** **(-5.66%)** **[-0.06 kPa]**	**0.60°C** **(-5.17%)** **[-0.06 kPa]**

The UCM2 has smaller T2m biases than the LSM, but performed similar for the non-urban stations. UCM2 had an average RH bias of 0.02% for barren land, which is misrepresented by the large positive RH bias from the WU network (~10.51%) in response to averaging smaller negative biases into the calculation. The correlation coefficients for RH are moderate-to-strong and have an overall range from 0.65-0.80 with the strongest accounting for barren land and evergreen forest. The high and medium urban intensities have the lowest RH correlation. T2m correlations are strongest for barren land and are no less than 0.86 overall. UCM1 has the strongest correlations among the urban models followed by both LSM and UCM2.

Table 9. T2m (RH) [e_a] RSMEs for LSM, UCM1, UCM2, and NC categorized by LULC.

LULC	LSM	UCM1	UCM2	NC
High Intensity	2.71°C (12.56%) [0.14 kPa]	2.39°C (11.58%) [0.14 kPa]	2.52°C (12.06%) [0.14 kPa]	2.00°C (11.48%) [0.14 kPa]
Medium Intensity	3.37°C (16.78%) [0.20 kPa]	2.55°C (14.79%) [0.19 kPa]	3.13°C (16.30%) [0.19 kPa]	2.50°C (15.40%) [0.20 kPa]
Low Intensity	2.91°C (11.77%) [0.13 kPa]	2.36°C (10.36%) [0.13 kPa]	2.88°C (11.45%) [0.13 kPa]	2.41°C (11.18%) [0.14 kPa]
Barren	2.47°C (11.87%) [0.15 kPa]	2.09°C (11.55%) [0.15 kPa]	2.36°C (11.58%) [0.15 kPa]	2.40°C (12.05%) [0.16 kPa]
Shrub	3.13°C (13.23%) [0.10 kPa]	2.85°C (12.70%) [0.10 kPa]	3.14°C (13.14%) [0.10 kPa]	3.05°C (13.23%) [0.11 kPa]
Evergreen Forest	2.74°C (12.74%) [0.08 kPa]	2.74°C (12.79%) [0.09 kPa]	2.74°C (12.65%) [0.09 kPa]	2.73°C (12.75%) [0.09 kPa]
Average	**2.88°C (13.16%) [0.13 kPa]**	**2.50°C (12.30%) [0.13 kPa]**	**2.80°C (12.86%) [0.13 kPa]**	**2.52°C (12.68%) [0.14 kPa]**

Statistical significances for e_a show less error than RH, with the best correlation in the rural sections (i.e. shrub and evergreen forest). For biases, e_a agrees with the other parameters on having the smallest differences in the barren area. For urban classifications, e_a has the largest RMSE and bias for medium intensity, while high- and low-intensity areas have similar statistical results. The correlation coefficient of e_a is moderately strong, and similar among models and LULC categories that range between 0.84-0.88.

Although the error statistics of NC simulations were more exceptional than UCM2 and LSM, the diurnal range for all models were systematically smaller than the

observations, resulting in NC simulations comparing better against observations. By following the UHI concepts, the LSM, UCM1, and UCM2 successfully capture a UHI effect relative to the NC simulation.

Table 10. T2m (RH) [e_a] correlation coefficients for LSM, UCM1, UCM2, and NC categorized by LULC.

LULC	LSM	UCM1	UCM2	NC
High Intensity	0.90 (0.68) [0.85]	0.91 (0.69) [0.85]	0.91 (0.68) [0.85]	0.93 (0.72) [0.85]
Medium Intensity	0.88 (0.65) [0.84]	0.90 (0.67) [0.84]	0.88 (0.65) [0.84]	0.91 (0.69) [0.84]
Low Intensity	0.88 (0.76) [0.87]	0.91 (0.77) [0.86]	0.87 (0.75) [0.87]	0.91 (0.77) [0.86]
Barren	0.92 (0.77) [0.84]	0.94 (0.80) [0.85]	0.93 (0.79) [0.85]	0.92 (0.78) [0.83]
Shrub	0.88 (0.74) [0.88]	0.89 (0.74) [0.87]	0.88 (0.74) [0.87]	0.89 (0.74) [0.87]
Evergreen Forest	0.87 (0.79) [0.88]	0.87 (0.79) [0.88]	0.86 (0.79) [0.88]	0.87 (0.79) [0.88]
Average	**0.89** **(0.73)** **[0.86]**	**0.90** **(0.74)** **[0.86]**	**0.89** **(0.73)** **[0.86]**	**0.91** **(0.75)** **[0.86]**

4.6 White Roofing Scenario

The albedo was increased from 0.20 to 0.65 for rooftops in the city to simulate a mitigation method of white roofing. This particular scenario was simulated with UCM1. The exercise to increase the albedo was performed to evaluate the model's response to UHI adaptation and mitigation efforts to reduce in-city temperature (e.g. Gaffin et al.

2012; Jacobson and Ten Hoeve, 2012). To find how much cooler T2m would be in the city, the albedo simulation was simply subtracted from the T2m simulation of UCM1.

Figure 46 shows the spatial distribution changes in T2m from increasing the albedo. T_{max} within the city decreased ~1°-2°C in areas not containing open space or barren land which only decreased < 0.5°C. T_{min} also decreases, but with very little effect in comparison to T_{max}. There is not an obvious relationship of cooling due to white roofing for LULC categories. However, effects appear to be stronger in East Las Vegas.

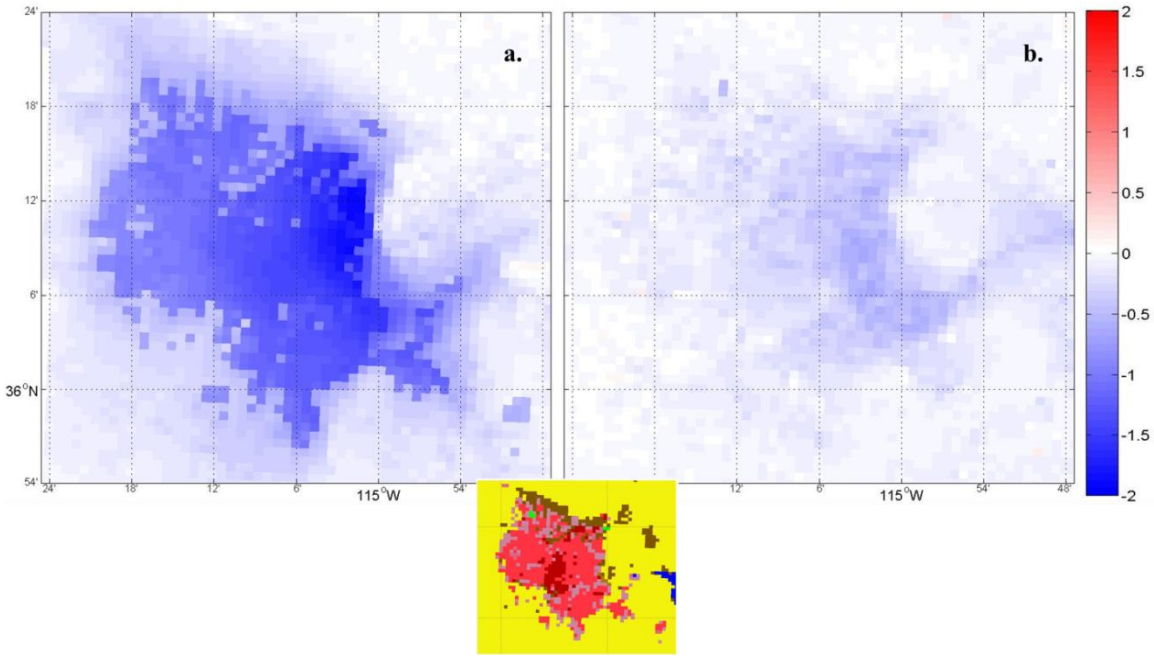

Fig. 46. The (a) T_{max} and (b) T_{min} changes (relative to UCM1) from increasing the albedo ("white roofing"). The inset map shows the urban LULC based on Figure 5.

Figure 47 shows that increasing the albedo only has a significant effect on cooling daytime (0900-1700 LST) temperatures over the city, and in return increasing daytime RH by ~5% in some areas (Figure 48). The increasing effect of RH is driven by T2m decreasing as this lowers e_s instead of increasing moisture. Table 11 displays UCM1 and the albedo simulated T_{max} along with the difference of UCM1 minus albedo. According to the simulations, increasing the albedo from 0.2 to 0.65 can decrease daytime temperatures by over 1°C in Las Vegas. Recall that this simulation was done for November 2012, and values are subject to be dissimilar under wetter conditions and changing of seasons. Furthermore, this simulation does not account for changes in energy use and emissions from white roofing that can further alter T2m. Rural sites do not show as strong of a response, even with smaller scale urban influences as Indian Springs cooled only by 0.43°C.

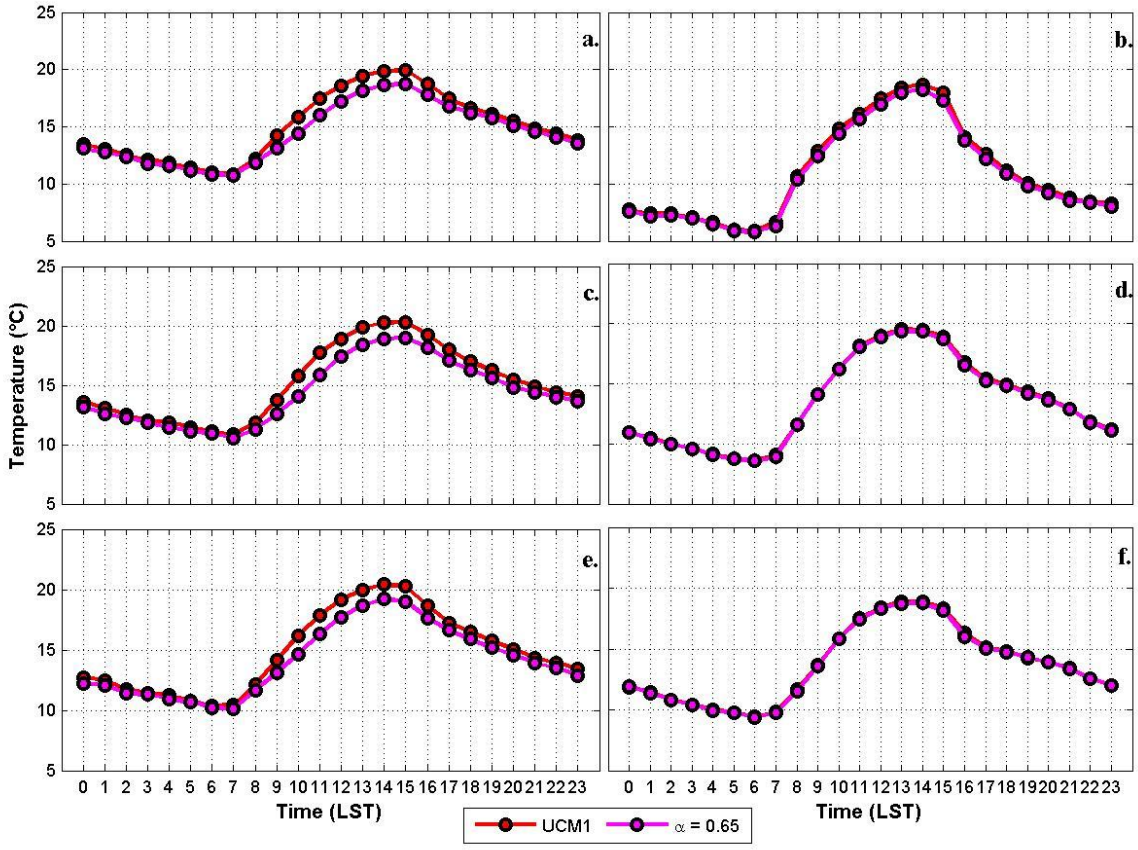

Fig. 47. Simulated diurnal cycle of T2m for UCM1 and increased albedo (α) for November 2012. Stations analyzed are: (a) McCarran, (b) Indian Springs, (c) Las Vegas, (d) Mojave Desert Shrub, (c) West, and (f) Yucca Gap.

Table 11. T_{max} of the diurnal cycle (Fig. 47) for the UCM1 and albedo simulations. The differences show the simulated effect "white roofing" has for each location.

Station	UCM1 T_{max}	$\alpha = 0.65$ T_{max}	UCM1-α
McCarran	19.90°C	18.73°C	1.17°C
Las Vegas	27.72°C	25.88°C	1.31°C
West	20.41°C	19.19°C	1.22°C
Indian Springs	18.69°C	18.26°C	0.43°C
Mojave Desert Shrub	19.52°C	19.36°C	0.16°C
Yucca Gap	18.91°C	18.76°C	0.15°C

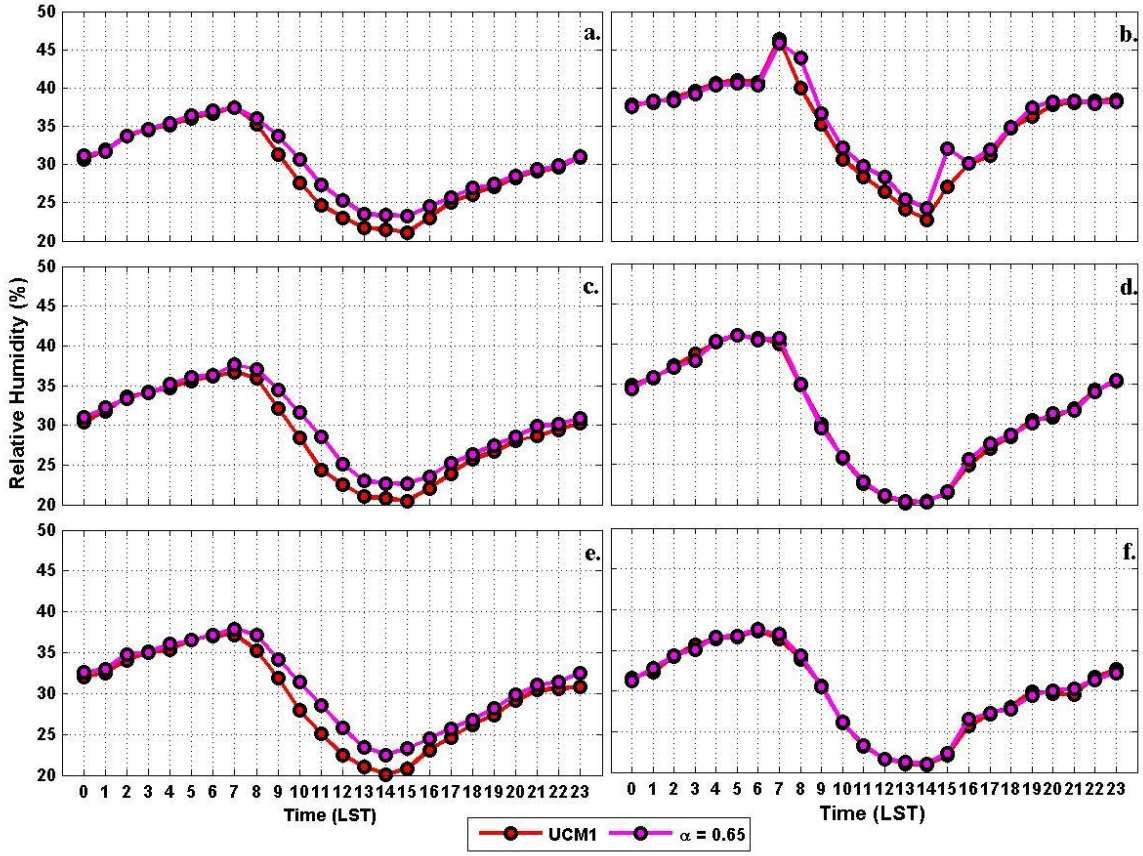

Fig. 48. Simulated diurnal cycle of RH for UCM1 and increased albedo (α) for November 2012. Stations analyzed are: (a) McCarran, (b) Indian Springs, (c) Las Vegas, (d) Mojave Desert Shrub, (c) West, and (f) Yucca Gap.

5. Discussion

5.1 In-City versus Regional Long-Term Trends

For the region of Southern Nevada, there is a marked warming trend in T_{min} with relatively small warming trends in T_{max}, which to some extent relate to the Las Vegas urban expansion and the UHI (Guhathakurta and Gober, 2010; Major et al., 2011). Local climate change adaptation and mitigation strategies for Las Vegas recommends that planting trees and increasing green space and canopy coverage would alleviate the UHI

effect. Recent results from Black (2013) suggested that such adaptation strategies appear to have a positive impact in reducing UHI trends. However, the results presented in this research suggests the existence of regional/statewide temperature trends (Figs. 10 and 11) could have contributed to such in-city local changes. Only after isolating the global/regional climate trends can one argue local climate effects due to urban growth and any adaptation measures.

Xian (2008) analyzed McCarran T_{min} long-term data and estimated a warming trend of about 0.07°C/yr, which is fairly equivalent to the 61-year result (~0.68°C/decade) in Chapter 3.1. Using remote sensing tools, Xian (2008) suggested that high intensity urban areas are responsible for most warming trends, followed by medium- and low-intensity urban developments. Xian and Crane (2006) found daytime cooling primarily in low-intensity space, but from 1984 to 2002 the cooling effect had reduced. To some extent our analyses of observed T2m agree. Anomalous T2m shows a small increase in T_{max} from 1984 to 2002 for local and statewide trends (Figs. 8-11). However, T_{max} and T_{min} have currently been experiencing a slight cooling trend in relation to global teleconnection patterns (e.g. PDO). Xian and Crane (2006) concluded a daytime UCI of -0.84°C and -0.35°C for 1984 and 2002, respectively. Although our results show a daytime UCI of -0.15°C, it is important to note that these results were established through: a different and longer period of time, the removal of statewide trends, and from surface observations rather than remote sensing data. Xian (2008) suggests the daytime cooling effect of Las Vegas is contributed to trees, lawns, and other green areas in

contrast to the dry desert surroundings. We believe ET is the primary driver of daytime cooling in these particular LULC areas (Hart and Sailor, 2009).

After isolating the local in-city effect from the regional trends, this research showed that the Las Vegas T_{amp} has decreased through the past 50 years from urban growth. The declination of T_{amp} is a well-known effect of urban development in dry (Svoma and Brazel, 2010) and moist (Kim and Baik, 2005) climates. The urban development has also shown to shift T_{max} and T_{min} timing. In Phoenix, Svoma and Brazel (2010) found that T_{max} and T_{min} tend to occur about 1 hour earlier, which is presumably related to thermal inertia from in-city heat storage. This research found little evidence to support this claim, though the Nellis JJA and SON diurnal cycle composites (Fig. 16) suggest similar trends for Las Vegas in low-intensity urban zones. The extent to which this shifting effect in the diurnal cycle being solely attributed to local rather than regional changes has not been demonstrated.

The urban minus regional residual approach implemented here and the results from several observation methods (station based and GDPs) show high consistency in the UHI/UCI detection. The magnitudes of UHI and UCI varied with season, showing stronger UHI activity during DJF while UCI was most evident for MAM and JJA. Other major cities in the world have found that UHI is more intense during JJA due to increased solar radiation and the increase of electricity consumption from air conditioning (Oke, 1973; Kimura and Takahashi, 1991; Fast et al., 2005; Aguado and Burt, 2007; Lin et al., 2008). In Tokyo, however, the UHI appears to be more intense during DJF, presumably related to increased hotel occupation during the cold season (Ichinose et al. 1999). The

maximum UCI intensity found during MAM and JJA supports Chow and Svoma (2011) findings for Phoenix, who attributed such cooling to the increased urban vegetation relative to the surrounding desert. For Las Vegas, Nellis contributes to a larger UCI effect than McCarran. Reasons to such contributions may be partial to the high albedo of the surface and/or advection from the medium- and low-intensity areas outside of Nellis. However, based on the confidence interval between the 1950s and 2000s, daytime T2m changes were insignificant resulting in the UCI failing the significance test at 95%.

On another note, a proposition was created in 2003 to buy out Las Vegas residencies to remove their turf grass. Although this strategy was implemented to conserve water demand, it counteracts the actions suggested by researchers to combat the UHI threat by planting more vegetation in order to cool the city (HARC, 2009). Despite the heavy droughts experienced after 2000, Las Vegas showed positive residuals and regression for e_a and T_d, respectively. Regardless, it is possible that the city may be an example of a creeping environment as Lake Mead levels have severely plummeted since the drought in 2000 occurred, and interannual activity from global teleconnections became more fixed than in earlier decades. Furthermore, the frequency of negative PDO with positive AMO activity may have liberated the post-2000 drought.

The UHI/UCI activity has strong influence in the surface RH. Observations show that Las Vegas is experiencing a decrease in RH_{amp} via increasing daytime RH and decreasing nighttime/morning RH (Akindobe et al., 2008). Furthermore, the urban core is subjected to RH deficits due to less available vegetation (Mohan and Arumugam, 1996). In this research, long-term trends in T_d, K_o, and VPD were estimated as proxies for

moisture availability in Las Vegas. Trends from these parameters were not significant at the 95% confidence level which makes it difficult to determine if there are indeed strong moisture changes within the city. Hence, it is likely that RH observed changes that are merely related to temperature trends. Furthermore, using observed e_a to further explore moisture trends was difficult to establish as conservation practices of removing turf grass occurred during strong drought activity. What is certain is that Lake Mead levels have declined ~40 m through the millennium which poses a threat to Las Vegas, and signifies attention for water demands.

5.2 The CF Approach

To estimate observed spatial patterns in Las Vegas, an experimental CF based on the average temperature of Γ_e was estimated to reduce the temperatures from all observation sites to obtain a single reference altitude. Results were composited according to the predominant LULC category in their surroundings. From August 2012-April 2013 low-intensity urban areas showed larger T2m values. This may be partial to some of the low-intensity sites having open space (i.e. natural desert landscape within the city) that contains less vegetation. In addition, there were only two observed sites for high-intensity urban areas, which may be a misrepresentation compared to the sample sizes of low- and medium-intensity sites.

Nighttime/early morning drainage flows from surrounding sierras create significant limitations in applying this approach as cool air tends to concentrate over low-elevation areas (e.g. eastern LV). Further work should be performed to include such mountain-valley circulations in the spatial characterization of the UHI/UCI effect. This

work has shown that seasonality and synoptic effects can also be important factors. The CF method provided some aspect of UHI/UCI effect by showing smaller diurnal temperature ranges in the city, smaller UHI signals from cooler and wetter months that are consistent with long-term trend results presented here, and also as a function of LULC (e.g. high-intensity having the warmest T_{min}).

5.3 The GDP Results

GDPs were analyzed by averaging the data over three different regions: core, outer-core, and rural area defined in Chapter 2.2. T_{max} and T_{min} trends from January 1980-December 2011 have similar long-term variability to observations with T_{min} increasing and T_{max} having little effect in change. Differences were noticeable when calculating the overall trends. The core domain for PRISM 800 m showed a more intense warming trend than McCarran for T_{min}, while Daymet showed a more intense warming trend than Nellis for T_{max}. When comparing T_{max}, Daymet has a larger warming trend than PRISM 800 m, while PRISM 800 m has a more prominent T_{min} warming trend. Based on the warming differences of the observations and GDPs, the GDPs are likely to underpredict the UHI and UCI.

The sparseness of rural station siting and the complex topography creates challenges in the interpolations of GDPs (Daly, 2006). However, PRISM 800 m shows T_{min} warming trends confined to the in-city area, whereas Daymet lacks a coherent warming structure related to the Las Vegas urban development. The Daymet interpolation approach uses local linear regression to relate temperature to elevation without accounting for climate transitions that are terrain-induced (Daly, 2006). PRISM 800 m

accounts for mountain-valley circulations which could modulate T_{min} by incorporating the effect of cold air pooling, inversions, and other atmospheric boundary layer mechanisms. It is unknown whether LULC is considered in the interpolation procedures on the outlined GDPs.

5.4 The UCM as a Tool for Urban Climate Studies and LULC Scenarios

WRF-UCM models adequately simulate T2m, and its diurnal and day-to-day variability. The models were sensitive and showed intricate responses for urban LULC categories. Two high-intensity observed sites located in lower urban elevated zones were analyzed and simulated best among other in-city LULC categories. Miao et al. (2009) analyzed 11 high-intensity sites for Beijing that showed the smallest RMSEs for T2m compare to other LULC categories from UCM1 simulations. This agrees to some extent with the error statistics in Chapter 4.5 as UCM1 simulated the urban categories quite well.

In an attempt to simulate the effect of a city in an arid environment and their UHI and UCI characteristics, the urban modeled simulations were subtracted by the NC simulation. Urban simulations successfully produce a UHI_{sim} and simulated UCI_{sim}. Low-intensity pixels showed the most cooling during T_{max} while high intensity pixels showed the most warming during T_{min}. Lee et al. (2011) found the LSM to overestimate sensible heat flux which may be the reason for stronger UHI_{sim} intensity for T_{min}. UCI_{sim} was evident over the city for UCM1 and UCM2 simulations during T_{max}, while the LSM showed insignificant cooling. Although the LSM provides an urban bulk parameterization approach, it was originally designed to simulate natural surfaces, while

the UCM has been designed to treat man-made surfaces (Chen et al., 2011). Other researchers have found that the LSM, unmodified and without UCM treatment, is not reliable as it does not account for seemingly important processes such as: the urban vegetation and urban hydrological processes (Lee et al., 2011). Hence, the lack of latent heating for the urban environment can enhance the daytime sensible heat flux and fail to clearly simulate the intensity of the UCI_{sim}.

Results show less skill in simulating RH relative to T2m and e_a. Overall, all models showed negative RH biases with the largest over medium-intensity sites, and the smallest over barren sites. Yang et al. (2012) showed lower values of simulated RH over urban areas than rural areas for Nanjing, China. This held true for the nighttime results in Las Vegas. However, RH during the daytime was larger in the urban environment relative to surrounding rural areas according to the spatial analysis conducted in this research (figure not shown). UCM1 simulations in Tokyo by Kusaka et al. (2012) showed smaller biases (2.2%) and RMSE (7.8%) for RH when compared to the results in Chapter 4.5. However, WRF-UCM results can be synoptic, seasonal, and climate dependent which institutes simulated differences for a sensitive variable such as RH. It is also important to establish that the LULC surrounding Las Vegas vastly differs from cities similar to Nanjing or Tokyo. Furthermore, the simulations from this research are conducted well above sea level without a strong influence of sea breeze. In addition, other grid and model configurations, including selection of PBL, microphysics, convection and radiation schemes can affect overall results.

Simulations for e_a provided better statistics for moisture than RH. Similar to the outputs of T2m and RH, the rural stations simulate e_a best. For urban simulations, the models had the most difficulty simulating e_a for medium-intensity stations. RMSEs for medium-intensity LULC differed by at least 0.5 kPa compared to other LULC categories in the urban regime. Overall, e_a observations and simulations correlated well in every LULC category (0.83-0.88). Of note is that the UCM1 had some difficulty simulating RH and e_a at Indian Springs. Simulated artifacts consisted of: anomalous RH increases at 0700 and 1500 LST (Fig. 42b), and e_a increases at 1500 LST on November 14, 24, and 25. A more in-depth analysis should be conducted as remote urban influences in arid/semi-arid environments may somehow be affecting the performance of the UCM1 model.

According to the McCarran simulation in Chapter 4.4.2, UHI_{sim} was more noticeable during days of clear skies, light winds, and low RH. Under these conditions the LSM had the strongest UHI_{sim} activity, but under the events of the moisture surge occurring November 17-19 the UCM2 favored larger UHI_{sim} intensity. Although the wind slightly increased during that time period, wind speeds under 7 m s^{-1} have been known to have little effect on relieving UHI in dry arid regions (Fast et al., 2005). As expected from the previous simulations, UCM1 simulated a more intense UCI_{sim}.

Lastly, the white roofing scenario implemented in this research showed that the model had greater effects for daytime T2m decreasing T_{max} ~1°-2°C which supports the findings of Jacobsen and Ten Hoeve (2012). In addition, the effects of the albedo

simulations reduced the diurnal range of T2m and RH, but showed little effect on nighttime/early morning results.

6. Summary and Conclusions

This document addresses the UHI and UCI in Las Vegas through several approaches consisting of: removing long-term regional trends, implementing a correction factor, normalizing station data, assessing the ability of GDPs to observe UHI/UCI, and running modeled simulations. Issues with the observational data consisted of: missing data, limited number of stations available for long-term analysis, limited number of rural sites near Las Vegas, and station maintenance among other issues on quality and quantity of data. These issues are of importance to address as they also affect the quality and robustness of the GDPs that interpolate from surface observations. Furthermore, a few networks were rejected from this study due to the poor quality that stemmed from a lack of maintenance and records.

This work shows that approaches to isolate the city long-term climate trends from those related to global/regional trends is a necessary step for any urban growth attribution and local climate effect relationships. The effects of global/regional trends show warming in T_{min} and interdecadal variability for T_{max}, while isolated long-term trends showed a UHI of ~1.63°C that was strongest during DJF. UCI was evident during daytime with a magnitude of ~-0.15°C and was most prominent during MAM and JJA. Furthermore, the city has shown to warm faster than the rural area in response to urban and population growth and activity.

The GDPs were able to highlight the climatological influence of the city over time. However, due to some well-known limitations of the interpolation procedures the GDPs tend to underemphasize the UHI in comparison to the normalized observations in Chapter 3.6. PRISM 800 m had a UHI bias of -0.71°C while Daymet data showed a bias of -1.38°C. The UCI was slightly overemphasized by 0.24°C and 0.31°C from PRISM 800 m and Daymet, respectively. Based on the spatial analysis, PRISM 800 m did a better job at interpreting an urban footprint. However, due to uncertainties of small-scale forcings, the spatial contrast of warm and cool spots in the city may be inaccurate. Furthermore, GDP interpolations become more credible with network enhancements. This could have some effect on comparing past and present changes.

The DRI-UHI experimental network (20 new sites) was set out to accomplish the task of enhancing current urban networks, and provide an unbiased representation of unsampled areas in and around Las Vegas. Five other regional and in-city surface station networks were available for this study totaling 29 sites. Extensive QA/QC protocols were performed to create a solid, reliable, and consistent dataset for this research. However, rural and high-intensity areas still remain undersampled relative to low- and medium-intensity urban areas. Furthermore, the DRI-UHI recorded only T2m and RH while other networks logged more variables to assess the climate. Data for the DRI-UHI network will be made available to the public on the Nevada Climate Change Portal at: *http://sensor.nevada.edu/NCCP/Default.aspx*. As of the time of this thesis report, DRI-UHI is still functional. The observations can further enable in-city hydrological studies,

create and calibrate remote sensing relationships, and further evaluate high-resolution models.

Five, one month high-resolution simulations (1 km grid size) for November 2012 created opportunities to evaluate model sensitivity, and developed an adaptation and mitigation scenario to reduce the observed warming trends. In general, several WRF-UCM configurations (using UCM default city parameters) were found to be very sensitive for the case of Las Vegas. To our knowledge this was the first time Las Vegas was simulated using the UCM, and it is suggested that further exploration be necessary to assess proper calibration of the model to adequately simulate the arid/semi-arid climates. Furthermore, it is recommended to update the LULC data (NLCD 2006 was used in this research) to incorporate more recent urban changes and growth.

We argue that the WRF-UCM is an adequate tool to explore the effects of city growth on local and remote climate, and assess the potential effect of adaptation and mitigation strategies such as: reforestation, cool paving, white roofing, landscape replacement, and designs of future urban developments. These strategies can further be explored by simulating the effects of water and electrical resource management before and after mitigation practices.

Recommendations to improve this research suggests: using remote sensing to elaborate on the current spatial thermal effects of Las Vegas, setting up more surface stations to enhance the network (especially in high-intensity and rural areas), using a different approach for the WRF-UCM simulations (i.e. updating the LULC maps, changing the physics and urban parameters from the default settings, etc.), and observe

more atmospheric variables and features above the surface level. Furthering this research can help get a better idea of the effects of current conservation practices and confirm climatological changes in Las Vegas.

7. References

Aguado, E. and J. E. Burt, 2007: Chapter 14: Human Effects : Air Pollution and Heat Islands. Understanding Weather and Climate, Fourth Edition. Pearson Prentice Hall, Upper Saddle River, NJ, 428-449.

Akindobe, O. M., A. O. Eludoyin, and O.A. Fashae, 2008: Temperature and relative humidity distributions in a medium-size administrative town in southwest Nigeria. *J. Eniviron. Manage.*, **87,** 95-105, doi: 10.1016/j.jenvman.2007.01.018.

Alghannam, A. R. O. and M. R. A. Al-Qahtnai, 2012: Impact of vegetation cover on urban and rural areas of arid climates. *Aust. J. Agr. Eng.*, **3,** 1-5.

Allwine, K. J. and C. D. Whiteman, 1988: Ventilation of pollutants trapped in valleys: A simple parameterization for regional-scale dispersion models. *Atmos. Environ.,* **22,** 1839-1845.

Akbari, H., H. D. Matthews, and D. Seto, 2012: The long-term effect of increasing the albedo of urban areas. *Environ. Res. Lett.,* **7,** doi:10.1088/1748-9326/7/2/024004.

Beard, J. B. and R. L. Green, 1994: The role of turfgrasses in environmental protection and their benefits to humans. *J. Environ. Qual.,* **23,** 452-460.

Benson, L., B. Linsley, J. Smoot, S. Mensing, S. Lund, S. Stine, and A. Sarna-Wojcicki, 2003: Influence of the Pacific Decadal Oscillation on the climate of the Sierra Nevada, California and Nevada. *Quaternary Res.,* **59,** 151-159, doi: 10.1016/s0033-5894(03)00007-3.

Black, Adam Leland, 2013: Temperature Trends and Urban Heat Island Intensity Mapping of the Las Vegas Valley. *University of Nevada, Las Vegas.*

Bolton, D., 1980: The computation of equivalent potential temperature. *Mon. Wea. Rev,* **108,** 1046-1053.,

Ca, V. T., T. Asaeda, and Y. Ashie, 1999: Development of a numerical model for the evaluation of the urban thermal environment. *J. Wind Eng. Ind. Aerodyn.,* **81,** 181-196.

Cai, M. and E. Kalnay, 2003: Impact on urbanization and land-use change on climate. *Nature,* **423, No. 6939,** 528-531, doi: 10.1038/nature01952.

Castro, C. L., H. I. Chang, F. Dominguez, C. Carillo, J. K. Schemm, and H. M. H. Juang, 2012: Can a regional climate model improve the ability to forecast the North American Monsoon? *J. Clim.,* **25,** 8212-8237, doi: 10.1175/JCLI-D-11-0441.1.

Changnon, S. A., 1981: METROMEX: A Review and Summary. *Meteor. Monogr.,* **18, No. 40,** Amer. Meteor. Soc., 181 pp.

Chen, F., H. Kusaka, M. Tewari, J. W. Bao, and H. Hirakuchi, 2004: Utilizing the coupled WRF/LSM/urban modeling system with detailed urban classification to simulate the urban heat island phenomena over the greater Houston area. Preprints, 5th Conference on Urban Environment, Vancouver BC, Canada.

Chen, F., H. Kusaka, R. Bornstein, J. Ching, C. S. B. Grimmond, S. Grossman-Clarke, T. Loridan, K. W. Manning, A. Martilli, S. Miao, D. Sailor, F. P. Salamanca, H. Taha, M. Tewari, X. Wang, A. A. Wyszogrodzki, and C. Zhang, 2011: The integrated WRF/urban

modelling system: development, evaluation, and applications to urban environmental problems. *Int. J. Climatol.,* **31,** 273-288, doi: 10.1002/joc.2158.

Chow, W. T .L. and B. M. Svoma, 2011: Analyses of nocturnal temperature cooling-rate response to historical local-scale urban land-use/land cover change. *J. Appl. Meteor. Clim.,* **50,** 1872-1883, doi: 10.1175/JAMC-D-10-05014.1.

Coniglio, M. C., K .L. Elmore, J. S. Kain, S. J. Weiss, M. Xue, and M. L. Weismann, 2010: Evaluation of WRF model output for severe weather forecasting from the 2008 NOAA Hazardous Weather Testbed spring experiment. *Weather Forecast.,* **25,** 408-427, doi: 10.1175/2009WAF2222258.1.

Daly, C., 2006: Guidelines for assessing the suitability of spatial climate data sets. *Int. J. Climatol.,* **26,** 707-721, doi: 10.1002/joc.1322.

Daly, C., M. Halbleib, J. I. Smith, W. P. Gibson, M. K. Doggett, G. H. Taylor, J. Curtis, and P. P. Pasteris, 2008: Physiographically sensitive mapping of climatologically temperature and precipitation across the conterminous United States. *Int. J. Climatol.,* **28,** 2031-2064, doi: 10.1002/joc.1688.

Earman, S., A. R. Campbell, B. D. Newman, and F. M. Phillips, 2006: Isotopic exchange between snow and atmospheric water vapor: Estimation of the snowmelt component of groundwater recharge in the southwestern United States. *J. Geophys. Res.,* **111,** D09302, doi:10.1029/2005JD006470.

Emmanuel, R. and H. J. S. Fernando, 2007: Urban heat islands in humid and arid climates: role of urban form and thermal properties in Colombo, Sri Lanka and Phoenix, USA. *Clim. Res.*, **34,** 241-251, doi: 10.3354/cr00694.

Enfield, D. B., A. M. Mestas-Nuñez, and P. J. Trimble, 2001: The Atlantic Multidecadal Oscillation and its relation to rainfall and river flows in the continental US. *Geophys. Res. Lett.*, **28,** 2077-2080, doi: 10.1029/2000GL012745.

EPA, 2008: Reducing Urban Heat Islands: Compendium of Strategies. Urban Heat Island Basics. <http://www.epa.gov/heatisland/resources/compendium.htm>.

Fast, J. D., J. C. Torcolini, and R. Redman, 2005: Pseudovertical temperature profiles and the urban heat island measured by a temperature datalogger network in Phoenix, Arizona. *J. Appl. Meteor.*, **44,** 3-13.

Gaffin, S. R., M. Imhoff, C. Rosenzweig, R. Khanbilvardi, A. Pasqualini, A. Y. Y. Kong, D. Grillo, A. Freed, D. Hillel, and E. Hartung, 2012: Bright is the new black—multi-year performance of high-albedo roofs in an urban climate. *Environ. Res. Lett.*, **7,** 014029, doi:10.1088/1748-9326/7/1/014029.

Gober, P., A. Brazel, R. Quay, S. Myint, and S. Grossman-Clarke, 2010: Using watered landscapes to manipulate urban heat island effects: How much water will it take to cool Phoenix? *J. Am. Plann. Assoc.*,**76,** 109-121, doi: 10.1080/01944360903433113.

Grossman-Clarke, S., J. A. Zehnder, T. Loridan, and C. S. B. Grimmond, 2010: Contribution of land use changes to near-surface air temperatures during recent summer extreme heat events in the Phoenix metropolitan area. *J. Appl. Meteorol. Clim.,* **49,** 1649-1664, doi: 10.1175/2010JAMC2362.1.

Guan, X. D., J. P. Huang, N. Guo, J. R. Bi, and G. Y. Wang, 2009: Variability in soil moisture and its relationship with surface albedo and soil thermal parameters over the Loess Plateau. *Adv. Atmos. Sci.,* **26,** 692-700, doi: 10.1007/s00376-009-8198-0.

Guhathakurta, S. and P. Gober, 2010: Residential land use, the urban heat island, and water use in Phoenix: A path analysis. *J. Plan. Educ. Res.,* **30,** 40-51, doi: 10.1177/0739456X10374187.

Hansen, J., R. Ruedy, M. Sato, M. Imhoff, W. Lawrence, D. Easterling, T. Peterson, and T. Karl, 2001: A closer look at United States and global surface temperature change. *J. Geophys. Res.,* **106,** 23947-23963.

Hart, M. A. and D. J. Sailor, 2009: Quantifying the influence of land-use and surface characteristics on spatial variability in the urban heat island. *Theor. Appl. Climatol.* **95,** 397-406, doi: 10.1007/s00704-008-0017-5.

Holt, T. and J. Pullen, 2007: Urban canopy modeling of the New York City metropolitan area: A comparison and validation of single- and multilayer parameterizations. *Mon. Wea. Rev.,* **135,** 1906-1930, doi: 10.1175/MWR3372.1.

Holthaus, E., 2014: Gulp: The Lake That Supplies Vegas with Most of Its Water Is Now at Record-Low Levels. Future Tense. <http://www.slate.com> (Accessed on 18.07.14).

Huang, G., W. Zhou, and M. L. Cadenasso, 2011: Is everyone hot in the city? Spatial pattern of land surface temperatures, land cover and neighborhood socioeconomic characteristics in Baltimore, MD. *J. Enviorn. Manage.,* **92,** 1753-1759.

Ichinose, T., K. Shimodozono, and K. Hanaki, 1999: Impact of anthropogenic heat on urban climate in Tokyo. *Atmos. Environ.,* **33,** 3897-3909.

Ikeda, R. and H. Kusaka, 2010: Proposing the simplification of the multilayer urban canopy model: Intercomparison study of four models. *J. Appl. Meteor. Clim.,* **49,** 902-919, doi: 10.1175/2009JAMC2336.1.

Jacobson, M. Z. and J .E. Ten Hoeve, 2012: Effects of urban surfaces and white roofs on global and regional climate. *J. Clim.,* **25,** 1028-1044, doi: 10.1175/JCLI-D-11-00032.1.

Jin, M. S., 2012: Developing an index to measure urban heat island effect using satellite land skin temperature and land cover observations. *J. Clim.,* **25,** 6193-6201, doi: 10.1175/JCLI-D-11-00509.1.

Jonsson, P., 2004: Vegetation as an urban climate control in the subtropical city of Gaborone, Batswana. *Int. J. Climatol.,***24,** 1307-1322.

Kim, J. J. and D. Y. Kim, 2009: Effects on building's density on flow in urban areas. *Adv. Atmos. Sci.,* **26,** 45-56, doi: 10.1007/s00376-009-0045-9.

Kim, Y. and J. Baik, 2005: Spatial and temporal structure of the urban heat island in Seoul. *J. Appl. Meteor.,* **44,** 591-605.

Kimura, F. and S. Takahashi, 1991: The effects of land-use and anthropogenic heating on the surface temperature in the Tokyo metropolitan area: A numerical experiment. *Atmos. Eniviron.,* **25B,** 155-164.

Kjelgren, R., and T. Montague, 1998: Urban tree transpiration over turf and asphalt surfaces. *Atmos. Environ.,* **32,** 35-41.

Kloss, C. and C. Calarusse, 2006: Rooftops to rivers: Green strategies for controlling stormwater and combined sewer overflows. Natural Resource Defense Council.

Kondo, H., Y. Genchi, Y. Kikegawa, Y. Ohashi, H. Yoshikado, and H. Komiyama, 2005: Development of a multi-layer urban canopy model for analysis of energy consumption in a big city: Structure of the urban canopy model and its basic performance. *Bound-Lay Meteor.,* **116,** 395-421, doi: 10.1007/s10546-005-0905-5.

Kunkel, K. E., S. A. Changnon, B. C Reinke, and R. W. Arritt, 1996: The July 1995 heat wave in the Midwest: A climatic perspective and critical weather factors. *Bull. Amer. Meteor. Soc.,* **77,** 1507-1518.

Kusaka, H., H. Kondo, Y. Kikegawa, and F. Kimura, 2001: A simple single-layer urban canopy model for atmospheric models: Comparisons with multi-layer and slab models. *Bound-Lay Meteor.,* **101,** 329-358.

Kusaka, H. and F. Kimura, 2004: Coupling a single-layer urban canopy model with a simple atmospheric model: Impact on urban heat island simulation for an ideal case. *J. Meteor. Soc. Jpn.,* **82,** 67-80.

Kusaka, H. and F. Kimura, 2004: Thermal effect of urban canyon structure on the nocturnal heat island: Numerical experiment using a mesoscale model coupled with an urban canopy model. *J. Appl. Meteor.,* **43,** 1899-1909.

Kusaka, H., F. Chen, M. Tewari, J. Dudhia, D. O. Gill, M. G. Duda, W. Wang, and Y. Miya, 2012: Numerical simulation of urban heat island effect by the WRF model with 4-km grid Increment: An inter-comparison study between the urban canopy model and slab model. *J. Meteorol. Soc. Jpn.,* **90B,** doi: 10.2151/jmsj.2012-B03.

Lee, S. H., S. W. Kim, W. M. Angevine, L. Bianco, S. A. McKeen, C. J. Senff, M. Trainer, S. C. Tucker, and R. J. Zamora, 2011: Evaluation of urban surface parameterizations in the WRF model using measurements during the Texas Air Quality Study 2006 field campaign. *Atmos. Chem. Phys.,* **11,** 2127-2143, doi: 10.5194/acp-11-2127-2011.

Li, H., J. T. Harvey, T. J. Holland, and M. Kayhanian, 2013: The use of reflective and permeable pavements as a potential practice for heat island mitigation and stormwater management. *Environ. Res. Lett.,* **8,** doi:10.1088/1748-9326/8/1/015023.

Li, S., H. Mo, and Y. Dai, 2011: Spatio-temporal pattern of urban cool island intensity and its eco-environment response in Chang-Zhu-Tan urban agglomeration. *Commun. Inform. Sci. Manage. Eng.,* **1,** 1-6.

Lin, C. Y., F. Chen, J. C. Huang, W. C. Chen, Y. A. Liou, W. N. Chen, and S. C. Liu, 2008: Urban heat island effect and its impact on boundary layer development and land-sea circulation over northern Taiwan. *Atmos. Environ.,* **42,** 5635-5649, doi:10.1016/j.atmosenv.2008.03.015.

Lindén, J., 2011: Nocturnal cool island in the Sahelian city of Ouagadougou, Burkina Faso. *Int. J. Climatol.,* **31,** 605-620, doi: 10.1002/joc.2069.

Liu, H. Z., B. M. Wang, and C. B. Fu, 2008: Relationships between surface albedo, soil thermal parameters and soil moisture in the semi-arid area of Tongyu, northeastern China. *Adv. Atmos. Sci.,* **25,** 757-764, doi: 10.1007/s00376-008-0757-2.

Major, D. C., A. Omojola, M. Dettinger, R. T. Hanson, and R. Sanchez-Rodriguez, 2011: Chapter 5: Climate change, water, and wastewater in cities. Climate Change and Cities: First Assessment Report of the Urban Climate Change Research Network. Rosenzweig, C., W.D. Solecki, S.A. Hammer, and S. Mehorta, Eds., Cambridge University Press, Cambridge, UK, 113-143.

Mantua, N. J. and S. R. Hare, 2002: The Pacific Decadal Oscillation. *J. Oceanogr.,* **58,** 35-44.

McCabe, G. J., M. A. Palecki, and J. L. Betancourt, 2004: Pacific and Atlantic Ocean influences on multidecadal drought frequency in the United States. *P. Natl. Acad. Sci. USA.,* **101,** 4136-4141, doi: 10.1073/pnas.0306738101.

McEvoy, D. J., Hobbins, M. T., Huntington, J. L., and A. Wood, 2014: Tracking Flash Drought with Land-Atmospheric Feedbacks. *American Meteorological Society Annual Meeting, Atlanta, GA, February 2-6.*

Mendonca, F., 2009: Urban heat and urban cool islands: Influences of vegetation and soil surface in some cities, Southern Brazil. Preprints, The seventh International Conference on Urban Climate, International Association for Urban Climate, Yokohama, Japan.

Mensing, S., S. Strachan, J. Arnone, L. Fenstermaker, F. Biondi, D. Devitt, B. Johnson, B. Bird, and E. Fritzinger, 2013: A network for observing Great Basin climate change. *Eos*, **94, No. 11,** 105-106.

Miao, S., F. Chen, M. A. LeMone, M. Tewari, Q. Li, and Y. Wang, 2009: An observational and modeling study of characteristics of urban heat island and boundary layer structures in Beijing. *J. Appl. Meteor. Clim.*, **48,** 484-501, doi: 10.1175/2008JAMC1909.1.

Middel, A., A. J. Brazel, S. Kaplan, and S. W. Myint, 2012: Daytime cooling efficiency and diurnal energy balance in Phoenix, Arizona, USA. *Clim. Res.*, **54,** 21-34, doi: 10.3354/cr01103.

Mohan, S. and N. Arumugam, 1996: Relative importance of meteorological variables in evapotranspiration: Factor analysis approach. *Water Resour. Manag.*, **10,** 1-20, doi: 10.1007/BF00698808.

Mueller, E. C., and T. A. Day, 2005: The effect of urban ground cover on microclimate, growth and leaf gas exchange of oleander in Phoenix, Arizona. *Int. J. Biometeor.,* **49,** 244-255.

NCA (National Climate Assessment), 2013: A Review of the Draft 2013 National Climate Assessment.

NCAR (National Center for Atmospheric Research), 2013: ARW Version 3 Modeling Systems User Guide.

Neelin, J. D., 2011: Chapter 2: Basics of Global Climate. Climate Change and Climate Modeling. Cambridge University Press, New York, NY, 34-70.

Nehrkorn, T., J. Henderson, M. Leidner, M. Mountain, and J. Eluszkiewicz, 2013: WRF Simulations of the Urban Circulation in the Salt Lake City Area for CO_2 Modeling. *J. Appl. Meteor. Clim.*, **52,** 323-340, doi: 10.1175/JAMC-D-12-061.1.

Oke, T., 1973: City size and the urban heat island. *Atmos. Environ.*, **7,** 769-779.

Oke, T. and G. B. Maxwell, 1975: Urban heat island dynamics in Montreal and Vancouver. *Atmos. Environ.,* **9,** 191-200.

Oke, T. R., 1987: Boundary Layer Climates, 2nd Edition. Methuen. 291.

Reheis, M. C. and F. E. Urban, 2011: Regional and climatic controls on seasonal dust deposition in the southwestern US. *Aeolian Res.*, **3,** 3-21, doi: 10.1016/j.aeolia.2011.03.008.

Roberts, S. M., T. R. Oke, C. S. B. Grimmond, and J. A. Voogt, 2006: Comparison of four methods to estimate urban heat storage. *J. Appl. Meteor. Clim.,* **45,** 1766-1781.

Scheitlin, K. N. and P. G. Dixon, 2010: Diurnal temperature range variability due to land cover and airmass types in the southeast. *J. Appl. Meteor. Clim.*, **49,** 879-888, doi: 10.1175/2009JAMC2322.1.

Schneider, N. and B. D. Cornuelle, 2005: The forcing of the Pacific decadal oscillation. *J. Clim.*, **18,** 4355-4373, doi: 10.1175/JCLI3527.1.

Scully, Rebecca, 2010: Intercomparison of PRISM and Daymet Temperature Interpolation from 1980 to 2003. *Utah State University.*

Shorr, N., R. G. Najjar, A. Amato, and S. Graham, 2009: Household heating and cooling energy use in the northeast USA: Comparing the effects of climate change with those of purposive behaviors. *Clim. Res.*, **39,** 19-30, doi: 10.3354/cr00782.

Skamarock, W. C., J. B. Klemp, J. Dudhia, D. O. Gill, D. M. Barker, W. Wang, and J. G. Powers, 2005: A Description of the Advanced Research WRF Version 2, NCAR Technical Note, NCAR/TN-468+STR, 88p.

Smith, K. R. and P. J. Roebber, 2011: Green roof mitigation potential for a proxy future climate scenario in Chicago, Illinois. *J. Appl. Meteor. Clim.,* **50,** 507-522, doi: 10.1175/2010JAMC2337.1.

Spronken-Smith, R. A. and T. R. Oke, 1999: Scale modelling of nocturnal cooling in urban parks. *Bound-Lay. Meteorol.,***93,** 287-312, doi: 10.1023/A: 1002001408973.

Svoma, B. M. and A. Brazel, 2010: Urban effects on the diurnal temperature cycle in Phoenix, Arizona. *Clim. Res.,* **41,** 21-29, doi: 10.3354/cr00831.

Taha, H., 1997: Urban climates and heat islands: albedo, evapotranspiration, and anthropogenic heat. *Energ. Buildings,* **25,** 99-103.

Theeuwes, N. E., A. Solcerová, and G. J. Steeneveld, 2013: Modeling the influence of open water surfaces on the summertime temperature and thermal comfort in the city. *J. Geophys. Res. Atmos.,* **118,** 8881-8896, doi: 10.1002/jgrd.50704.

Thornton, P. E., S. W. Running, and M. A. White, 1997: Generating surfaces of daily meteorological variables over large regions of complex terrain. *J. Hydrol.,* **190,** 214-251, doi: 10.1016/S0022-1694(96)03128-9.

Titus, T. N., K. Becker, F. Tosi, M. T. Capria, M. C. De Sanctis, E. Palomba, D. Grassi, F. Capaccioni, E. Ammannito, J. -Ph. Combe, T. B. McCord, J. -Y. Li, C. T. Russell, and C. A. Raymond, 2013: Analysis of temperature and thermal inertia of the surface of Vesta using Dawn VIR survey observations. Preprints. 44th Lunar and Planetary Science Conference, The Woodlands, Texas.

Tripathi, O. P. and F. Dominguez, 2013: Effects of spatial resolution in the simulation of daily and subdaily precipitation in the southwestern US. *J. Geophys. Res.,* **118,** 7591-7605, doi:10.1002/jgrd.50590.

UNEP, 2014: Las Vegas. Environmental Change Hotspots. Division of Early Warning and Assessment (DEWA). United Nations Environment Programme (UNEP). <http://na.unep.net/atlas/webatlas.php?id=2224> (Accessed on 19.05.14).

Van Den Heever, S. C. and W. R. Cotton, 2007: Urban aerosol impacts on downwind convective storms. *J. Appl. Meteor. Clim.,* **46,** 828-850, doi: 10.1175/JAM2492.1.

Van Heerwaarden, C. C. and J. Vilà-Guerau De Arellano, 2008: Relative humidity as an indicator for cloud formation over heterogeneous land surfaces. *J. Atmos. Sci.,* **65,** 3263-3277, doi: 10.1175/2008JAS2591.1.

Wallace, J. M. and P. V. Hobbs, 2006: Chapter 9: The Atmospheric Boundary Layer. Atmospheric Science, Second Edition: An Introductory Survey. Dmowska, R., Hartmann, D., and H. T. Rossby, Eds., Academic Press, Burlington, MA, 63-111.

Wang, Z-H., E. Bou-Zeid, and J. A. Smith, 2013: A coupled energy transport and hydrological model for urban canopies evaluated using a wireless sensor network. *Q.J.R. Meteorol. Soc.,* **139,** 1643-1657, doi: 10.1002/qj.2032.

Watts, A., 2009: Is the U.S. Surface Temperature Reliable? The Heartland Institute, Chicago, IL, 1-29.

Wickham, J. D., S. V. Stehman, L. Gass, J. Dewitz, J. A. Fry, and T. G. Wade, 2013: Accuracy assessment of NLCD 2006 land cover and impervious surface. *Remote Sens. Environ.,* **130,** 294-304.

Winguth, A. M. E. and B. Kelp, 2013: The urban heat island of the North-Central Texas region and its relation to the 2011 severe Texas drought. *J.Appl. Meteor. Clim.,***52,** 2418-2433, doi: 10.1175/JAMC-D-12-0195.1.

Xian, G., 2008: Satellite remotely sensed land surface parameters and their climatic effects for three metropolitan regions. *Adv. Space Res.,***41,** 1861-1869, doi:10.1016/j.asr.2007.11.004.

Xian, G. and M. Crane, 2006: An analysis of urban thermal characteristics and associated land cover in Tampa Bay and Las Vegas using Landsat satellite data. *Remote Sens. Environ.,* **104,** 147-156, doi:10.1016/j.rse.2005.09.023.

Yang, B., Y. Zhang, and Y. Qian, 2012: Simulation of urban climate with high-resolution WRF Model: A case study in Nanjing, China. *Asia-Pac. J. Atmos. Sci.*, **48,** 227-241, doi: 10.1007/s13143-012-0023-5.

Yates, D., K. Averyt, F. Flores-Lopez, J. Meldrum, S. Sattler, J Sieber, and C. Young, 2013: A water resources model to explore the implications of energy alternatives in the southwestern US. *Environ. Res. Lett.,* **8,** doi: 10.1088/1748-9326/8/4/045004.

Yu, C. and W. N. Hien, 2006: Thermal benefits of city parks. *Energ. Buildings,* **38,** 105-120, doi: 10.1016/j.enbuild.2005.04.003.

Yushkov, V. P., R. D. Kouznetsov, and M. A. Kallistratova, 2009: The spatial and temporal variability of the wind speed within the urban boundary layer. Preprints. The Seventh International Conference on Urban Climate, Yokohama, Japan.

Zhang, S. Q., M. Zupanski, A. Y. Hou, X. Lin, and S. H. Cheung, 2013: Assimilation of precipitation-affected radiances in a cloud-resolving WRF ensemble data assimilation system. *Mon. Wea. Rev.,* **141,** 754-772, doi: 10.1175/MWR-D-12-0005.1.

8. Appendix

Appendix A: Featured stations analyzed in this study along with their specific location (latitude and longitude), elevation, length of observation record, and recorded parameters. The "*" are represented as homes, "**" are represented as CCSD sites, and "***" are represented as golf courses for the DRI-UHI network. Parameters available: T2m, T_d, RH, wind vectors (Wind), surface pressure (P), precipitation (precip) solar radiation (SR), cloud cover (CC), and visibility (Vis).

Station Name	Network	Latitude	Longitude	Elevation (m ASL)	Recording Period	Parameters
Boulder City	CEMP	35.985°	-114.841°	734	1999-current	T2m, RH, wind, SR, precip
Henderson	CEMP	36.007°	-114.966°	670	1999-current	T2m, RH, wind, SR, precip
Indian Springs	CEMP	36.574°	-115.676°	964	1999-current	T2m, RH, wind, SR, precip
Las Vegas	CEMP	36.114°	-115.149°	623	1999-current	T2m, RH, wind, SR, precip
Boulder City Municipal	NWS	35.947°	-114.861°	653	2010-current	T2m, Td, P, wind, precip, CC, Vis
Desert Rock	NWS	36.621°	-116.028°	990	1978-current	T2m, Td, P, wind, precip, CC, Vis
Henderson Executive	NWS	35.976°	-115.133°	740	2004-current	T2m, Td, P, wind, precip, CC, Vis
McCarran	NWS	36.072°	-115.163°	663	1948-current	T2m, Td, P, wind, precip, CC, Vis
Nellis	NWS	36.250°	-115.033°	577	1928-current	T2m, Td, P, wind, precip, CC, Vis
Blackbrush	NevCAN	36.520°	-115.163°	1670	2011-current	T2m, RH, P, wind, SR
Mojave Desert Shrub	NevCAN	36.435°	-115.355°	900	2011-current	T2m, RH, P, wind, SR
Montane	NevCAN	36.591°	-115.215°	2320	2011-current	T2m, RH, P, wind, SR
Pinyon Juniper	NevCAN	36.575°	-115.205°	2065	2011-current	T2m, RH, P, wind, SR
KNVHENDE6	WU	36.032°	-115.075°	625	Unknown	T2m, RH, Td, P, wind, precip
KNVHENDE15	WU	36.001°	-115.078°	714	Unknown	T2m, RH, Td, P, wind, precip
KNVHENDE21	WU	35.995°	-115.070°	688	Unknown	T2m, RH, Td, P, wind, precip
KNVHENDE25	WU	35.945°	-115.104°	878	Unknown	T2m, RH, Td, P, wind, precip
KNVLASVE11	WU	36.045°	-115.286°	832	Unknown	T2m, RH, Td, P, wind, precip
KNVLASVE35	WU	36.206°	-115.330°	914	Unknown	T2m, RH, Td, P, wind, precip
KNVLASVE71	WU	36.082°	-115.250°	743	Unknown	T2m, RH, Td, P, wind, precip
KNVNORTH6	WU	36.264°	-115.148°	632	Unknown	T2m, RH, Td, P, wind, precip
KNVNORTH9	WU	36.232°	-115.171°	656	Unknown	T2m, RH, Td, P, wind, precip
MC7282	WU	36.040°	-115.095°	618	Unknown	T2m, RH, Td, P, wind, precip
MD5799	WU	36.047°	-115.186°	699	Unknown	T2m, RH, Td, P, wind, precip

MUP076	WU	36.029°	-115.227°	738	Unknown	T2m, RH, Td, P, wind, precip
Desert NWR	RAWS	36.579°	-115.144°	2197	2002-current	T2m, RH, wind, SR, precip
Yucca Gap	RAWS	36.437°	-115.331°	972	2004-current	T2m, RH, wind, SR, precip
Kyle Canyon	RAWS	36.267°	-115.600°	2065	1998-current	T2m, RH, wind, SR, precip
Red Rock	RAWS	36.135°	-115.477°	1266	1990-current	T2m, RH, wind, SR, precip
Blue Diamond**	DRI-UHI	36.048°	-115.406°	1029	2012-current	T2m and RH
Cheyenne Transportation**	DRI-UHI	36.215°	-115.149°	625	2012-current	T2m and RH
Clough*	DRI-UHI	36.144°	-115.330°	908	2012-current	T2m and RH
Collins*	DRI-UHI	35.989°	-114.986°	758	2012-current	T2m and RH
DL Dickens**	DRI-UHI	36.260°	-115.091°	599	2012-current	T2m and RH
Fenstermaker*	DRI-UHI	36.271°	-115.250°	717	2012-current	T2m and RH
Kim*	DRI-UHI	36.120°	-115.267°	764	2012-current	T2m and RH
Las Vegas High**	DRI-UHI	36.146°	-115.031°	534	2012-current	T2m and RH
Miller*	DRI-UHI	36.317°	-115.280°	775	2012-current	T2m and RH
Peacock*	DRI-UHI	36.031°	-115.204°	722	2012-current	T2m and RH
Piechota*	DRI-UHI	35.988°	-115.118°	744	2012-current	T2m and RH
Pitchford*	DRI-UHI	36.095°	-115.129°	616	2012-current	T2m and RH
Pohlmann*	DRI-UHI	36.022°	-115.077°	653	2012-current	T2m and RH
Roos*	DRI-UHI	36.251°	-115.283°	744	2012-current	T2m and RH
Spangler*	DRI-UHI	36.120°	-115.106°	584	2012-current	T2m and RH
Summerlin***	DRI-UHI	36.192°	-115.287°	796	2012-current	T2m and RH
Sunrise Acres**	DRI-UHI	36.165°	-115.113°	561	2012-current	T2m and RH
Wallin**	DRI-UHI	35.932°	-115.089°	918	2012-current	T2m and RH
West**	DRI-UHI	36.194°	-115.168°	631	2012-current	T2m and RH
Wildhorse***	DRI-UHI	36.056°	-115.078°	596	2012-current	T2m and RH

Appendix B: Photographs of DRI-UHI sites.

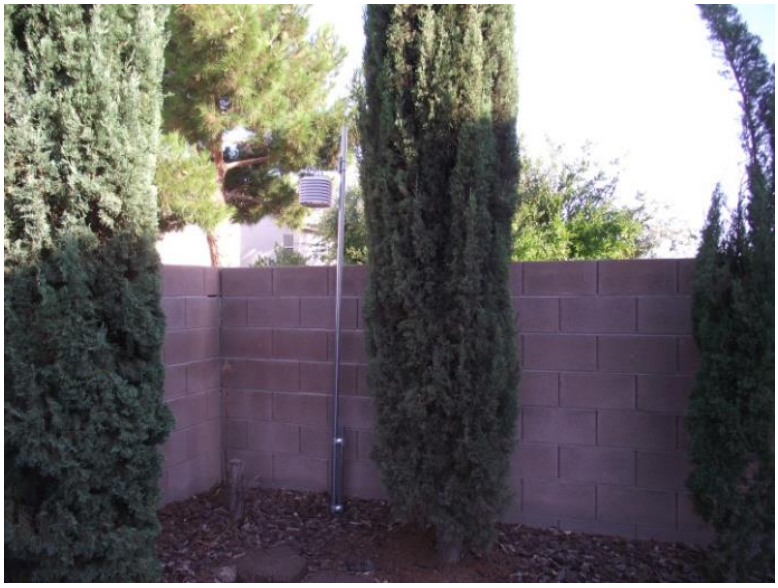

Kim residential site.

Charles West Middle School CCSD site.

Wildhorse Golf Course.

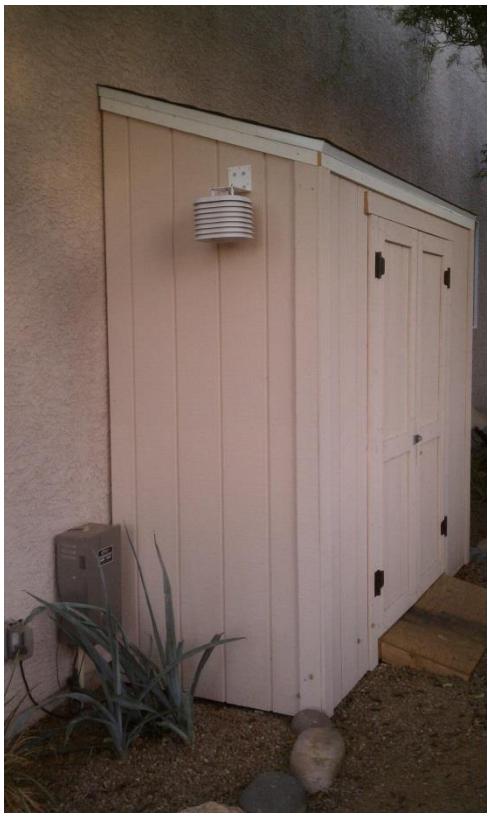

Pohlmann residential site.

Appendix C: LULC categories for each surface station based on the 2006 NLCD and Landsat imagery. Station LULC categories range in 6 different categories which are: High-intensity urban (High Int), medium-intensity urban (Med Int), low-intensity urban (Low Int), barren, shrub, and evergreen forest (EF). LULC classification was updated based on current visual and Landsat analysis.

Station Name	**Network**	**Latitude**	**Longitude**	**Elevation (m)**	**LULC 2006**	**LULC Updated**
Boulder City	CEMP	35.985°	-114.814°	734	Low Int	Low Int
Henderson	CEMP	36.008°	-114.966°	670	Med Int	Med Int
Indian Springs	CEMP	36.574°	-115.676°	964	Low Int	Shrub
Las Vegas	CEMP	36.114°	-115.149°	623	High Int	High Int
Boulder City Municipal	NWS	35.947°	-114.861°	653	Shrub	Shrub
Desert Rock	NWS	36.621°	-116.028°	990	Shrub	Shrub
Henderson Executive	NWS	35.976°	-115.133°	740	Shrub	Shrub
McCarran	NWS	36.072°	-115.163°	663	High Int	High Int
Nellis	NWS	36.250°	-115.033°	577	Barren	Barren
Blue Diamond	DRI-UHI	36.048°	-115.406°	1029	Shrub	Shrub
Cheyenne Transportation	DRI-UHI	36.215°	-115.149°	625	Barren	Barren
Clough	DRI-UHI	36.144°	-115.330°	908	Shrub	Med Int
Collins	DRI-UHI	35.989°	-114.986°	758	Shrub	Low Int
DL Dickens	DRI-UHI	36.260°	-115.091°	599	Barren	Low Int
Fenstermaker	DRI-UHI	36.271°	-115.250°	717	Med Int	Low Int
Kim	DRI-UHI	36.120°	-115.267°	764	Med Int	Med Int
Las Vegas High	DRI-UHI	36.146°	-115.031°	534	Barren	Low Int
Miller	DRI-UHI	36.317°	-115.280°	775	Low Int	Low Int
Peacock	DRI-UHI	36.031°	-115.204°	722	Shrub	Low Int
Piechota	DRI-UHI	35.988°	-115.118°	744	Low Int	Med Int
Pitchford	DRI-UHI	36.095°	-115.129°	616	Med Int	Med Int
Pohlmann	DRI-UHI	36.022°	-115.077°	653	Med Int	Med Int
Roos	DRI-UHI	36.251°	-115.283°	744	Med Int	Low Int
Spangler	DRI-UHI	36.120°	-115.106°	584	Med Int	Med Int
Summerlin	DRI-UHI	36.192°	-115.287°	796	Med Int	Med Int
Sunrise Acres	DRI-UHI	36.165°	-115.113°	561	Med Int	Med Int
Wallin	DRI-UHI	35.932°	-115.089°	918	Shrub	Med Int
West	DRI-UHI	36.194°	-115.168°	631	Med Int	Med Int
Wildhorse	DRI-UHI	36.056°	-115.078°	596	Med Int	Med Int
Blackbrush	NevCAN	36.520°	-115.163°	1670	Shrub	Shrub

Mojave Desert Shrub	NevCAN	36.435°	-115.355°	900	Shrub	Shrub
Montane	NevCAN	36.591°	-115.215°	2320	EF	EF
Pinyon Juniper	NevCAN	36.575°	-115.205°	2065	EF	EF
HENDE6	WU	36.032°	-115.075°	625	Med Int	Med Int
HENDE15	WU	36.001°	-115.078°	714	Med Int	Low Int
HENDE21	WU	35.995°	-115.070°	688	Shrub	Low Int
HENDE25	WU	35.945°	-115.104°	878	Med Int	Low Int
LASVE11	WU	36.045°	-115.286°	832	Low Int	Low Int
LASVE35	WU	36.206°	-115.330°	914	Low Int	Low Int
LASVE71	WU	36.082°	-115.250°	743	Med Int	Low Int
NORTH6	WU	36.264°	-115.148°	632	Barren	Barren
NORTH9	WU	36.232°	-115.171°	656	Low Int	Low Int
MC7282	WU	36.040°	-115.095°	618	Med Int	Med Int
MD5799	WU	36.047°	-115.186°	699	Low Int	Low Int
MUP076	WU	36.029°	-115.227°	738	Shrub	Shrub
Desert NWR	WU	36.579°	-115.144°	2197	Shrub	Shrub
Yucca Gap	WU	36.437°	-115.331°	972	Shrub	Shrub
Kyle Canyon	WU	36.267°	-115.600°	2065	EF	EF
Red Rock	WU	36.135°	-115.477°	1266	Shrub	Shrub

Appendix D: Daily dominant cloud cover and maximum simulated UHI (UCI) at McCarran Airport for the month of November 2012.

Day	Cloud Cover	LSM UHI	UCM1 UHI	UCM2 UHI
1	Broken	3.64°C (none)	1.53°C (-3.08°C)	3.24°C (-1.31°C)
2	Scatter	2.66°C (-0.33°C)	1.49°C (-2.62°C)	1.57°C (-1.30°C)
3	Scatter	3.02°C (-0.99°C)	1.17°C (-2.42°C)	1.67°C (-1.77°C)
4	Clear	3.24°C (-0.73°C)	1.76°C (-2.52°C)	2.09°C (-1.66°C)
5	Clear	4.18°C (-2.04°C)	1.82°C (-3.72°C)	2.65°C (-2.95°C)
6	Clear	3.35°C (-0.74°C)	1.41°C (-2.53°C)	1.63°C (-1.61°C)
7	Clear	2.88°C (-0.34°C)	1.51°C (-1.91°C)	2.21°C (-1.51°c)
8	Broken	2.03°C (-1.04°C)	1.33°C (-0.94°C)	1.98°C (-1.35°C)
9	Scatter	1.84°C (-0.66°C)	0.73°C (-1.01°C)	1.48°C (-1.42°C)
10	Scatter	3.16°C (-0.66°C)	0.97°C (-2.01°C)	2.92°C (-1.83°C)
11	Clear	4.12°C (-0.18°C)	1.74°C (-2.74°C)	3.77°C (-1.45°C)
12	Scatter	2.74°C (-0.64°C)	1.21°C (-2.37°C)	2.84°C (-1.03°C)
13	Clear	2.89°C (-1.41°C)	0.86°C (-2.65°C)	2.86°C (-1.67°C)
14	Broken	3.16°C (-1.75°C)	1.38°C (-3.06°C)	3.29°C (-1.71°C)
15	Broken	2.05°C (-1.35°C)	0.54°C (-2.28°C)	1.91°C (-1.01°C)
16	Scatter	2.45°C (-1.62°C)	1.27°C (-3.10°C)	2.85°C (-1.16°C)
17	Broken	3.63°C (-0.49°C)	2.13°C (-3.77°C)	3.78°C (-1.47°C)
18	Scatter	2.69°C (-0.50°C)	1.28°C (-1.51°C)	2.58°C (-1.06°C)
19	Scatter	3.54°C (-0.40°C)	2.48°C (-2.12°C)	3.70°C (-0.91°C)
20	Clear	1.80°C (-1.18°C)	0.56°C (-2.84°C)	1.71°C (-1.70°C)
21	Scatter	2.50°C (-0.33°C)	0.68°C (-1.97°C)	2.27°C (-0.66°C)
22	Scatter	3.67°C (-1.50°C)	2.00°C (-2.83°C)	4.01°C (-1.37°C)
23	Clear	3.23°C (-1.09°C)	1.79°C (-2.17°C)	2.53°C (-1.21°C)
24	Clear	3.77°C (-1.21°C)	1.76°C (-2.50°C)	2.88°C (-1.27°C)
25	Scatter	2.58°C (-0.75°C)	1.82°C (-2.30°C)	2.09°C (-0.68°C)
26	Clear	2.78°C (-0.94°C)	1.33°C (-2.57°C)	2.98°C (-1.04°C)
27	Broken	2.03°C (-1.07°C)	0.76°C (-2.37°C)	1.68°C (-1.19°C)
28	Scatter	1.89°C (-0.72°C)	1.56°C (-2.01°C)	2.64°C (-0.83°C)
29	Broken	2.34°C (-0.90°C)	1.23°C (-0.76°C)	2.45°C (-0.79°C)
AVERAGE		**2.89°C (-0.91°C)**	**1.38°C (-2.37°C)**	**2.56°C (-1.34°C)**